TABLE OF CONTENTS

FOREWORD

I defended a PhD thesis entitled "Molecular Clouds in the Cepheus Region" at the Mathematical Faculty of the University of Belgrade on November, 22. 2001. The thesis was divided into two parts - the first 6 chapters were basically a broad introduction to the topic of research, while the results were presented in the further 5 chapters, mostly in extended forms of the papers published or submitted/intended for submission in a near future. The papers included are given in the list below:

I – **S. Nikolić**, Cs. Kiss, L.E.B. Johansson, J.G.A. Wouterloot, L.V. Tóth, 2001, "L 1274: a multiwavelength study of a dark cloud in the Cep – Cas void", *Astron. Astrophys.* **367**, 694

II – **S. Nikolić**, L.E.B. Johansson, J. Harju, 2003, "Star forming cores in L 1251: maps and molecular abundances", *Astron. Astrophys.* **409**, 941

III – **S. Nikolić**, M. Juvela, 2003, "Modeling HCO^+ disks of CO outflow sources IRAS 22343+7501 and IRAS 22129+7000 ", *Astron. Astrophys. intended*

IV – M. Kun, **S. Nikolić**, P. Ábrahám, 2000, "Star Formation in the Cepheus Flare: L 1219 and L 1251", in the *Star formation from the small to the large scale*, Proc. of the 33rd ESLAB Symp., eds. Favata F., Kaas A.A., Wilson A., ESA–445, pg. 441

V – **S. Nikolić**, 1998, "Comparison of Chemical and Traditional Temporal Indicators", in the Proc. of the XII National Conference of Yugoslav Astronomers, *Publ.Astron.Obs.Belgrade* **65**, 93

However, having in mind the main aim of this monography, to introduce new topics of molecular radio spectroscopy and star formation studies to Serbian astronomical community, the PhD text had to undergo some changes. The main difference is the PhD's chapter *Molecular Excitation and Radiative Transfer*, which has as such, disappeared. The results from that work are, however, included in the appropriate chapters of this monography. I gathered that it would be more welcomed as a contribution to a separate monography devoted solely to radiative transfer problem in astrophysics. The later chapters of the thesis required a new organization and partly new content with both the results not previously included in the thesis. The list of those new papers is below:

VI – Cs. Kiss, L.V. Tóth, A. Moór, F. Sato, **S. Nikolić**, J.G.A. Wouterloot, 2000, "Low mass clouds in the Cepheus–Cassiopeia Void I: Khavtassi 15", *Astron. Astrophys.*, **363**, 755

VII – Cs. Kiss, **S. Nikolić**, A. Moór, L.V. Tóth, 1997, "Multiwavelength studies of Kh 15", in the Proc. of the XXX YERAC, *Acta Cosmologica*, Universitas Iagellonica, XXIII-2, pg. 95.

VIII – **S. Nikolić** & L. E. B. Johansson, 2002, "Molecular line observations of low–mass star formation in L 1251", in the Proc. of the conference *"Chemistry as a Diagnostic of Star Formation"* University of Waterloo, Canada, C. L. Curry & M. Fich eds. pg.371

IX – **S. Nikolić** & M. Kun, 2003, "Star formation in the L 1219/L 1217 molecular cloud I. CO observations and dust distribution", *Astron. Astrophys. in prep.*

Financial or "just a" support from Prof. Roy Booth, the director of the Onsala Space Observatory, Prof. Lajos Balázs the director of the Konkoly Observatory of the Hungarian Academy of Sciences, Prof. Balint Erdi the current and the late head of the Department of Astronomy of the Lorán Eötvos University in Budapest Prof. Miklos Marik, Dr. Milan Dimitrijević who was director of the Astronomical Observatory in Belgrade (AOB) during my doctoral studies and my supervisor, Dr. Ištvan Vince, is acknowledged.

It was my pleasure to meet or work or simply share the same several cubic meters with Lars, Per, Arto, Roger (tack såmycket!), John (thank you!), Steve (gun robh math agad!), Jiyune (gamsahapnyda!), Cathy (merci!), Mika, Jorma (kiitos!), Jan (bedankt!), Duilia (obrigada!), Maria, Laszlo, Csaba, Viktor (köszönöm!), Sanja and Snežana (hvala!)

To my family.

25. January, 2003. Gothenburg, Sweden

Silvana Nikolić

Chapter 1
INTRODUCTION

There are many indications that the interstellar medium in the Cepheus – Cassiopeia region ($100 \leq \ell \leq 140°, 0 \leq b \leq 25°$, Cep - Cas region) is highly disturbed due to one or more supernova explosions in the last 10^6 years. The area between the Cepheus and Cassiopeia molecular cloud complexes is virtually free of CO emission. This CO "hole" is filled with an excess soft X-ray radiation whose origin might be a supernova that exploded roughly 10^4 years ago at a distance of about 300 pc (Grenier et al. 1989). Along the eastern border of the Cepheus cloud complex runs a ridge of the one of the major radio-continuum loops, Loop III (Berkhuijsen 1973). Loop III has an estimated distance of 150 pc and the projected center at $\ell \approx 125°$ and $b \approx 15°$ (Berkhuijsen 1973). It is generally accepted that the radio-continuum loops are $\sim 10^6$ years old supernova remnants (SNRs). Another SN explosion might have occured in the Cep OB2a association about 3×10^6 years ago. Kun et al. (1987) have proposed that the "Cepheus Bubble", a giant ($\approx 10°$ in angular diameter) dust ring around the Cep OB2, association had been created by the strong stellar wind/UV radiation and the subsequent supernova explosion of the most massive star in the older subgroup Cep OB2a. Ábrahám et al. (2000) investigated the spatial and velocity distribution of atomic hydrogen associated with the Cepheus Bubble. The kinematics and size of this shell is best modeled by a supernova explosion that occurred in Cep OB2a at the distance of ~ 560 pc (De Zeeuw et al. 1999) about $\sim 1.7 \times 10^6$ years ago. Since the ages of several parts of the Cepheus Bubble are considerably higher than the age of the expanding shell, the supernova probably exploded in a pre-existing cavity, and its shock front might have interacted with the already existing star forming regions Sh2-140, IC 1396, and NGC 7129, leading to a new wave of star formation there. As a last example of this brief lists of SNs candidates in this region, the space velocity of a recently discovered runaway star HD203854 suggests that some $5 \times 10^5 - 10^6$ years ago this star might have been a companion of a supernova located close to the center of the Cep - Cas CO Void (Kun et al. 2000).

The ISM in Cepheus ($100° \leq \ell \leq 120°$, $b \geq 10°$) is distributed over large spatial and velocity range, $-15 \leq v_{\rm LSR} \leq 20\,{\rm km\,s^{-1}}$ (see e.g., Lebrun 1986, Yonekura et al. 1997). Distances of the molecular clouds were determined using optical star counts and three major absorbing layers were identified (Kun 1998). These layers are located at the distances of 200, 300 and 450 pc from the Sun, all at $z \approx 90$ pc from the Galactic plane. Study of A–type stars in the region resulted in the same spatial distribution

of the clouds (Kun et al. 2000).

The dust in the Cep – Cas region also seems to be disturbed. The Cepheus Bubble was discovered from the IRAS 60 μm and 100 μm maps of Cepheus Region (Kun et al., 1987). Moreover, from the 100μm ISSA images Tóth et al. 1996 and Kiss et al. 2003, in preparation have defined in the second Galactic quadrant in total 135 FIR loops. On the sky molecular clouds appear to follow many of those FIR loops, supporting the hypothesis that these loops trace dust and gas swept out by strong stellar winds and/or supernova explosions.

While a number of other star-forming regions is well studied e.g., Orion (the presumably high-mass star forming region) and Taurus (where exclusively stars of low-masses are formed) molecular cloud complex, the Cepheus region, although nearby, was ignored. However, there are indications that Cepheus is not simply a more massive and somewhat more distant sibling of the Taurus complex. Recent studies of the YSOs distribution (Kun 1998) and the ^{13}CO mapping by Yonekura et al.(1997) have provided for the first time a basis for further, more comprehensive studies.

We have selected four dark clouds for studies of physical and chemical conditions in molecular clouds possibly disturbed by shocks. Both pre-(proto)stellar and star-forming clouds/cores are included in the sample:

∘ L 1274 (Lynds 1962) is located north of the Cassiopeia cloud complex. With no visible signs of any star – formation it is regarded as a pre – stellar dark cloud. Preview maps in ^{13}CO (Sato F. 1995, priv.comm.) have suggested L 1274 to be a possible face – on shocked cloud.

∘ Kh 15 is small, non-star forming cloud in the Upper Cepheus – Cassiopeia region. In the extinction maps (Khavtassi 1960) it appears as an E–W elongated banjo-shaped feature, suggesting edge-on shock-cloud collision.

∘ L 1219 lies in the southern edge of the Cepheus molecular cloud complex. The 100 μm image indicated a 'head–tail' structure as well as presence of two cold clumps surrounding the identified embedded YSOs (Kun 1998).

∘ L 1251 is a cometary-shaped E–W directed cloud (Sato & Fukui 1989, Sato et al. 1994) with a rich on-going star formation. Kun & Prusti (1993) have found 12 H α emission line stars and 16 IRAS point sources with far infrared spectra typical of young stellar objects (YSOs). The H α emission line stars i.e., T Tauri candidate stars are located almost exclusively in the eastern part of the cloud. This suggests that star formation in this part of the cloud has been going on over a time scale much longer than in the western part of the cloud.

The structure of this monography is as follows: general overview of the interstellar medium is given in Chapter 2; Chapter 3 deals with basic molecular structure, line radiation, and molecular clouds in general; in Chapter 4 principles of star-formation are given, with an emphasis on low-mass stars; chemistry is discussed in Chapter 5, in Chapters 6–10 results of the research papers are presented.

Chapter 2
THE INTERSTELLAR MATTER

The space between the stars is not empty - there is an interstellar medium (ISM) of gas and dust in the disk of the Galaxy.[1] The ISM is observed to be highly inhomogeneous, with much of the mass concentrated in clouds - both atomic and molecular - which occupy a small fraction of the volume, with warmer intercloud gas filling the rest of the volume. Generally, the ISM is referred as to a three – phase gas that co–exists: the Hot Interstellar Medium (HIM) is very dilute gas with kinetic temperatures of about $T \approx 10^6\,\mathrm{K}$. This gas is highly ionized, with densities of typically 0.01 hydrogen atom per cm^3. The Warm Interstellar Medium (WIM) is partly ionized gas with temperatures of $T \approx 10^4\,\mathrm{K}$ and densities less or about 1 hydrogen atom per cm^3. The third phase of the ISM gas is the Cold Neutral Medium (CNM). The CNM gas has temperatures of $T \sim 1 - 100\,\mathrm{K}$ and densities that can reach up to 10^6 molecules per cm^3 (see e.g., McKee 1990, 1995 and references therein). Generally, molecular clouds are not considered as a "fourth phase" in the sense of being another state of matter in a pressure equilibrium with the rest of the ISM, since most molecular gas in the Galaxy is self–gravitating. Moreover, the clumpy molecular structure (e.g., Falgarone & Puget 1988) suggested that molecular clouds alone may be a three phase media, where dense and cold H_2 clumps are surrounded with the CNM and WIM interclump medium.

The ISM is observed to be extremely turbulent. Based on the observational data, McKee (1990) estimated the ISM turbulence pressure to be 3.6 times higher than the ISM thermal pressure. Spitzer (1978) showed that supernovae are the primary energy sources, although an exact rate of supernovae occurrence remained uncertain. In our immediate neighborhood the filling factor of hot gas is close to unity, since we reside inside the so–called Local Bubble of hot gas (see e.g., Cox & Raynolds 1987, Bystrova 1998 and other contributions in the same reference). The North Polar Spur, a most prominent radio–continuum feature of the Northern sky (e.g., Berkhuijsen et al. 1971), is a wall of the hot bubble directly adjacent to the Local Bubble. Apart from disturbing the ISM, supernova shocks might also help formation of molecular clouds. In clouds already formed, supernovae shocks may initiate or speed up process of star – formation (e.g., Elmegreen 1987).

This "classical" interpretation of the open frothy structure of the interstellar medium as an indication of stellar winds and supernovae (Brand & Zealey 1975) was

[1] General references: Beichman (1987); Dickey & Lockman (1990); Combes (1991).

challenged by recent results where the observed ISM structure is interpreted in terms of a hierarchical fractal model with clumps inside other clumps (Elmegreen 1997, Elmegreen & Falgarone 1996). Elmegreen (1997) derived the low density volume filling factor of nearly 80%, which indicates that a turbulent ISM should be mostly empty, with bulk of it's mass in a form of clouds that occupy only a small fraction of the volume.

2.1. GALAXY MOLECULAR SURVEYS

The 21–cm emission line of atomic H I, predicted by van de Hulst (1945) and first observed by Ewnen & Purcell (1951), has been a principal tool to study the ISM and its large scale distribution for two decades. The first large–scale or all–sky surveys by Muller & Westerhout (1957) and Kerr et al. (1959) were followed by the surveys of Heiles & Habing (1974) and Stark et al. (1992). The latest survey was the Leiden/Dwingeloo survey (Burton & Hartmann 1994) which is an improvement over a magnitude in kinematic coverage, sensitivity, spatial and kinematical resolution respective to any survey previously made. On the other side, molecular hydrogen, H_2, was firstly directly observed in the UV absorption lines (Carruthers 1970). Since the hydrogen molecule does not radiate in the radio spectrum, a convenient tracer was necessary. That appeared to be the CO line, first detected by Wilson et al. (1970). The 2.6 mm $J = 1 \rightarrow 0$ transition is induced by collisions with the H_2 molecule, even on low temperatures. Since the pioneering surveys (see Dame 1998 and references therein) of the selected Galactic plane areas, the high–latitude sky and of individual nearby clouds and cloud complexes, the most complete survey, with spatial resolution of $\sim 30'$, was conducted with twin 1.2-m telescopes (Cambridge, Massachusetts, USA and Cerro Tololo, Chile) in a "superbeam mode", where spatial resolution was sacrifices to larger sky coverage. The CO $J = 1 \rightarrow 0$ survey was completed by late 1980s (Dame et al. 1987). Roughly half of the ($-25° \leq b \leq +25°$) area remained unsurveyed. This survey was combined with the new, high–resolution ($\sim 7.5'$) surveys of the entire Galactic plane ($b = \pm 2 - 5°$) and surveys of all large local clouds at higher latitudes, into a "composite CO survey" of the Galaxy (Dame et al. 2001). Based on an existing cross–correlation of the CO and the H I column density derived from the Leiden–Dwingeloo 21 cm survey (Burton & Hartmann 1994), Dame at al. argued that the CO survey was nearly a complete. The CO column density was derived from the IR 100 μm emission of the new reprocessed composite of the DIRBE and the IRAS all – sky maps by Schlegel et al. (1998). Parts of the Galaxy were surveyed with much better resolution (e.g., Lebrun 1986, Clemens et al. 1986 etc.).

Currently, two new Galactic plane surveys are ongoing: University of Tokio's twin telescopes with 60 cm apertures that operate in Japan and ESO in Chile and are surveying the Galaxy at the CO (2–1) line, thus having the same spatial resolution as the CO (1–0) survey (Hasegawa 1997); Nagoya University uses two 4 m telescopes in Japan and Las Campanas Observatory in Chile to make the ^{13}CO (1–0) survey with HPBW of $2.'7$ (Fukui & Yonekura 1997).

The large scale CO emission is widely different from the H I distribution: H_2 molecules, and consequently CO, dominate the central ISM, while the atomic H I gas

is much more important in the outer parts of the Galaxy. To determine an H_2/CO conversion ratio is not easy. The main problem are high optical depths of the ^{12}CO lines (even higher transitions may be optically thick). Because of the high optical depths of the main isotopomer–CO line, rarer CO isotopomers, ^{13}CO and eventually C^{18}O, were used in order to determine the H_2/CO conversion ratio (Dickman 1978, Frerking et al. 1982, Cernicharo & Guélin 1987). Linear relationships, albeit with a large scatter, were found between the ^{13}CO and the C^{18}O column densities and the hydrogen column density. The large scatter implies that there might not be only one, 'universal', conversion factor, i.e., that the CO/H_2 ratio varies from molecular cloud to molecular cloud (even within a sigle cloud). Another possibility is that a combination of multiple factors e.g., line saturation, various levels of subthermal excitation temperatures averaged out in the observing beam, etc., resulted in the scatter. The rarer isotopomers might be used with more confidence if the ^{12}CO/^{13}CO abundance ratio is constant and universal. Unfortunately, it is not. The ratio depends mainly on a star-formation history and amount of an exposure to the UV radiation field, where ^{13}CO can be much enriched by fractionization. On a large scale, for the Galaxy, the conversion factor derived from CO (1–0) and H I maps has a mean value of $(1.8 \pm 0.3) \times 10^{20}\,\mathrm{cm^{-2}\,K^{-1}\,s}$ (Dame et al. 2001) and shows little systematic variation with the Galactic latitude. Based on a study of a diffuse, high–energy γ–ray emission Strong & Mattox (1996) have estimated the overall Galaxy conversion factor to be $(1.9 \pm 0.2) \times 10^{20}\,\mathrm{cm^{-2}\,K^{-1}\,s}$. For the Cepheus region in particular Digel et al. (1996) have found significatly lower value - $(0.9 \pm 0.14) \times 10^{20}\,\mathrm{cm^{-2}\,K^{-1}\,s}$.

Chapter 3
MOLECULES AND MOLECULAR CLOUDS

3.1. BASIC MOLECULAR STRUCTURE AND RADIATION

Compared to atoms, molecules have a complicated structure. Thus, the Schrödinger equation of the system is correspondingly complex, involving positions and motions of both the nuclei and the electrons[2]. However, due to nuclei large masses we can neglect parts of Hamiltonian operator that describe the kinetic energy of a nuclei. This separation between nuclear and electronic motions is so–called Born – Oppenheimer approximation. Accordingly, transitions in a molecule can be separated as for energies involved:

$$W^{\rm total} = W^{\rm el} + W^{\rm nuclei} \equiv W^{\rm el} + W^{\rm vib} + W^{\rm rot}, \tag{3.1}$$

where $W^{\rm el}$ is the energy of the electrons, typically of a few eV - in such transitions lines are in the visual or UV regions of the spectrum; $W^{\rm vib}$ is the vibrational energy of the nuclei, with typical energies in the range of $0.1 - 0.01\,{\rm eV}$, these transitions correspond to lines in the infrared region of the spectrum and $W^{\rm rot}$ is the rotational energy of the nuclei, with typical value of $\cong 10^{-3}\,{\rm eV}$. These rotational transitions, caused by the rotation of the nuclei, have lines in the *cm* and *mm* wavelength range — the region of interest in the *mm*-radio astronomy. Only sometimes transitions between different vibrational levels are involved, e.g., rotational transitions between vibrationally excited states of HC_3N (Wyrowski et al. 1999), SiO (Mollaaghababa et al. 1991), SiC_2 (Gensheimer & Snyder 1997) and more "exotic" molecules CH_3CN (Olmi et al. 1996) and C_2H_3CN (Nummelin & Bergman 1999). Occasionally, differences in the geometrical arrangement of the nuclei result in a doubling of the energy levels, such is the case of inversion doubling of ammonia (e.g., Wilson et al. 1993).

3.1.1. ROTATIONAL SPECTRA OF DIATOMIC MOLECULES AND LINEAR POLYATOMIC MOLECULES

The solution of the Schrödinger equation for a diatomic slightly elastic molecule results in the eigenvalues for the rotational energy:

$$E_{\rm rot} = W(J) = \frac{\hbar^2}{2\,\Theta_e}\,J(J+1) - h\,D\,[J(J+1)]^2, \tag{3.2}$$

[2]General references used in this chapter are Rohlfs & Wilson 1996 and Townes & Schawlow 1975.

where $\Theta_e = m\, r_e^2$ is the moment of inertia (m is the reduced mass, and r_e is the equilibrium distance between two nuclei), D is the centrifugal stretching constant and $J = 0, 1, 2, ...$ is the quantum number of angular momentum. If we introduce the rotational constant

$$B_e = \frac{\hbar}{4\,\pi\,\Theta_e}, \tag{3.3}$$

the pure rotational spectrum for electric dipole transitions $\Delta J = \pm 1$ is given by:

$$\nu(J) = \frac{1}{h}\,[W(J+1) - W(J)] = 2\,B_e\,(J+1) - 4\,D\,(J+1)^3. \tag{3.4}$$

Typically, $D \approx 10^{-5}$ of the magnitude of B_e, so for low J rotational transitions of a molecule can be approximated by rotational transitions of a rigid rotor. However, even in a ground vibrational state there is still a zero point vibration, and B_e should be substituted by $B_0 = B_e - \alpha_e\left(v + \frac{1}{2}\right)$, where $v = 0, 1, 2...$ is the vibrational quantum number and α_e is the change in the B_e equilibrium value due to excitation of the vibration. The change is usually $< 10^{-2}\,B_e$ (see Townes & Schawlow 1975 for details).

Dipole radiative transitions will occur between different rotational states only if the molecule possesses a permanent dipole moment. Homonuclear diatomic molecules like H_2, O_2 or N_2 will not produce such lines. In quantum mechanics, dipole radiative transitions occur with a change in the angular momentum quantum number by one, $\Delta J = \pm 1$, and the parity of the initial and final states must be opposite.

Compared to the spectrum of a diatomic molecule, the spectrum of a linear polyatomic molecule is more complex, mostly due to different possible modes of vibration. If degenerate modes (i.e., modes which have the same frequency and the same value of α_i) of vibration of a linear molecule are counted as a single vibration, then the rotational constant, B_0, is

$$B_0 = B_e - \sum_i\, \alpha_i\, \left(v_i + \frac{d_i}{2}\right), \tag{3.5}$$

where d_i is the degree of the degeneracy. If we consider triatomic molecule, a simplest and most common polyatomic molecule, any arbitrary relative vibration of the atoms in the molecule can be described as a sum of four types of normal modes of vibrations, two of which are degenerate. The rotational constant would then be $B_0 = B_e - \alpha_1\left(v_1 + \frac{1}{2}\right) - \alpha_2(v_2+1) - \alpha_3\left(v_3 + \frac{1}{2}\right)$. Bending or perpendicular modes of oscillation in a linear polyatomic molecule introduce a new phenomenon, so-called l–type doubling. If a molecule is not rotating then it may bend in two perpendicular planes, with exactly the same frequencies of oscillation (these are the two degenerate modes). However, if a molecule is rotating, then bending in two planes would not be equivalent, the effective moments of inertia about the axis of rotation being different. After a proper quantum mechanical treatment, rotational frequencies of such a molecule would be:

$$\nu(J) = 2\,B_0\,(J+1) - 4\,D\,(J+1)[(J+1)^2 - l^2], \tag{3.6}$$

where the angular momentum has values $l = v, v-2, v-4, ..., -v$. A degeneracy between $+l$ and $-l$ is indicated here, and when l–type doubling is fully included, the rotational frequency for e.g., $|l| = 1$, becomes:

$$\nu(J) = [\, 2\, B_0 \pm \frac{q_l}{2}\, (v_2 + 1)\, J\,]\, (J+1) - 4\, D\, (J+1)[(J+1)^2 - l^2], \tag{3.7}$$

where v_2 is the quantum number of degenerate vibration, and q_l is the l–type doubling constant (for details see Townes & Schawlow 1975).

Examples of the interstellar linear polyatomic molecules are OCS (carbonyl sulfide), HCN (hydrogen cyanide), HNC (hydrogen isocyanide), N_2O (nitrous oxide), HC_3N (isocyanoacetylene).

3.1.2. SYMMETRIC–TOP AND ASYMMETRIC–TOP MOLECULES

The moment of inertia of a molecule may be represented by an ellipsoid which has a fixed orientation in space and whose center coincides with the center of mass of the molecule. If the coordinate system is oriented so that x, y and z are along the principal axes of the ellipsoid of inertia, then

$$\frac{x^2}{\Theta_x^2} + \frac{y^2}{\Theta_y^2} + \frac{z^2}{\Theta_z^2} = 1, \tag{3.8}$$

where Θ_x, Θ_y and Θ_z are the moments of inertia along the directions of the principal axes. If $\Theta_x \neq \Theta_y \neq \Theta_z$ the molecule is called an asymmetric rotor or asymmetric–top, and the principal moments of inertia are denoted $\Theta_{\rm A}$, $\Theta_{\rm B}$ and $\Theta_{\rm C}$ in increasing order of size. If $\Theta_{\rm A} = \Theta_{\rm B}$ or $\Theta_{\rm B} = \Theta_{\rm C}$ the molecule is a symmetric–top (a linear polyatomic molecule is a special case of a symmetric–top molecule). If all $\Theta_{\rm A} = \Theta_{\rm B} = \Theta_{\rm C}$ the molecule is a spherical top.

If we define rotational constants as

$$A = \frac{\hbar}{2\,\Theta_{\rm A}} \qquad B = \frac{\hbar}{2\,\Theta_{\rm B}} \qquad C = \frac{\hbar}{2\,\Theta_{\rm C}}, \tag{3.9}$$

then for a symmetric–top ($\Theta_{\rm A} = \Theta_{\rm B}$) the quantum solution (in a rigid–body approximation) for rotational energy levels is:

$$W(J,K)/h = B\, J\, (J+1) + (C-B)\, K^2, \tag{3.10}$$

where $J = 0, 1, 2, ...$ is the quantum number of total moment of inertia, $K = 0, \pm 1, \pm 2, ...$ $\pm\, J$ is the quantum number of the z–projection of the moment of inertia (assuming rotation around z axis). The levels with $K > 0$ are doubly degenerate. Note that for a spherical–top the energy level depends only on the total angular momentum. The selection rules for dipole radiation of symmetric–top molecules are $\Delta J = \pm 1$ and $\Delta K = 0$.

If we include centrifugal effects, the frequency due to a rotational transition becomes

$$\nu = 2\, (J+1)\, (B - D_{JK}\, K^2) - 4\, D_J\, (J+1)^3, \tag{3.11}$$

where B is previously defined rotational constant, and D_{JK}, D_J are the centrifugal distortion constants (Townes & Shawlow 1975). The $\Delta K = 0$ selection rule is valid for the case of dipole transitions; however octopole transitions are possible and would require $\Delta K = \pm 3$. Since such transitions are very slow, there is a high probability that meanwhile collisions will cause an exchange of population between different K–ladders (Rohlfs & Wilson 1996).

As for asymmetric–top molecules there is no generally useful model for the quantum mechanical case, neither is the classic treatment simple. Various parameters may be used to indicate the degree of asymmetry, e.g., so–called Ray's asymmetry parameter is defined as $\kappa = \frac{2B-A-C}{A-C}$, and has values $-1 < \kappa < +1$. For a prolate symmetric–top, i.e., for $B = C$, $\kappa = -1$; for an oblate symmetric–top, i.e., if $B = A$, $\kappa = +1$. In case of "a slightly asymmetric" prolate– or oblate–top an approximative formula for rotational energy levels is easy to obtain. But in general, each molecule must be treated as a particular case with specific amount of asymmetry. Several approximate methods have been developed and short description of each and it is applicability are given in Townes & Shawlow (1975). In the microwave region of spectra centrifugal distortion is far more important in asymmetric rotors then in symmetric–tops. For some light molecules centrifugal distortion can shift the observed microwave lines significantly.

Examples of the interstellar symmetric–top molecules are: NH_3 (ammonia), CH_3CN (methylcyanide), CH_3NC (methylisocyanide), CH_3C_2H (methylacetylene); and for asymmetric–tops: SO_2 (sulfur dioxide), H_2O (water), HN_3, H_2S (hydrogen sulfide), O_3 (ozone).

3.2. MOLECULAR CLOUDS

3.2.1. ATOMS AND MOLECULES IN THE ISM TRACED BY RADIATION AT RADIO FREQUENCIES

At radio wavelengths spectral line radiation has been detected only from a few atomic species. If we set the upper limit of radio frequencies at 1 THz, then the following atoms (neutral and ions) have fine and hyperfine transitions that emit radiation in the radio spectrum: H I (the transition between hyperfine structure levels $^2S_{1/2}, F = 1-0$ emits radiation at $\lambda = 21$ cm), D I (the deuterium analog $^2S_{1/2}, F = 3/2 - 1/2$ hyperfine transition; detected only at a 4σ level Chengalur et al. 1997), $^3He^+$ (spin–flip transition Bell 2000 and references therein) and C I (the $^3P_1 - ^3P_0$ and the $^3P_2 - ^3P_1$ transitions, see van der Veen et al. 1998, Gerin et al. 1998 and references therein).

When an ionized atom recombines at some level with the principal quantum number $n > 1$, the atom will produce recombination line emission on cascading down to the ground state. Lines corresponding to the transition $n + 1 \rightarrow n$ are most intense and are called α lines; for $n + 2 \rightarrow n$ transitions we talk about β lines; for $n + 3 \rightarrow n$ transitions about γ lines etc. In the radio spectrum, recombination lines with high principal numbers of H, He, C and S atoms were observed. Such are the C 575 α, 225 α and 205 α lines at 34.5, 560 and 770 MHz respectively (Kantharia et al. 1998a); the H 270–273 α lines at 327 MHz (Roshi & Anantharamaiah 2000); at 1.4 GHz the

Table 3.1: The 123 reported interstellar, including comets, and circumstellar molecules as for April, 2002. (`http://www.cv.nrao.edu/ awootten/allmols.html`).

diatomic	triatomic	four atoms	five atoms	six atoms	seven atoms
H_2	† C_3	c-C_3H	C_5	C_5H	C_6H
AlF	C_2H	l-C_3H	C_4H	l-H_2C_4	CH_2CHCN
AlCl	C_2O	C_3N	C_4Si	C_2H_4	CH_3C_2H
† C_2	C_2S	C_3O	l-C_3H_2	† CH_3CN	HC_5N
CH	CH_2	C_3S	c-C_3H_2	CH_3NC	$HCOCH_3$
CH^+	† HCN	† C_2H_2	CH_2CN	† CH_3OH	NH_2CH_3
† CN	HCO	CH_2D^+ ?	† CH_4	CH_3SH	c-C_2H_4O
† CO	† HCO^+	HCCN	† HC_3N	HC_3NH^+	CH_2CHOH
† CO^+	HCS^+	$HCNH^+$	HC_2NC	HC_2CHO	
CP	HOC^+	† HNCO	† HCOOH	† NH_2CHO	
CSi	† H_2O	HNCS	H_2CHN	C_5N	
HCl	† H_2S	$HOCO^+$	H_2C_2O		
KCl	† HNC	† H_2CO	H_2NCN		
NH	HNO	H_2CN	HNC_3		
NO	MgCN	† H_2CS	SiH_4		
NS	MgNC	† H_3O^+	H_2COH^+		
NaCl	N_2H^+	† NH_3			
† OH	N_2O	SiC_3			
PN	NaCN				
† SO	† OCS				
SO^+	† SO_2				
SiN	c-SiC_2				
SiO	CO_2				
SiS	NH_2				
† CS	H_3^+				
HF	SiCN				
SH	AlNC				
FeO(?)					

eight atoms	nine atoms	ten atoms	eleven atoms	thirteen atoms
CH_3C_3N	CH_3C_4H	CH_3C_5N ?	HC_9N	$HC_{11}N$
† $HCOOCH_3$	CH_3CH_2CN	$(CH_3)_2CO$		
CH_3COOH(?)	$(CH_3)_2O$	NH_2CH_2COOH ?		
C_7H	CH_3CH_2OH			
H_2C_6	HC_7N			
CH_2OHCHO	C_8H			

† Molecules that have also been found in Comet 1995 O1 Hale–Bopp.

? Tentative detections.

168 α lines of H, C and S (Kantharia et al. 1998b); at $\sim$ 4.5 GHz the H 92 α, 110 α and 166 α lines, and the He 92 α line at $\sim$ 8 GHz (Garay et al. 1998).

Observationally, the molecular ISM in the Galaxy (hence, not including comets) was detected in late 1930s, when the methylidine radical, CH, was found in absorption towards bright stars (Dunham & Adams 1937, Dunham 1937, Swings & Rosenfeld 1937). Few years later, another molecule, cyanide radical, CN, was detected in absorption towards ζ Oph (Sanford 1940). Detections of CH^+ in spectra of some carbon stars, the detected molecular radiation coming from the envelopes of those stars, followed shortly afterwards (Douglas & Herzberg 1941, Keenan 1942). However, how

widespread molecular gas is was only realized in mid–1960s, after a chain of new molecules detections. Weinreb et al. (1963) detected at λ=18 cm OH lines in absorption towards the Cas A SNR. That was the first detection of an interstellar maser line. During first few years of molecular line radio spectroscopy only 2–atomic molecules were detected, what was thought to be a natural limit due to the low densities in the ISM. Ammonia, NH_3, is the first larger molecule detected in the ISM (Cheung et al. 1969). As it turned later to be, the most important trace molecule in the ISM, carbon monoxide, CO, was detected in SNRs (Scoville et al. 1977), Sharpless H II regions (Kazes et al. 1977) and towards Galactic center (Bania 1977) in mid– 1970s. After these detections the number of newly detected molecules steadily increased. Today, more then 120 different molecules are detected in the ISM (see Table 3.1), 92 of them are considered to be organic, i.e., have a C–atom as one of the constituents. The largest detected molecule has 13 atoms, but it is probably not the upper limit of the ISM molecules size. Some detected molecules are commonly found on Earth, others, such as OH, CN, CO^+, CH^+, HCO^+, N_2H^+, are chemically unstable and under laboratory conditions quickly combine to form more chemically stable species. It turned out that formation of even diatomic molecules in the Space requires chemistry much different from that one on the Earth. Variety of different conditions in the ISM provide a clue when searching for new molecules in the ISM: only some molecules and some transitions can be seen in certain regions, thus limiting possibilities for confusing new transitions of already known molecules and a radiation from a new molecule. An example of such a search is given in Figure 1 which shows a 2–GHz span of the OSO–20 m deep spectral scan (Kalenskii et al. 2003, in prep.) towards two well known Galactic H II regions.

3.2.2. GAS CONTENT OF MOLECULAR CLOUDS

The ISM is not homogeneously distributed in the Galaxy, but organized in clouds (atomic or molecular) which are embedded in the intercloud medium. Molecular clouds consist mainly from molecules, $\geq$98% of their mass is in form of H_2 and $\leq$1% mass is contributed by numerous 'trace' molecules. The remaining $\approx$1% of the cloud's mass is dust. However, molecular clouds can have "envelopes" with relative large abundances of atomic hydrogen and carbon (e.g., Wannier et al. 1983, Tielens & Hollenbach 1985). This is to say that the molecules in the outer parts of a cloud exposed to the InterStellar Radiation Field (ISRF) and/or strong ambient UV radiation can easily be destroyed. Regions where most of the molecular content is destroyed are called photodissociation regions or more precisely, photon–dominated regions (PDRs; general reference for PDRs is e.g., Hollenbach & Tielens 1997). Moreover, since the evidence of a clumpy structure of molecular clouds is increasing (e.g., Falgarone et al. 1991, Falgarone & Philips 1996, Juvela 1997, Stutzki et al. 1998, Goodman et al. 1998) probably even the interiors of molecular clouds have appreciable percentage of atomic hydrogen and carbon. Recent detection of C^+ from deep inside the NGC 6334 molecular cloud (Boreiko & Betz 1995) proves existence of ionized and neutral "interclump" medium. Generally accepted ratio of neutral carbon relative to carbon monoxide in molecular clouds is [C I]/[CO] $\cong$ 0.1 (Goldsmith 1987).

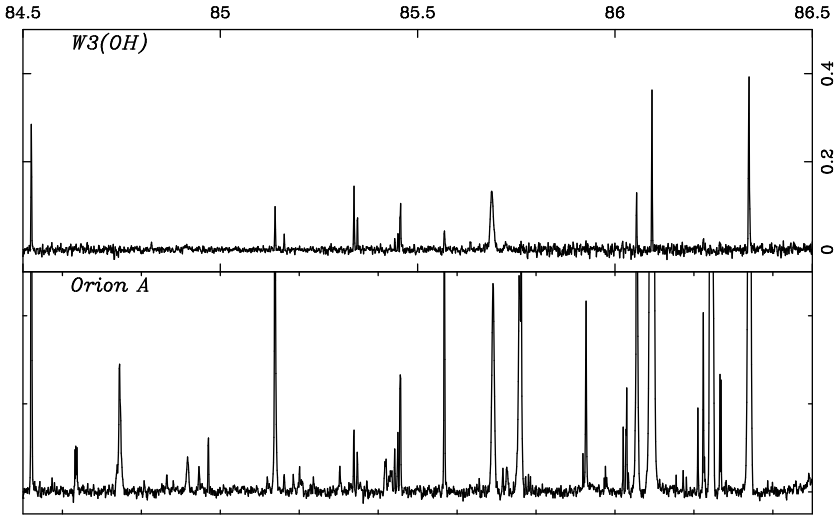

Figure 3.1: The 85.5–86.5 GHz wide deep spectral scan of the W 3 OH and Orion A region from Kalenskii et al., 2003, in prep., (courtesy the authors). The x– and the y–axes are the observed frequency, in GHz, and the antenna temperature, in K, respectively. The T_A^* scale is cut–of at 0.5 K. W 3 OH ($\ell = 133^\circ.95$, $b = +1^\circ.06$) is probably the most studied ultracompact H II region in our Galaxy. It has a powerful OH and CH_3OH maser emission, the central ionizing star being massive ($\approx 30\,M_\odot$) O9–O7 star and is about 2.2 kpc away. Orion A (or Orion KL, or Sharpless 2–281; $\ell = 209^\circ$, $b = -19^\circ.4$) is an H II region at the surface of the Orion A (the 'Ridge') cloud of the Orion giant molecular cloud complex, the nearest (≈ 450 pc) high – mass star forming region. Note different densities and spectral lines intensities in spite of the similar nature of the sources.

Molecular clouds can be either self–gravitating or pressure confined structures. Morphologically, molecular clouds can be divided in three categories with different masses, densities and average kinetic temperatures of the gas. Translucent/diffuse clouds are pressure confined. Typical gas kinetic temperatures in these filamentary structures are 30–50 K and average total gas densities are $n(\mathrm{H}) + 2\,n(\mathrm{H_2}) \approx 10^2 - 10^3\,\mathrm{cm^{-3}}$. Translucent clouds have masses up to $10^2\,M_\odot$ and sizes 0.5–5 pc. The remaining two categories of molecular clouds are fully or at least partly gravitationally bound. Dark clouds contain cold, dense gas with kinetic temperatures and densities typically about $T_{\mathrm{kin}} \sim 10$ K and $n(\mathrm{H_2}) \approx 10^{3-7}\,\mathrm{cm^{-3}}$, respectively. An average dark cloud masses and sizes are $10^2 - 10^3\,M_\odot$ and ≈ 10 pc, respectively. Finally, a goup of their own, Giant Molecular Clouds (GMCs, sometimes also referred to as giant molecular cloud complexes) have, on average, warmer gas than dark clouds do - typically about $T_{\mathrm{kin}} \sim 20 - 50$ K. GMCs gas number densities are, on the other side, similar to those of dark clouds. Linear extents of GMCs can be as much as ≥ 100 pc, thus a GMC may contain mass of up to $10^6\,M_\odot$. Molecular clouds are sites of star formation: low – mass stars are formed predominantly in dark clouds, while GMCs

give birth also to high – mass stars.

How are molecular clouds formed and how they survive up to 10^7 years or more, is not yet completely clear. They may be formed by shock compression of ambient gas, by agglomeration of smaller clouds or by spontaneous instabilities in the ambient medium (Elmegreen 1987). Thermal instability inside the shock – compressed layer produces a geometrically thin, dense layer which will further fragment into small molecular clouds (Koyama & Inutsuka 2000). Thermal instabilities in diffuse molecular clouds may trigger formation of molecular clouds of the dark clouds type (Grazziani & Black 1987). Gravitational instabilities occur continuously in the ambient medium in a galactic disk with rotation, shear and azimuthal magnetic field, with the rates enhanced in spiral density – wave crests and swept – up shells (Elmegreen 1989, 1987a). When one has two distinct fluids in pressure equilibrium across a common interface, Rayleigh-Taylor (when a heavy fluid rests on top of light fluid, due to gravitational acceleration perpendicular to the interface) and Kelvin-Helmholtz instability (due to a relative motion of the two fluids) may play a role in a weak magnetic fields areas (e.g. Hartquist & Dyson 1987, Hunter & Whitaker 1989, Hunter et al. 1997, Fleck 1989). In an ISM comprised of thermal gas, magnetic field and cosmic rays, confined to a thin layer by the vertical gravity of the Galaxy, Parker-Jeans instability (to some extent analog to the hydrodynamical Rayleigh-Taylor instability, but with certain unique features due to the freezing of the magnetic field lines) plays a significant role. In a skewed (i.e. the field line direction is a function of the height) magnetic fields the Parker instability preferentially forms large-scale structures like giant molecular clouds (Hanawa et al. 1992, Elmegreen 1982); also molecular clouds with coherent filamentary structure may be attributed to the Parker-Jeans instability of gaseous disk under the influence of rotation (Chou et al. 2000).

Magnetic field plays an important role in the further life of a molecular cloud: it may give support to stabilize the cloud through the magnetic field pressure (e.g. Boss 1997, Lizano 1989, Langer 1978) or fluctuating transverse fields (Gammie & Ostriker 1996). On the other side, it is also another source of turbulent energy which can be released through an instability driven by ambipolar diffusion (Zweibel 1998). A cloud may also be destroyed by the excess turbulent internal motions (e.g. Bonazzola et al. 1987, Fleck 1980).

Dark molecular clouds which are not restricted to the spiral arms probably survive one or more rotation periods of the Galaxy, thus having lifetimes of $\geq 10^8$ years. Giant molecular clouds are probably assembled and dispersed as they cross the spiral arms on a time – scale of $\sim 10^7$ years (e.g., Bash & Peters 1976).

3.2.3. DUST IN MOLECULAR CLOUDS

Although dust abundance in molecular clouds is only 10^{-12} by number relative to hydrogen, what is $\sim$1% by mass, it is essential for many physical and chemical processes. Foremost, the most important route for the hydrogen molecule formation is the association of hydrogen atoms on the dust surfaces i.e., $H+H \rightarrow H_2$ (see e.g., van Dishoeck & Black 1988). Dust particles catalyze some important part of chemistry. They accrete molecules from gas to form ices, probably being responsible for the observed significant CO depletion in molecular clouds (Caselli et al. 1999, Kramer

et al. 1999). Dust particles also act as a shield against the UV starlight, protecting from destruction molecules for which self–shielding doesn't operate (as it does for H_2 and CO). Furthermore, the dust grains can carry a substantial fraction of the charge, thus having influence on magnetic fields in the clouds as general (see e.g., Ciolek & Mouschovias 1993) and on the structure of C–type shocks propagating through a molecular cloud (Wardle 1998). They are also responsible for absorption, scattering and polarization of star light. The latter process can be used to measure magnetic fields by multiwavelength submillimeter or IR polarization measurements, to differentiate between the emission in warm and cool dust components (Schleuning et al. 2000, Coppin et al. 2000, Matthews & Wilson 2000). And finally, it has been shown that the upper mass limit of newly formed stars is directly related to the presence of solid particles (Yorke et al. 1993, 1995). Thermal continuum emission from dust grains at IR and submm/mm wavelengths is excellent tracer of cold protostars, circumstellar disks and envelopes around young stellar objects (see Chapter 5.3).

The molecular clouds dust population is a multi–component system, containing grains of different chemical composition and structure, usually assumed to have graphite or silicate cores. In the dense regions of molecular clouds, adsorption of gas phase species and surface chemistry leads to the formation of ice mantles, usually composed of water, methanol, carbon oxide and carbon dioxide (H_2O, CH_3OH, CO and CO_2) and some other simple molecules, with impurities. Current grain models usually are three–component; in order to explain both the IR emission in diffuse H I clouds and the interstellar extinction curve Désert et al. (1990) proposed the following dust composition: PAHs (Polycyclic Aromatic Hydrocarbons), very small grains (VSGs, with diameter of a dust particle $\leq 10\,\mathrm{nm}$) and large grains (graphite or silicate, still with the diameter $\leq 1\,\mu\mathrm{m}$; traditional dust component historically inferred from optical studies).

3.2.4. HEATING AND COOLING OF GAS

The physics of the molecular gas in a cloud is characterized by its kinetic temperature, density, ionization degree, velocity field, total mass and cloud size.

The temperature is controlled by the balance between various heating and cooling processes. Heating is provided by collisions with dust grains, atoms, ions and electrons. The electrons are either released from dust grains by the photoelectric effect or are created by the cosmic ray ionization of hydrogen, other molecules or atoms. The hydrogen cosmic ray ionization is a prime source of new electrons, and this production is persistant at a rate of $10^{-16}\,\mathrm{s}^{-1}$. Such electrons can have an excess kinetic energy which they may transfer to the gas by collisions. Further heating can be provided by energy released in chemical reactions or by collisional de-excitation of H_2. The drag between ions and neutrals due to a magnetic field is another source of additional heat. When present, turbulent motions in the gas can release heat through the dissipation of turbulence. Shocks also depose energy, as does a shearing due to the differential rotation etc. Cooling is mainly due to radiation from molecules, ions, atoms and dust; but other processes may contribute, such as e.g., adiabatic expansion.

Ionization degree, i.e., magnetic field contributes to the heating of the gas via electron-gas particles collisions, and to the cooling, by excitation of trace molecules.

Magnetic fields also act as a support of the cloud against gravitational collapse (collisions between charged particles, tied to the magnetic field, and neutral particles, give rise to a frictional force).

The cloud size and density distribution and the total mass of the cloud are determined by the competition between 'confining' and 'dispersing' forces, such as self-gravitation, internal and external gas and radiative (UV, $\lambda > 91.2\,\mathrm{nm}$) pressure, coupling to magnetic fields, tidal forces, shocks from expanding star envelopes, supernovae, etc.

3.2.5. PROBES OF PHYSICAL CONDITIONS

The UV radiation needed to excite H_2 emission does not penetrate bulk of the cloud. There are some special cases, however: in shocked regions H_2 emits rovibrational lines that are useful for the kinetic temperature and the velocity field probe (e.g., Draine & McKee 1993); some vibrational transitions were seen in absorption in the near-infrared (NIR) in only a few molecular clouds (Lacy et al. 1994). Gamma rays do probe all the material in molecular clouds (e.g., Strong et al. 1994), but so far these studies suffer from low spatial resolution and uncertainties in the cosmic ray flux determination and were mostly used for large scales studies.

Essentially, all probes of physical conditions in molecular clouds rely on the trace constituents, dust and molecules other than H_2. Dust particles attenuate light at short wavelengths (UV to NIR) and emit at longer wavelengths (far infrared (FIR) to millimeter). Assuming that the ratio of dust extinction at a given wavelength to the gas column density is constant, one can use optical extinction to map the gas column density in molecular clouds. Through catalogs and atlasses of Barnard (1927), Bok & Reilly (1947) and Khavtassi (1955) molecular clouds were mapped in that way long before it was known that they contain any molecules. Palomar Observatory Sky Survey (POSS) photo – plates and prints were used to make Lynds (1962), Clemens & Barvainis (1988) and Blitz et al. (1984) catalogs of dark clouds, small clouds (i.e., globules) and high – latitude clouds, respectively. More recently, NIR surveys are used to probe the densest parts of molecular clouds: the $H - K$ color excess can trace the gas column density up to an equivalent visual extinction of $\sim$30 mag (Lada et al. 1994, Alves et al. 1998). Continuum emission from dust at long wavelengths can trace large column densities and thus provide an independent mass estimate. It is well established that the dust opacity decreases with increasing wavelength as $\kappa(\lambda) \propto \lambda^{-\beta}$, with $\beta \sim 1 - 2$ (Hildebrand 1983).

However, since the discovery of interstellar molecules, rotational transitions at the millimeter or the submillimeter wavelengths are used as a prime probe for molecular gas properties. The most abundant molecule after H_2, carbon monoxide ($^{12}C^{16}O$, the main isotopomer, usually is written only as CO) is also the most common tracer of molecular gas. In a region of a high gas column density, N, CO fails to trace the column density and progressively rarer isotopomers are used to trace progressively higher values of N. Recent studies of some particularly opaque regions indicate severe depletion of all isotopomers of CO onto dust grains (Kuiper et al. 1996, Bergin & Langer 1997, Caselli et al. 1999). Alves et al. (1999) found that $C^{18}O$ can trace column density only up to $A_V = 10$.

Sizes of clouds, characterized by a radius, are measured by mapping the cloud in a particular tracer. The size along the line of sight (depth) can be in most cases only constrained by making geometrical assumptions (e.g. spherical or cylindrical cloud). So far, only one possible probe of the cloud's depth is the H_3^+ molecule, which has a calculable, constant density in molecular clouds. Thus, a measurement of $N(H_3^+)$ yields a measure of cloud depth (Geballe & Oka 1996).

The mass of a cloud could be estimated if we know it's size and the hydrogen column density, by integrating the column density N over an area a:

$$M_N = \int N \, da. \tag{3.12}$$

Another possibility to asses a cloud's mass is to estimate so-called virial mass (e.g., Johansson et al. 1998)

$$M_V = 150 \, d \, \Delta v^2 \ \mathrm{M}_\odot, \tag{3.13}$$

where d is the diameter of the cloud in [pc], Δv is the line width at half maximum in [$\mathrm{km\,s^{-1}}$]. Finally, the mass of a cloud can also be estimated from integrating the CO emission over the cloud and using an empirical relation between mass and the CO luminosity, $L(\mathrm{CO})$.

Density (n) and gas kinetic temperature (T_K) are both measured by determining the population in molecular energy levels and comparing the results to calculation of molecular excitation. In general, collision and radiative processes compete to establish level populations. For some levels in some molecules, radiative rates are unusually low, collisions dominate, $T_{ex} = T_K$, and observational determination of these "thermalized" level populations yield T_K. Unthermalized level populations depend both on the density and the kinetic temperature, and with a knowledge of T_K one can use observational determination of these populations yield n. However, the observations themselves always involve some average over the finite beam and along the line of sight, consequently to interpret the observations a model of the cloud is needed. Tracers of temperature are CO, and molecules in which transitions between certain levels are forbidden by selection rules e.g., different K ladders of symmetric tops like NH_3, CH_3CN, CH_3CCH etc. (Ho & Townes 1983, Loren & Mundy 1984, Kuiper et al. 1984) or different K_{-1} ladders in H_2CO (Mangum & Wootten 1993). To determine the density, observations of several transitions that are not in the local thermodynamic equilibrium (LTE) are needed. Then the ratio of populations, or equivalently T_{ex}, can be used to constrain the density. Often a detection of a particular transition is taken to imply that a density is larger then the critical density for the particular transition. In general, the excitation technique measures the total density of collision partners, $n \simeq n(H_2) + n(He)$. Table 3.2 adopted from Evans (1999) gives for some commonly observed lines the transition involved, the frequency of the transition, the energy above the effective ground state, the critical densities, n_c, at $T_K = 10\,\mathrm{K}$ and $T_K = 100\,\mathrm{K}$, and for comparison, n_{eff}, the density needed to produce a line of $1\,\mathrm{K}$ calculated with the large velocity gradient (LVG) code. However in opaque regions, trapping of line photons enhance the effect of collisions, so to obtain n we need at least two transitions with different critical densities $n_c(jk)$ to be able to determine the line optical depth.

Table 3.2: Molecules Probing Densities[1]

Molecule	Transition	ν GHz	E_{up} K	$n_c(10\,\mathrm{K})$ cm^{-3}	$n^2_{\rm eff}(10\,\mathrm{K})$ cm^{-3}	$n_c(100\,\mathrm{K})$ cm^{-3}	$n_{\rm eff}(100\,\mathrm{K})$ cm^{-3}
CS	J=1→0	48.9909780	2.4	4.6×10^4	7.0×10^3	6.2×10^4	2.2×10^3
CS	J=2→1	97.9809500	7.1	$3.0\ 10^5$	$1.8\ 10^4$	$3.9\ 10^5$	$4.1\ 10^3$
CS	J=3→2	146.9690330	14	$1.3\ 10^6$	$7.0\ 10^4$	$1.4\ 10^6$	$1.0\ 10^4$
CS	J=5→4	244.9356435	35	$8.8\ 10^6$	$2.2\ 10^6$	$6.9\ 10^6$	$6.0\ 10^4$
CS	J=7→6	342.8830000	66	$2.8\ 10^7$	...	$2.0\ 10^7$	$2.6\ 10^5$
CS	J=10→9	489.7510400	129	$1.2\ 10^8$	...	$6.2\ 10^7$	$1.7\ 10^6$
HCO^+	J=1→0	89.1885280	4.3	$1.7\ 10^5$	$2.4\ 10^3$	$1.9\ 10^5$	$5.6\ 10^2$
HCO^+	J=3→2	267.5576190	26	$4.2\ 10^6$	$6.3\ 10^4$	$3.3\ 10^6$	$3.6\ 10^3$
HCO^+	J=4→3	356.7342880	43	$9.7\ 10^6$	$5.0\ 10^5$	$7.8\ 10^6$	$1.0\ 10^4$
HCN	J=1→0	88.6318473	4.3	$2.6\ 10^6$	$2.9\ 10^4$	$4.5\ 10^6$	$5.1\ 10^3$
HCN	J=3→2	265.8861800	26	$7.8\ 10^7$	$7.0\ 10^5$	$6.8\ 10^7$	$3.6\ 10^4$
HCN	J=4→3	354.5054759	43	$1.5\ 10^8$	$6.0\ 10^6$	$1.6\ 10^8$	$1.0\ 10^5$
H_2CO	$J=2_{12}\rightarrow1_{11}$	140.8395020	6.8	$1.1\ 10^6$	$6.0\ 10^4$	$1.6\ 10^6$	$1.5\ 10^4$
H_2CO	$J=3_{13}\rightarrow2_{12}$	211.2114680	17	$5.6\ 10^6$	$3.2\ 10^5$	$6.0\ 10^6$	$4.0\ 10^4$
H_2CO	$J=4_{14}\rightarrow3_{13}$	281.5269290	30	$9.7\ 10^6$	$2.2\ 10^6$	$1.2\ 10^7$	$1.0\ 10^5$
H_2CO	$J=5_{15}\rightarrow4_{14}$	351.7686450	47	$2.6\ 10^7$	...	$2.5\ 10^7$	$2.0\ 10^5$
NH_3	(1,1)*inv*	23.6944955	1.1	$1.8\ 10^3$	$1.2\ 10^3$	$2.1\ 10^3$	$7.0\ 10^2$
NH_3	(2,2)*inv*	23.7226333	42	$2.1\ 10^3$	$3.6\ 10^4$	$2.1\ 10^3$	$4.3\ 10^2$

[1] Adopted from Evans (1999); ... means no value, *inv* means inversion transition

[2] $n_{\rm eff}$ is the density needed to produce a line of 1 K. The values of $n_{\rm eff}$ were calculated in a large velocity gradient (LVG) approximation to account for trapping, assuming $\log(N/\Delta v) = 13.5$ for all species but NH_3, for which $\log(N/\Delta v) = 15$ was used.

To determine the velocity field of molecular clouds, in principle maps of a line profile over a cloud should suffice. However, since only motions along the line of sight produce Doppler shifts, and line profiles average over the beam and along the line of sight, it is difficult to decode the observations. So far we are able to say that a typical molecular cloud in the Galaxy experiences neither overall collapse (Zuckerman & Evans 1974) nor rapid rotation (e.g. Goodman et al. 1993). Most clouds appear to have velocity fields dominated by turbulence, because the typical line widths are much larger then expected from thermal broadening (see e.g., Myers 1995).

Both the magnetic field strength and direction are difficult to measure. Zeeman effect probes the line-of-sight component $B_\parallel$. Almost all measurements done so far use the OH lines, although possible molecules suitable for observations may be CN and CCS (Crutcher 1999). The magnetic field direction projected on the plane of the sky is measured by observing the polarization of a thermal emission of dust grains. The thermal emission is polarized perpendicular to $B_\perp$ (Hildebrand 1988). Finally, the ionization fraction, x_e may be determined by calculating relative fractional abundance of some molecules, e.g., $HC^{18}O^+$, or by chemical analysis, by considering deuterium fractionization reactions, as discussed by van Dishoeck & Blake (1998).

Chapter 4
STAR FORMATION

The Galaxy is a thin, rotating disk of stars, gas and dust, embedded in a more tenuous and more spherical halo. Most of the luminous mass in the Galaxy is in stars which formed $\sim 10^9$ years ago[3]. Only a small fraction of the galactic mass, about 1%, is involved in the production of new stars (Myers 1995). The recent estimated galactic average of star-production is $3 M_\odot \, \mathrm{year}^{-1}$ (Scalo 1986). At the same time, in form of mass loss from evolved stars, around $1-2 \, M_\odot \, \mathrm{year}^{-1}$ (e.g., Knapp & Morris 1985) of gas is returned back to the Interstellar Medium (ISM). Overall star forming efficiency (SFE; defined as the ratio $M_{star}/(M_{star}+M_{gas})$, where M_{gas} is the total gas mass of a molecular cloud) for the Galaxy is estimated to be only $\sim$2% (Myers et al. 1986).

Depending on the degree of influence of external processes, star formation can be spontaneous or stimulated. Spontaneous star formation occurs without external influence, and stimulated or triggered star formation is induced by external events (e.g., supernova shock fronts, ionization fronts, stellar winds, spiral density waves, cloud collisions). In a review Elmegreen (1992) discusses various mechanisms for star formation in details. The mechanisms of spontaneous star formation are dissipation-collapse scenario, when a cloud loses additional internal energy (e.g., turbulent, magnetic, rotational energy) by the virial theorem gravitational binding energy will increase, thus making a collapse inevitable. Mechanisms of triggered star formation in principle only change the initial or boundary conditions and in that way speed up the spontaneous star formation. Shock fronts increase the density of the gas on small scales through compression and thus enhance turbulent energy loss and loss of rotational energy. If the pressure front is perpendicular to the direction of the magnetic field loss of magnetic energy is also enhanced. The issue which process is dominant is still unresolved. The current prevailing opinion is that although on the small scales spontaneous star formation is predominant, on the large scales star formation is induced (Elmegreen 1992).

In a molecular cloud with only thermal support, collapse should occur whenever the mass exceeds the Jeans mass (1928)

$$M_J = \left(\frac{\pi \, k \, T_K}{\mu \, m_\mathrm{H} \, G} \right)^{\frac{3}{2}} \rho^{-\frac{1}{2}} \equiv 18 \, T_K^{\frac{3}{2}} \, n^{-\frac{1}{2}} \, M_\odot, \tag{4.1}$$

[3]General references: Evans (1999); Shu et al. (1987).

where T_K is the kinetic temperature in [K], ρ is the mean mass density in [$\mathrm{g\,cm^{-3}}$], n is the total particle density in [$\mathrm{cm^{-3}}$] (in a molecular cloud $n = n(\mathrm{H_2})+n(\mathrm{He})$), m_H is the mass of the hydrogen atom, μ is the mean mass per particle (equal to 2.29 in a fully molecular cloud with 25% helium by mass). Without pressure support collapse would occur in a free – fall time (e.g., Spitzer 1978)

$$t_{ff} = \left(\frac{3\,\pi}{32\,G\,\rho}\right)^{\frac{1}{2}} \equiv 3.4 \times 10^7\,n^{-\frac{1}{2}} \quad \text{years.} \tag{4.2}$$

Our Galaxy contains $\sim 1 - 3 \times 10^9\,\mathrm{M_\odot}$ of molecular gas (e.g., Combes 1991). Most of the gas is incorporated into giant molecular clouds (GMCs) with masses that exceed $10^4\,\mathrm{M_\odot}$ (Elmegreen 1985). The Jeans mass derived for typical conditions in the Galactic molecular clouds is $\sim 80\,\mathrm{M_\odot}$ (e.g., Shu et al. 1987), much less than the GMCs masses. Free-fall collapse in such environments would lead to a star formation rate of more than $200\,\mathrm{M_\odot\,year^{-1}}$ (Zuckerman & Palmer 1974), much higher than the observed one. Clouds' life times of $\sim 4 \times 10^7$ years (e.g., Leisawitz et al. 1989) suggest another support mechanism besides thermal support. Fragmentation and collapse of a molecular cloud will occur when such support is lost. Magnetic fields (e.g., Chandrasekhar & Fermi 1953, Mestel 1965, Spitzer 1968, Mouschovias 1976), rotation (e.g., Field 1978) and turbulence (e.g., Larson 1981) could be such a support.

Since the discovery of CO in molecular clouds it has been known that the CO linewidths correspond to very supersonic fluid motions. Typical linewidths for GMCs are $\sim 10\,\mathrm{km\,s^{-1}}$ and for dark clouds $\sim 2 - 3\,\mathrm{km\,s^{-1}}$, much broader than the corresponding Doppler broadening by thermal motions. For temperatures typical for GMCs i.e., at 30 K, the Doppler broadening is $\sim 0.2\,\mathrm{km\,s^{-1}}$ and for typical dark clouds' temperatures i.e., at around 10 K, the thermal line widths are $\sim 0.1\,\mathrm{km\,s^{-1}}$ (Myers 1995). When interpreted as a turbulence, these velocities approach virial values $\Delta v \sim \left(\frac{2\,G\,M}{R}\right)^{1/2}$, where R is the radius of the cloud, M is the mass of the cloud and Δv is the full width at half maximum (FWHM) of the molecular line. The difficulty with supersonic turbulence is that it is highly dissipative in the absence of magnetic fields (e.g., Goldreich & Kwan 1974). Moreover, turbulence would lead to forces which may balance self – gravity only if the turbulent "pressure" has a gradient. Unfortunately, the observations have shown that in molecular clouds the turbulent pressure is constant, $\rho\,v^2 \approx const.$ (Fleck 1981). Interstellar polarization maps (Vrba et al. 1976) show that the directions of the embedded magnetic fields are well ordered over dimensions of the clouds. This implies that turbulence does not dominate over magnetic fields.

Measured rotation rates of dark clouds are low, of order $0.1 - 1\ \mathrm{km\,s^{-1}\,pc^{-1}}$ (e.g., Fuller & Myers 1987, Goodman et al. 1993). This suggests that the clouds are magnetically controlled i.e., that they are subcritical regions and are not contracting rapidly as a whole (Shu et al. 1987). Observations of rotation rates in the GMCs and hot cores are fairly scarce: in ρ Ophiuchi and Orion few clumps with masses of $\leq 10\,\mathrm{M_\odot}$ have rotation rates between 25 and $50\,\mathrm{km\,s^{-1}}$ (Wadiak et al. 1985, Harris et al. 1983). The faster rotation and larger masses within a given radius imply that these cores have formed from a supercritical background that is itself contracting (Shu et al. 1987).

All these facts indicate that magnetic fields play a crucial role for a clouds support against the self gravity. The mass for which the magnetic fields can provide appreciable mechanical support is numerically calculated (Mouschovias & Spitzer 1976)

$$M_{cr} \equiv M_B = 0.13 \frac{\Phi}{\sqrt{G}} \cong 10^3 \left(\frac{B}{30\,\mu\mathrm{G}}\right) \left(\frac{R}{2\,\mathrm{pc}}\right)^2 \mathrm{M}_\odot. \tag{4.3}$$

Here Φ is the magnetic flux, B is the magnetic field strength and R is the radius of the (spherical) cloud. For highly flattened clouds the numerical coefficient should be replaced by the $(2\,\pi)^{-1}$ factor (Li & Shu 1996). Since the magnetic fields cannot provide support along the direction of the fields, the clouds are probably rather flattened than spheres (Shu et al. 1987). By measuring the Zeeman splitting of the thermal OH lines, the component $\vec{B}$ along the line of sight could be measured. For some hot cores measured field strengths have values of $\sim 10 \leq B_{\|} \leq 130\mu$G (e.g., Heiles 1987). For a random field orientation, the total field strengths are probably larger, on average by a factor of 2 (Shu et al. 1987).

Alfvén waves (Alfvén 1947) may provide requisite support along $\vec{B}$ if a fluctuating part of the wave (perpendicular to the direction of the static field) is comparable with the static part of the magnetic field i.e. if $\delta\vec{B} \sim \vec{B}_0$, and if the characteristic damping length is comparable with the size of the cloud. Both conditions seem to be fulfilled in cases of dark molecular clouds (Zweibel & Josafatsson 1983). Additionally, only the waves propagating outwards support the cloud against self – gravity; the waves propagating inwards tend to compress the cloud (Shu et al. 1987). Alfvén waves generated by the spin of the molecular cloud core relative to its envelope may be responsible for the low values of the rotational angular velocity commonly observed in molecular cloud/cores. Significant magnetic braking occurs when the amount of envelope material affected by the outward propagating Alfvén waves has a moment of inertia equal to that of the core. Characteristic time scale for braking the angular velocity component along the magnetic field is for $\rho_{\mathrm{core}} \gg \rho_{\mathrm{envelope}}$ much larger than the characteristic time scale for braking the velocity component perpendicular to the mean magnetic field direction (Mouschovias & Paleologou 1980). This lower efficiency of parallel magnetic braking leaves the spin axes of molecular cloud cores aligned parallel to $\vec{B}$ (Shu et al. 1987).

The ionization fraction in molecular clouds is low. Typically, for dark clouds ionization fraction is determined from the $HC^{18}O^+$ fractional abundance and is estimated to be $\sim 10^{-8}$ (Williams et al. 1998, Caselli et al. 1998, Anderson et al. 1999). An upper limit of 10^{-6} can be set from deuterium fractionization reactions (Dalgarno & Lepp 1984). For such low ionization fraction, magnetic fields support molecular clouds against collapse via process of ambipolar diffusion - the process in which magnetic fields (and the charged plasma to which they are coupled) drift relative to background of neutrals (e.g., Mestel & Spitzer 1956). The neutrals can be supported against their self-gravity only through the frictional drag that they experience as they slip relative to the ions. Ambipolar diffusion will allow neutral gas to move across the

magnetic field lines with a time–scale of (Spitzer 1978, Shu et al. 1987, Evans 1999)

$$t_{AD} \sim \frac{R^2}{\mathcal{D}} \sim \frac{R}{v_d} \equiv \frac{3}{4\,\pi}\,\frac{1}{G\,\rho\,\tau_{ni}} \simeq 7.3 \times 10^{13}\,x_e \quad \text{years}\,, \tag{4.4}$$

where $\mathcal{D}$ is so-called diffusion coefficient, v_d is the drift velocity of the ions (nearly comove with the electrons) relative to the neutrals, ρ is the density of the combined medium (ions+neutrals), τ_{ni} is the ion-neutral collision time and x_e is the ionization fraction. For ionization fraction of 10^{-7} the ambipolar diffusion time-scale is $\sim 10^6$ years. However, this time-scale may be too long to account for the observations. Fatuzzo & Adams (2002) have explored how fluctuations in the background magnetic fields affect the rate of ambipolar diffusion. Considering one–dimensional slab geometry and assuming *a priori* forms for the fluctuations they showed that a long–wavelength fluctuations may be able to shorten the ambipolar diffusion by a factor of $\Lambda \sim 1 - 10$.

4.1. BIMODAL STAR FORMATION: HIGH – MASS AND LOW – MASS STAR FORMATION

Herbig (1962) pointed out that some molecular clouds, like Taurus, harbor only low-mass stars with stellar masses $\sim$2 $M_\odot$, while others, like Orion, contain both high– and low-mass stars. Mezger & Smith (1977) indicated that the birth sites of high– and low-mass stars may be spatially distinct, with the OB stars being born primarely in GMCs situated in the spiral arms of the Galaxy. The possibility of two separate mechanisms of star formation was often discussed (e.g., Elmegreen & Lada 1977, Gusten & Mezger 1982). Today, the "bimodal star formation" has changed the emphasis from "low-mass vs. high-mass" to "loosely-aggregated (isolated) vs. closely-packed (clustered)" mode of stellar birth (e.g., Shu et al. 1987, Shu 1991). If gravitational collapse occurs independently for individual small cores to form single stars (or binaries), we have loosely-aggregated star formation mode. On the other side, if a large piece of a GMC collapses and produces a tight group of stars created more–or–less simultaneously, we have the closely-packed star formation mode. This tight group may, but need not form a bound cluster (Lada et al. 1984, Elmegreen & Clemens 1985).

If we assume that the magnetic fields provide molecular clouds prime support against their self-gravity, there is an obvious theoretical explanation of the proposed different modes of star formation (Mestel 1985, Shu et al. 1987). In the supercritical regime, when $M_{\rm cloud} > M_{cr}$, molecular clouds cannot be held up by magnetic fields alone, and must collapse as a whole to form a closely packed group of stars. From initially subcritical assemblage, the supercritical regime may be reached either by agglomeration of the discrete clouds/clumps (Blitz & Shu 1980) or by shock-induced forced motions of stable cold clumps (Elmegreen 1989). On the other side, in the subcritical case, when $M_{\rm cloud} < M_{cr}$, if the magnetic field is frozen, i.e. if Φ is conserved, gravitational collapse cannot be induced by any amount of increased external pressure. As long as magnetic fields do not leak out by the process of ambipolar diffusion, the cloud is stable (e.g., Nakano 1979, Shu et al. 1987). The relatively long

time-scale for ambipolar diffusion might explain why the star formation in subcritical molecular clouds (i.e. dark, cold clouds) is generally inefficient process.

Recently Adams & Myers (2001) argued that star – forming environments should be classified into finer division. The three suggested modes or classes are as follows: **I** Isolated single stars and multiple systems, including binaries, triples and other few body systems with $N_* \leq 10$; **II** Groups, consisting of intermediate numbers of stars with $10 < N_* \sim 100$, and **III** Clusters, consisting of large numbers of stars with $N_* > 100$. The criteria to distinguish these modes of star formation depend on many different (and sometimes coupled) physical processes: the longevity of stellar systems, the stellar IMF (Initial Mass Function), The UV mass – luminosity relationship for stars, the minimum progenitor mass for a supernova, the brightness of stellar populations, the formation time for clusters and the scattering cross sections for solar system disruption.

4.2. EVOLUTION OF LOW – MASS PROTOSTARS

Current theory of isolated star formation, often cited as "the standard theory", was analytically developed by Shu et al. (1987), although it was sketched by numerical modeling much earlier (Larson 1969). Formation of low-mass stars can be separated into several well defined stages. The first stage is fragmentation of a molecular cloud into a number of gravitationally-bound cores, once the initial support against self-gravity is lost. During a probably brief initial phase, the released gravitational energy is freely radiated away and the collapsing fragment stays roughly isothermal. This "runaway" isothermal collapse phase tends to produce a strong central concentration of matter with a radial density gradient $\rho \propto r^{-2}$ at small radii, essentially independent of initial conditions (e.g., Foster & Chevalier 1993). According to numerical calculations this phase ends with the formation of an opaque, hydrostatic protostellar object in the center (e.g., Bate 1998). The standard theory considers a static singular isothermal spheroid (SIS) with a

$$\rho \sim \frac{a^2}{2\,\pi\,G}\,\frac{1}{r^2} \tag{4.5}$$

density distribution (e.g., Chandrasekhar 1939, Shu 1977, Shu et al. 1987, Li & Shu 1996), where a is the isothermal sound speed, i.e., the speed with which the collapse propagates outward. This phase in the standard theory is known as an "inside – out collapse".

The next phase is main accretion phase during which the central object builds up its mass $M_\star$ from a surrounding infalling envelope of mass $M_{\rm env}$ and accretion disk, while progressively warming up. In the standard theory the accretion rate is

$$\dot{M}_{\rm acc} \sim \frac{a^3}{G}, \tag{4.6}$$

and is considered constant in time. However, the observations show that the accretion rate is generally time – dependent (e.g., André et al. 1993). During this phase the mass of the envelope is much larger than the mass of the protostar, $M_{\rm env} \gg M_\star$. When

freely falling material in the envelope reaches the hydrostatic surface of the star at $R_\star$, it dissipates the energy in accretion shocks producing the luminosity (Shu et al. 1987)

$$L = G\, M_\star\, \dot{M}_{\rm acc}/R_\star. \tag{4.7}$$

Here we assume that all kinetic energy of the infall is converted into radiation. The main accretion phase is always accompanied by a powerful ejection of a small fraction of the accreted material in the form of prominent bipolar jets/outflows (e.g., Cabrit et al. 1997, Bachiller & Tafalla 1999).

When the central object has accumulated most ($> 90\%$) of its final main – sequence mass, it becomes a pre – main sequence (PMS) star which evolves further approximately at fixed mass on the Kelvin – Helmholtz (K – H) contraction time – scale (e.g., Shu et al. 1987, Stahler & Walter 1993). The K – H time – scale is the time required to reach the internal thermal equilibrium and is calculated as $t_{\rm KH} = G\, M_\star^2\, /R_\star\, L_\star$. However, the question is when exactly and why the termination of the infall occurs? In the standard theory the protostar accumulates matter of ever increasing specific entropy, hence remains radiative, until the ignition of deuterium, which starts when $M_\star \sim 0.3{\rm M}_\odot$ (Stahler et al. 1980, Shu et al. 1987). Deuterium burning in a low – mass star can drive convection, which when coupled with a presence of differential rotation can produce dynamo action and generate magnetic activity (Parker 1979). The released energy may then power the intense stellar surface activity in young stellar objects (YSOs). The resulting stellar wind eventually reverses the infall and therefore defines a mass of a newly formed star at the point when it first becomes optically visible. For the ideal gas of polytrope 1.5, with mean mass m, Chandrasekhar (1939) has calculated the temperature required for deuterium burning in the center of a sphere with mass $M_\star$ and radius $R_\star$ to be $T_c = 0.54\, GM_\star\, m/k\, R_\star$. An approximate criterion for deuterium burning for a completely ionized gas of cosmic abundance for $0.01{\rm M}_\odot \leq M_\star < 2{\rm M}_\odot$ can be obtained by setting the central temperature to 1×10^6 K in this relation (Shu et al. 1987). The equation $R_\star \approx 0.15 + 7.6\, M_\star$, where the radius and the mass are given in the Solar radius and mass, respectively, produces a birthline in the H – R diagram for pre – main sequence stars which agrees well with the observed upper envelope for T Tau stars.

4.2.1. OUTFLOWS

It seems that stars of all masses undergo energetic, generally bipolar, mass loss during their formation. More than 200 outflows have been cataloged so far (Wu et al. 1996). Outflows are observable over a wide range of wavelengths, from the ultraviolet (UV) to the radio domain. Outflow research started as early as 1950's when Herbig (1951) and Haro (1952) observed few peculiar nebulosities with emission line spectra. These so–called Herbig – Haro (HH) objects were later recognized to result from the interaction of highly supersonic stellar winds with ambient material (Schwartz 1975). When these winds interact with the surrounding molecular cloud, they give rise to so–called molecular outflows which are best observed in the millimeter–wave lines of CO. The outflowing material tends to lie in two lobes of gas, one blueshifted and the other redshifted relative to the CO emission velocity of the parent molecular cloud, with

YSO in the neck of such "hourglass" (see e.g., the reviews of Cabrit et al. 1997, Bachiller & Tafalla 1999, Richer et al. 2000).

Flow sizes range from less than 0.1 pc to several parsecs. Observed (unprojected) terminal velocities range from a few to $\sim 100\,\mathrm{km\,s^{-1}}$. Kinematical time-scale i.e., the flow length divided by the terminal velocity, ranges from about 10^3 yr to $\sim 10^5$ years. The total molecular mass of the outflowing material ranges from a few 10^{-2} to several $10^2\,\mathrm{M_\odot}$ (Bachiller & Tafalla 1999). Multiline observations of CO in a number of bipolar outflows have indicated the presence of clumping in the high–velocity gas (e.g., Bally 1982, Plambeck et al. 1983, Snell et al. 1984). Observations with high angular resolution have provided evidence that most of the outflowing gas is in form of dense clumps (e.g., Kitamura et al. 1990, 1992, Tafalla et al. 1994, Plambeck & Snell 1995).

Morphologically, bipolar outflows can be divided into so–called "classical" and "highly – collimated" outflows. Although an outflow's collimation depends on many factors e.g., ambient molecular gas density and energetics of the outflow, the two classes reflect to some extend the age of the outflow. Classical outflows are poorly collimated and extended. Structure of dense gas elongated perpendicular to the flow axes ("toroids") are found in many cases (e.g., Torrelles et al. 1983, also Chapter 7). The gas inside the lobes has shell geometry, with a cavity along the outflows axes devoid of molecular gas (e.g., in L 1551 outflow, Moriarty–Schieven & Snell 1988). This suggests that the outflow material *is* an ambient gas set into motion by (invisible) wind from the central YSO. The highest velocities are not reached near the YSO, but at some distance from it (Snell et al. 1984). The combination of momentum conservation and a density decrease away from the outflow source can explain such a pattern (Shu et al. 1991a). Energy is probably not conserved during outflow acceleration (it is radiated away), but the linear momentum most likely is, so the momentum in the CO outflow must equal the momentum in the invisible agent (e.g., Bachiller & Tafalla 1999).

Highly – collimated outflows (an example is given in Fig. 4.1) were only identified in late 1980's, with the new generation of high resolution mm-wave radio telescopes. Collimation increases systematically with velocity, and the fastest gas lies close to the outflow axes and has the highest bipolarity (e.g., Bachiller & Tafalla 1999). Still, these outflows show a shell-like gas distribution at the lowest velocities. The shells diverge away from the central source but converge at the end of the lobe, where strong H_2 (shocked) emission is observed, as seen in a best–to–date studied compact outflow HH 221, (Gueth & Guilloteau 1999). Highly collimated outflows tend to have additional velocity component, a fraction of extremely high velocity (EHV) gas moving at speeds up to $150\,\mathrm{km\,s^{-1}}$ (HH 7–11, Bachiller & Cernicharo 1990). This EHV component appears to form discrete condensations, often referred to as molecular "bullets", which have estimated typical sizes of 10^{-2} pc, typical masses of a few $10^{-4}\,\mathrm{M_\odot}$ and kinematical time scales from a few 10^2 to a few 10^3 yr (Bachiller et al. 1990). The bullets are best understood if there is some type of instability in the central source that gives rise to quasiperiodic ejection every $10^2 - 10^3$ years (Bachiller & Tafalla 1999). Highly collimated outflows are an order of the magnitude more energetic than the classical flows from sources of comparable luminosity.

The ideas of the outflows' evolution are still tentative, but a general picture seems to emerge. Highly collimated outflows are powered by Class 0 objects which are con-

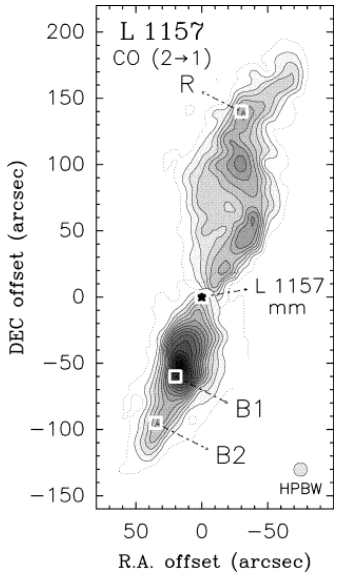

Figure 4.1: CO 2–1 emission from the L1157 outflow integrated over velocity intervals from -20 to 3 km s^{-1} (blueshifted gas to the south of the driving source) and from 3 to 30 km s^{-1} (redshifted gas toward the north of the source). Position offsets are in arcseconds from L1157-mm, the outflow-exciting source. First contour and step are 11 K km s^{-1}. The squares mark the positions in which the survey of molecular lines was carried out (from Bachiller & Pérez Gutiérrez 1997).

sidered the youngest protostars known (André et al. 1993), while classical outflows are excited by Class I YSOs, which represent a more evolved state. By the time a YSO reaches the Class I stage, its bipolar outflow has lost an appreciable part of its collimation and has formed an opening cavity in the parent cloud (Bachiller et al. 1995, Gueth & Guilloteau 1999). The broadness of such a cavity increases with time. There is a good correlation between the outflow momentum flux and the amount of circumstellar mass (Bontemps et al. 1996). As circumstellar mass is likely indicator of age (mass decreases as age increases), the correlation suggests that the outflow power decreases with time.

Radiation pressure from central YSO lacks enough momentum to drive a molecular outflow, therefore a mechanical agent like a stellar wind seems most likely responsible for this phenomenon (e.g., Bachiller & Tafalla 1999). The driving wind could be either ionized or neutral, and if neutral it could be either atomic or molecular. Theoretical models developed so far are not unique in a sense that they make an attempt either to explain the molecular gas acceleration starting with a given driving agent (jet, wide angle wind) either to explain the outflow launching by the central star/disk system. Wide angle wind theories, not surprisingly, explain better classical outflows' characteristics. In a model by Li & Shu (1996) density distribution with a little gas along the polar axes ("toroids") and winds with a stronger axial momentum component are able to successfully reproduce shell–like structure. Recently, a new class of models appeared, so–called "circulation" models, where most of the infalling circumstellar mate-

rial is diverted magnetically at large radii into a slow–moving outflow along the polar direction, while infall proceeds along the equatorial plane (Fiege & Henriksen 1996). Jet – driven outflow models of Masson & Chernin (1993) argue that for typical molecular cloud densities and typical jet velocities, the jet – cloud interaction is highly dissipative and a narrow bow shock forms at the jet end; the swept up material is accelerated mostly forward. Raga & Cabrit (1993) consider time–dependent flow velocity field when a bow shock compresses and sweeps ambient material, which later re–expands into the cavity left behind. As for wind launching models, only the family of magnetohydrodynamics (MHD) models stood the test of time: they seem to be capable to meet the energy and momentum requirements by converting a fraction of the gravitational energy released by mass accretion into outflow motion. If the magnetic field is coupled to the rotating matter (through flux freezing) and if it takes sufficiently large angle with the rotation axes ($> 30°$), corotation accelerates and ejects the material along the field lines. Two classes of models have been proposed: disk outflow models, where the outflow arises from a disk which is threaded by an inclined magnetic field (e.g., Blanford & Payne 1982, Ferreira & Pelletier 1993) and stellar surfaces outflow origin, where the advantage of natural curvature of the stellar surface near the equator is taken into account. Shu et al. (1988) have proposed that the magnetic field, emerging almost perpendicular to the star surface, makes the adequate angle to centrifugally drive a wind. However, that model would need much faster rotation rates than detected in T Tau stars (Hartmann et al. 1986), so either YSOs rotate much faster than the pre-main sequence stars, or the model needs some adjustments.

4.2.2. VISIBLE STAGES: T TAU STARS

T Tauri stars were soon after their discovery (Joy 1942) recognized as a population of very young (overall ages $\sim 10^7$ yr) low – mass stars. Newly born within dark clouds, they were invariably associated both spatially and kinematically with the "parent" cloud (e.g., Herbig 1977). T Tau stars are characterized by high variability and prominent emission lines, most notably the Balmer series of hydrogen and Fe II lines (see e.g., Herbig 1962). Observed in the IR band, T Tauri stars have an infrared excess emission which was suggested to origin in the circumstellar dust grains (Mendoza 1966). Spectral energy distribution in the IR of many T Tau stars was successfully modeled by a protostar surrounded by a more or less flat disk of circumstellar dust (Shu et al. 1987). In the ultraviolet band, T Tau stars exhibit strong UV emission lines and continuum excess. The UV activity has been interpreted either as an indication for a heavy chromospheric activity (e.g., Calvet et al. 1984), or as a process that results from a boundary layer – accretion disk interaction (Bertout et al. 1988). Photometric and Doppler imaging studies show rotation modulations of star spots that cover from a few percent up to about 50% of the surface with temperatures of approximately 500 – 1000 K for both classical T Tauri and weak T Tau stars (e.g., Bouvier et al. 1995). All T Tau stars are faint X–ray sources (e.g., Montmerle et al. 1983, Fiegelson & Montmerle 1999, Alcála et al. 2000). Most X–ray T Tau stars vary on time scales of months (classical T Tau, Montmerle et al. 1983) or days (weak T Tau stars, Preibisch 1997). Occasionally they exhibit a high–amplitude flare with

time scale of hours. Often the X–ray emission can be modeled as a mixture of a so–called "soft" component with $T_{\rm x} \simeq 2 - 5 \times 10^6\,{\rm K}$ and a "hard" component with temperatures as high as $T_{\rm x} \simeq 15 - 30 \times 10^6\,{\rm K}$ (Preibisch 1997).

T Tauri stars have strong magnetic fields, as revealed by measuring the Zeeman splitting on photospheric absorption lines. Magnetic enhancement of the equivalent width of the Fe I lines in the weak T Tau star LkCa16 can be interpreted as $B = 2.4\,{\rm kG}$ fields covering $f = 0.6$ of the stellar surface (Guenther et al. 1999). Classical T Tauri stars might have somewhat larger magnetic fields e.g., the spectrum of BP Tau shows broadening in the Zeeman–sensitive Ti I line at $2.2\,\mu$m corresponding to a total magnetic flux of $B \simeq 3.3 \pm 0.3\,{\rm kG}$ (Johns–Krull et al. 1999).

The overall activity of T Tauri stars may result simply from an adjustment needed to accommodate material recently acquired from the ISM to stellar conditions (Shu et al. 1987). This is supported by the observed decay of surface activity, infrared excess, intensity of the emission lines and X–ray activity (Cohen 1984) as T Tau stars age.

4.3. SPECTRAL EVOLUTION OF PROTOSTARS

Varying amount of gas and dust that surround an embedded YSO absorb and reprocess substantial amount of the energy radiated by the buried protostar. Consequently, YSOs radiate most of their luminous energy in the infrared (IR) part of the spectrum. The slope of the broad-band IR spectrum (from the near – IR to submillimeter region) of a YSO depends both on the nature and distribution of the surrounding material, and therefore probably is function of the state of evolution of the YSO (e.g., Lada 1999). The original classification scheme (Lada & Wilking 1984) for the IR sources in the near– to mid-infrared (i.e., $\sim 1 - 100\,\mu$m) is based on the value of a spectral index defined as $\alpha = d\log(\lambda\,F_\lambda)\,/\,d\log(\lambda)$. YSOs were divided into three distinct morphological classes: for a spectral index i.e. the slope of the spectral energy distribution (SED) between $2.2\,\mu$m and 10–$25\,\mu$m of $\alpha < -1.5$ YSO is classified as a Class III source; for $-1.5 \leq \alpha < 0$, sources belong to the Class II objects and if $\alpha \geq 0$ IR objects are classified as Class I sources. Class I sources are usually deeply embedded in molecular clouds and are not detected in the optical part of the spectrum, while both Class II and Class III objects are optically visible (e.g., Lada 1999).

This empirical classification is easily identified with different stages of evolution in the theory of the low – mass stars formation (Shu et al. 1987). Class III and Class II objects correspond to pre – main sequence (PMS) stars: "weak" (or "naked") and "classical" T Tau stars, respectively (e.g., André & Montmerle 1994, Lada 1999). Weak T Tau stars have a simple black body SED and age estimated $2 - 3 \times 10^7$ years (Wolk & Walter 1996). The SED shape indicates that Class III objects have little (optically thin at $\lambda \leq 10\mu$m) or no accretion disk. Classical T Tau stars have the SED with the IR part that departs from the spectral energy distribution of a cool atmosphere. This "excess IR part" shows that the Class II objects still have accretion disks, which is usually optically thick at $\lambda \leq 10\mu$m. All classical T Tau stars drive strong stellar winds with mass loss of $\sim 10^{-7}\,{\rm M}_\odot$/year, their ages being estimated to $0.5 - 3 \times 10^6$ years (Barsony & Kenyon 1992). Only the youngest Class II objects drive CO outflows. Objects of both classes have already dispersed their circumstellar

envelopes. SEDs for the both Class I and Class II sources are broader than a single black body spectrum, with many absorption features (e.g. Lada 1999). They are interpreted as relatively evolved protostars surrounded by both a disk of $\sim 10^2$ AU in size (e.g., Hogerheijde et al. 1999), and a diffuse circumstellar envelope of substellar ($< 0.1 - 0.3\,M_\odot$) mass (e.g. André & Montmerle 1994). Substantial fraction of their luminosity is delivered from accretion (André et al. 1993). Class I objects drive outflows, with a low(er) mass – loss rate and a wide(r) opening angles (e.g. Bontemps et al. 1996). The age of these objects is estimated to be $\sim 10^5$ years (Barsony & Kenyon 1992, Kenyon & Hartmann 1995).

Recently, as a class on their own, YSOs with extremely steep spectral index corresponding to a black body of 30–40 K are defined as Class 0 objects (André et al. 1993). These sources are defined by the following observational properties: there is only indirect evidence for a central YSO e.g., detection of a compact cm – radio continuum source (e.g. André et al. 1993, Ward–Thompson et al. 1995), a highly collimated powerful CO outflow (e.g., Barsony et al. 1998, Wolf–Chase et al. 1998, 2000) or an internal heating source as detected in X-rays (e.g., Feigelson & Montmerle 1999); centrally peaked but extended submillimeter continuum emission tracing the presence of a spheroidal circumstellar dust envelope (e.g., André & Montmerle 1994) and for the luminosity measured longward of 350 μm, $L_{\rm bol}/L_{\rm smm} \leq 200$, which indicates that the envelope mass exceeds the central stellar mass. Class 0 objects are extremely young objects with the estimated age of $\sim 10^4$ years (Barsony et al. 1998), deeply embedded in the circumstellar envelope. They have prominent disks that extend usually up to $10^3 - 10^4$ AU in radius (e.g., Hogerheijde et al. 1999).

Combining the IR and the submillimeter data we may define a complete, empirical evolutionary sequence for low – mass YSOs:

$$\text{Class 0} \;\rightarrow\; \text{Class I} \;\rightarrow\; \text{Class II} \;\rightarrow\; \text{Class III},$$

which likely corresponds to different stages of evolution: early main accretion phase, late accretion phase, PMS stars with protoplanetary disks and PMS stars with debris disks (e.g., André et al. 1993). The accretion phase is characterized by bipolar outflows simultaneous with undergoing infall (e.g., Evans 1999).

The sequence of evolution may be parameterized by the "bolometric temperature", $T_{\rm bol}$, defined as the temperature of a black body having the same mean frequency as the observed YSO spectrum (Myers & Ladd 1993). They proposed to use the $\log L_{\rm bol} - \log T_{\rm bol}$ diagram for embedded YSOs as a direct analog to the H – R diagram for optically visible stars. Chen et al. (1995) have found that the boundary lines in $T_{\rm bol}$ coincide with the IR classes: Class 0 objects have $T_{\rm bol} < 70$ K, Class I YSOs have $70 \leq T_{\rm bol} < 650$ K and Class II objects $650 \leq T_{\rm bol} < 2800$ K.

Further search for protostars can be done by employing various strategies: (sub) millimeter continuum mapping (e.g., Motte et al. 1998, 2000), HIRES processing of the *IRAS* data (e.g., Hurt & Barsony 1996, O'Linger et al. 1999), deep radio – continuum VLA (Very Large Array) surveys (e.g., Bontemps et al. 1995, Yun et al. 1996, Moreira et al. 1997, Gibb 1999), CO mapping (e.g. Bachiller et al. 1990, Bourke et al. 1997) and large – scale near – IR/optical imaging of shocked H_2 and [S II] emission (e.g. Hodapp & Ladd 1995, Wilking et al. 1997, Phelps & Barsony 1999).

Chapter 5
ASTROCHEMISTRY

Astrochemistry started with observations of visible absorption lines in the interstellar gas attributable to the diatomic molecules CH, CN, CH^+ (Dunham & Adamas 1937, Dunham 1937) coupled with the experiments in laboratory spectroscopy and with theoretical attempts to identify the processes through which molecules are formed and destroyed in the diffuse ISM. Molecules are found to survive in often hostile environments like e.g., circumstellar shells, H II regions, emission nebulae, planetary nebulae, Herbig – Haro objects, supernova remnants, supernova ejecta, novae, shocked gas subjected to outflows, photodissociation or photon-dominated regions, star – forming regions, accretion disks, cooling flows and external galaxies as distant as a red-shift of 4.69 (Dalgarno 2000). Such extreme conditions require unusual chemistry, compared to the Earth laboratories.

5.1. FORMATION AND DESTRUCTION PROCESSES

Because of low temperatures and densities in molecular clouds, chemistry is not in thermodynamical equilibrium, but controlled by two – body reactions. Three – body interactions are generally not important.[4] The abundances of different molecular species depend both on a current physical conditions (T, n, radiation field)and on the history of a given region - ISM is continuously enriched with heavy elements from dying stars through red–giant winds, novae and supernovae explosions.

There are two basic processes which form molecules in molecular clouds:

• *Radiative association*, $X + Y \rightarrow XY^* \rightarrow XY + h\nu$, where the new molecule is stabilized by emission of a photon. These reactions are very slow, having the rate coefficients $\sim 10^{-17} - 10^{-14}\,\mathrm{cm^3\,s^{-1}}$ (J. Black, private communication, see footnote 4). If both X and Y are in the ground state, molecule formation occurs only once in 10^{10} collisions. However, in the other radiative association processes, through excited states, inverse predissociation and inverse vibrational predissociation efficiency of the process may increase up to one formed molecule for every 10^5 collisions.

[4] As an example of two – body reaction one may take the $C^+ + H_2 \rightarrow CH_2^+ + h\nu$ reaction, with the reaction rate coefficient of $k \approx 10^{-15}\,\mathrm{cm^3\,s^{-1}}$, in the typical ISM conditions where the H_2 number density is $n(H_2) \approx 10^2\,\mathrm{cm^{-3}}$, each C^+ waits $\approx 10^3$ s; for the corresponding three – body reaction $C^+ + H_2 + H_2 \rightarrow CH_2^+ + H_2$ at the reaction rate coefficient of $k \approx 10^{-27}\,\mathrm{cm^3\,s^{-1}}$, each C^+ would have to wait $\approx 10^{23}$ s, a life – long time of the Universe (J. Black, 1998, *Lecture notes in Astrochemistry* and private communication).

• *Grain surface formation*, $X + Y : g \rightarrow XY + g$, where the grain carries off the released energy corresponding to the molecular bond. There are two different modes: in i) a diffusive mechanism the formation of a molecule proceeds in stages sticking – diffusion+molecule formation – desorption, $X + Y : g \rightarrow X : g : Y \rightarrow X - Y : g \rightarrow XY + g$, ii) in a direct mechanism a molecule is formed 'immediately' i.e., in the following stages - molecule formation – desorption $X + Y : g \rightarrow X - Y : g \rightarrow XY + g$.

The third possible process which can form molecules, an *associative detachment*, $X^- + Y \rightarrow XY + e$, plays a role only in partly ionized regions and early Universe, because the prerequisite process, $X + e \rightarrow X^- + h\nu$, the negative ions formation, is a very slow process which requires certain electron abundances.

Destruction of molecules may occur via the following three processes:

• *Photodissociation*, $XY + h\nu \rightarrow X + Y$, is important in the diffuse and translucent clouds, which are permeated by the intense ultraviolet radiation. Deep inside dark clouds, little of the ambient radiation penetrates, yet a weak UV field can be maintained by cosmic–rays induced photons, resulting from the excitation of H_2 by secondary electrons following cosmic ray ionization of H_2 (Gredel et al. 1989). In the unshielded radiation field, typical lifetime against photodissociation (or photoionization) is only 10^2–10^3 years.

• *Dissociative recombination*, $XY^+ + e \rightarrow X + Y$, is responsible for destruction of molecular ions. The reaction is very fast at low temperatures, typical of molecular cloud cores. Rate coefficients for this process of abundant molecular ions, including the key specie in the chemistry, H_3^+, are typically $10^{-6} - 10^{-7}\,\mathrm{cm^3\,s^{-1}}$ (see the review van Dishoeck 1998).

• *Collisional dissociation*, $XY + M \rightarrow X + Y + M$, is only important in the regions of very high temperatures ($> 3000\,\mathrm{K}$) and density, such as shocks in vicinity of young stars (outflows).

Once molecules are formed, molecular bonds can be rearranged by chemical reactions leading to more complex species. Such processes generally fall into three categories:

• *Ion – molecule reactions*, $X^+ + XY \rightarrow XY^+ + Z$, are very rapid at low temperatures. If the reaction is exothermic, the rate coefficient is independent of temperature, and has typically values of $\sim 10^{-9} - 10^{-8}\,\mathrm{cm^3\,s^{-1}}$. Because of the enhanced long–range attraction, reactions between ions and molecules with a permanent dipole are factors of 10–100 larger at low temperatures (see the review van Dishoeck 1998).

• *Charge-transfer reactions*, $X^+ + YZ \rightarrow X + YZ^+$, can neutralize both atomic and molecular ions, if the reactants are large molecules such as polycyclic carbonates (PAHs) or metals.

• *Neutral – neutral reactions*, $X + YZ \rightarrow XY + Z$, were originally thought to be very slow compared with the ion – molecule reactions at low temperatures. However, some reactions, e.g., radical – radical and radical – unsaturated molecule reactions have rate coefficients that are only a factor of ~ 5 lower then the ion – molecule reactions i.e., have rate coefficients of order of $\sim 10^{-10} - 10^{-9}\,\mathrm{cm^3\,s^{-1}}$.

5.1.1. GAS – PHASE CHEMISTRY

Interstellar clouds consist mainly of hydrogen and helium, with carbon, oxygen and nitrogen present only in trace amounts. If an atom or molecule can react with H or H_2, that process will be the dominant production path. Since some elements are needed to make grains, heavy elements are expected to be depleted from the gas-phase.

The chemistry starts with cosmic – ray ionization of the dominant species, with an estimated rate of $\zeta_0 = 1 - 5 \times 10^{-17}\,\mathrm{s}^{-1}$ (see e.g., van Dishoeck & Black 1986):

$$\begin{aligned} \mathrm{H} + \text{cosmic ray} &\rightarrow \mathrm{H}^+ + e + \text{cosmic ray}, \\ \mathrm{H_2} + \text{cosmic ray} &\rightarrow \mathrm{H_2}^+ + e + \text{cosmic ray}. \end{aligned} \tag{5.1}$$

The production of H_2^+ is followed by a rapid reaction leading to H_3^+:

$$\mathrm{H_2}^+ + \mathrm{H_2} \rightarrow \mathrm{H_3}^+ + \mathrm{H}. \tag{5.2}$$

H_3^+ ion plays a crucial role in the subsequent ion – molecule chemistry through proton – transfer (see e.g., van Dishoeck 1998). Because the destruction of the H_2 is initiated by line absorption, the lines can become optically thick, thereby shielding molecules deeper in the cloud from the dissociating radiation. The H_3^+ ion was detected only recently, through IR absorption line observations toward young stars embedded in dense molecular clouds (Geballe & Oka 1996). In a sample of dark clouds McCall et al. (1999) observed almost constant column densities of $N(\mathrm{H_3^+}) = 1 - 2 \times 10^{14}\,\mathrm{cm}^{-2}$, with almost constant number density of $n(\mathrm{H_3^+}) \sim 1 \times 10^{-4}\,\mathrm{cm}^{-3}$ independent of the total H_2 number density. At low temperatures, typical for dark clouds, only exothermic reactions can occur, which is the case with reactions between H and H_2 and small ions; most reactions of neutrals and large ions have substantial barriers, so that they do not proceed at the low temperatures (e.g., van Dishoeck & Blake 1998).

Next important transition in the chemistry is the eventual production of CO from neutral and ionized atomic carbon (e.g., Langer et al. 2000). The C^+ ion should be available in sufficient quantities, since atomic carbon is easily ionized by the penetrating UV radiation. There is a difference between chemistry in diffuse and in dark clouds, since the production of carbon monoxide may go through different paths (e.g., van Dishoeck 1995):

$$\begin{aligned} \mathrm{C^+ + H_2^+} &\rightarrow \mathrm{CH_2^+} + h\nu, \\ \mathrm{CH_2^+} + e &\rightarrow \mathrm{CH + H}, \\ \mathrm{CH + O} &\rightarrow \mathrm{CO + H}; \\ &\text{or} \\ \mathrm{CH + C^+} &\rightarrow \mathrm{C_2^+ + H}, \\ \mathrm{C_2^+ + C} &\rightarrow \mathrm{C_2 + C^+}, \\ \mathrm{C_2 + O} &\rightarrow \mathrm{CO + C}. \end{aligned} \tag{5.3}$$

However, there are other possible paths, and this branching in the carbon–network increases uncertainties (e.g., Fig. 6 in van Dishoeck 1995 for extensive carbon–network reactions):

$$\begin{aligned} C + H_3^+ &\rightarrow CH^+ + H_2, \\ CH^+ + H_2 &\rightarrow CH_2^+ + H. \end{aligned} \tag{5.4}$$

Another possibility to form CO molecules is through oxygen – network (e.g., van Dishoeck 1995):

$$\begin{aligned} OH + C^+ &\rightarrow CO^+ + H, \\ CO^+ + H &\rightarrow CO + H^+; \\ &\text{or} \\ OH + O &\rightarrow O_2 + H, \\ O_2 + C &\rightarrow CO + O; \\ &\text{or} \\ CO^+ + H_2 &\rightarrow HCO^+ + H, \\ HCO^+ + e &\rightarrow CO + H. \end{aligned} \tag{5.5}$$

For dark clouds with densities of $10^4 - 10^5\,\mathrm{cm}^{-3}$, CO will be produced within $10^5 - 10^6$ years (Langer et al. 2000).

Creation of more complex species and long carbon chains requires large abundances of both ionized and atomic carbon. Thus, the concentration of complex molecules tends to peak at early times ($\sim 10^5\,\mathrm{yr}$) and decline as equilibrium is reached (e.g., Langer et al. 2000).

Abundances of other trace elements, oxygen, nitrogen and sulphur depend on how their chemistry is linked to that of carbon (see e.g., van Dishoeck 1995, Langer et al. 2000).

The gas – phase oxygen chemistry is initiated by the cosmic rays ionization of atomic and molecular hydrogen (see Eq. 5.1). OH^+ then forms (van Dishoeck 1995, 1998) through

$$O + H_3^+ \rightarrow OH^+ + H \text{ or } H_2, \tag{5.6}$$

or, if the temperatures exceed 100 K via endothermic reaction:

$$\begin{aligned} O + H^+ &\rightarrow O^+ + H - 227\,\mathrm{K}, \\ O^+ + H_2 &\rightarrow OH^+ + H. \end{aligned} \tag{5.7}$$

The abundance of simple oxygen bearing molecules are low at early times, as OH, O_2 and H_2O react with C and C^+.

The primary N–bearing molecules, N_2 and NH_3, form via simple ion – molecule and neutral – neutral reactions, (e.g., van Dishoeck 1995, 1998)

$$\begin{aligned} N + H_3^+ &\rightarrow NH_2^+ + H, \\ NH_2^+ + e &\rightarrow NH + H, \\ NH + N &\rightarrow N_2 + H; \end{aligned}$$

$$
\begin{array}{rcl}
 & \text{or} & \\
\mathrm{NH} + \mathrm{O} & \rightarrow & \mathrm{NO} + \mathrm{H}, \\
\mathrm{NO} + \mathrm{N} & \rightarrow & \mathrm{N_2} + \mathrm{O}; \\
 & \text{and} & \\
\mathrm{N^+} + \mathrm{H_2} & \rightarrow & \mathrm{NH^+} + \mathrm{H}, \\
\mathrm{NH^+} & \stackrel{\mathrm{H_2}}{\rightarrow} & \mathrm{NH_2^+} \stackrel{\mathrm{H_2}}{\rightarrow} \mathrm{NH_3^+} \stackrel{\mathrm{H_2}}{\rightarrow} \mathrm{NH_4^+}, \\
\mathrm{NH_4^+} + e & \rightarrow & \mathrm{NH_3} + \mathrm{H},
\end{array}
\tag{5.8}
$$

and have slow, steady buildup in concentration until equilibrium is reached.

The most abundant sulphur–bearing molecules, CS and SO exhibit slight evolutionary difference, and the [CS]/[SO] abundance ratio is suggested as an age indicator (e.g., Nilsson et al. 2000). Namely, SO is produced mainly through a reaction of S with OH and O_2, and is destroyed by C producing CS. Thus, the chemistry of CS is linked to the carbon network which leads to slightly higher abundances at earlier times, while SO has larger concentrations in equilibrium (see e.g., van Dishoeck 1995, Langer et al. 2000).

A dichotomy exists in the gas phase chemistry: i) species linked to the carbon chemistry, such as CS, CN, HCN and complex carbon chains have larger abundances at earlier evolutionary stages; ii) molecules that are independent or destructively linked to the carbon chemistry such as N_2, NH_3, N_2H^+ and SO exhibit larger concentrations near equilibrium. This has been used to interpret observations of molecular clouds in terms of evolution in sources such as TMC–1, or L 134N (Lee et al. 1996, Millar et al. 1997; also Chapter 9).

5.1.2. GRAIN – SURFACE CHEMISTRY

Gas phase chemistry could explain the observed relative abundances of most, but not all molecules (see e.g., the review Herbst 2000). A need for grain chemistry was early recognized, since the most abundant molecule, H_2, could not be produced in 'sufficient' quantities by the two–body gas phase mechanisms involving electrons or protons as catalysts. These reactions are quite ineffective except where the level of ionizations is unusually high (e.g., Duley & Williams 1986). It is assumed now that the hydrogen molecules form at the surfaces of interstellar grains, through several distinct steps[5] (e.g., Barlow & Silk 1976, Duley & Williams 1986). In spite having large activation barriers, many reactions proceed on grain surfaces because the long time–scale ($\sim$1 day) available for reaction between two reactive species on a grain surface before another reactant is accreted from the gas phase (Tielens & Hagen 1982).

[5] 1) Collision of an H atom with a grain, collisional rate being $k_c = 3 \times 10^{-17}\, n_g\, n(\mathrm{H})$; 2) Sticking to the grain surface and adsorption, kinetic temperatures less then 40 K are needed so the H atom will not evaporate before forming H_2; 3) Retention on the grain surface until another H atom arrives, time collision for the second H atom with the grain is less then adsorption time for the hydrogen number density of 100 $\mathrm{cm^{-3}}$ if $T_{\mathrm{kin}} \leq 15$ K; 4) H–atom diffusion to a reaction site, the upper limit for the kinetic temperature for which the H–atom still has enough time to migrate over the surface of an average sized dust grain is $T_{\mathrm{kin}} \approx 20$ K; 5) recombination to form H_2 and 6) ejection of the newly formed molecule from the grain surface, possibly in an excited state (E.F. van Dishoeck, 1998, *Astrochemistry: Lecture Notes*)

In the developing the grain-surface reactions network two methods are used: the Monte Carlo (stochastic) and the rate equation approach (Herbst 2000). In the rate equation formalism, the rate of formation of species is defined by the surface rate coefficient which is the sum of the diffusion rates of the reactant species over the entire surface of the grain. This approach is justified when large number of species are reacting on a surface (Herbst 2000). In the Monte Carlo approach gas – phase species are randomly selected to adsorb onto a grain and, once on the grain, react with other species if this is more likely then evaporation. In case when more then one reactant is available, reactions would occur according to their relative probabilities. Tielens & Hagen (1982) first used 'semi–Monte Carlo approach' where the reaction times were not randomly sampled. However, true Monte Carlo methods are very computationally time consuming and may as well require parallel architecture (Charnley 1998).

Two physical processes specially contribute to the composition and evolution of the dust in molecular clouds: i) thermal processing of ice mantles driven by e.g., nearby newly born stars; and ii) energetic processing of ices by (F)UV photons and/or cosmic – ray particles bombarding (e.g., Langer et al. 2000). When an ice mantle is heated to a temperature near its sublimation point, outgassing will occur. In mixed molecular ices where two or more components have similar concentration, but different sublimation temperatures, the evaporation of each component is largely regulated only by its own sublimation behavior: experiments (Sandford & Allamandola 1990) have shown that CO/H_2O=1/2 and CO_2/H_2O=1/1 ices show early release of CO around 25 K and CO_2 around 85 K, with a small fraction of the CO and CO_2 locked in the water ice–crystal until around 120–130 K where H_2O has phase transition. Shalabiea & Greenberg (1994) suggested that the two key processes may be the UV photoprocessing of grain mantles and the explosive desorption, cosmic rays induced or induced by grain – grain collisions. Incorporation of these two processes into models have shown improvement for more then an order of the magnitude in certain key molecule abundances: H_2O, CO_2, NH_3, H_2CO, CH_2OH.

5.2. CHEMICAL MODELS

For models for a particular environment, specification of initial chemical and physical conditions is required and two important items should be considered seriously: the abundance of the elements and the abundance of various ions which drive ion – molecule chemistry. The Solar elemental abundances (relative to hydrogen) are not representative of the ISM in general, where they appear to be generally lower (see, e.g., Table 1 in the review of Wilson & Rood 1994). Additionally, significant fraction of heavier elements seems to be incorporated into grains (e.g., Kingdon & Ferland 1997). The second point is , Of the ions present in the ISM, the C^+ ion is essential for the reactions leading to more complex hydrocarbon molecules. In diffuse clouds, and in the envelopes of dark clouds, where C^+ is available in sufficient quantities (the ionization potential is smaller then 13.6 eV), the carbon chemistry is probably initiated by the slow radiative association reaction $C^+ + H_2 \rightarrow CH_2^+ + h\nu$ which has the rate coefficient of $\approx 10^{-15}\,\mathrm{cm^3\,s^{-1}}$ (van Dishoeck 1998). In dense clouds, shielded from

the UV radiation, the amount of ionized carbon is very low, hence the C – chemistry is probably initiated through the reactions $C+H_3^+ \rightarrow CH^- \rightarrow CH_2^+ \rightarrow CH_4^+$ (see e.g., van Dishoeck 1998). The production of complex hydrocarbons occur via three types of pathways (Herbst 1995): carbon insertation reaction, condensation reactions and radiative association reactions. The carbon insertation reactions are thought to be the dominant route, the necessary carbon ions being produced in small amount through destruction of carbon monoxide by ionized helium: $He^+ + CO \rightarrow C^+ + O + He$, where He^+ production is induced by cosmic rays.

Significant enhancement of various isotopes in the low temperature interstellar clouds can occur as a result of process called 'fractionation'. An extreme example is the deuterium fractionation initiated by the isotope exchange reactions, followed by deuterium transfer reactions which lead to DCO^+/HCO^+ and DCN/HCN abundance ratios that are up to a factor of 1000 larger then the overall [D]/[H] ratio of $\sim 1.6 \times 10^{-5}$ (van Dishoeck 1998). Another example of fractionation is process that occurs where there is available carbon i.e., not all carbon is locked up in CO, when ^{13}CO is incorporated preferentially in various molecules through exchange reactions such as $^{13}CO^+ + {}^{12}CO \leftrightarrows {}^{12}CO^+ + {}^{13}CO + 36\,K$. However, in this case isotope selective dissociation of ^{13}CO tends to counteract this enhancement process. Again, the relative isotopic ratios in nearby ISM differ from those in the present day Solar system, which in turn differ from the 'protosolar' values. It is known that the isotopic ratios of C, N, O, S and Si depend on the area in the Galaxy, they are different for the Galactic center, the 4 kpc molecular ring, in the Local ISM and in the outer Galaxy (see Table 4 in Wilson & Rood 1994).

In principle, chemical models can be divided into two separate classes: those which are constrained only for gas – phase reactions, and those which extend the chemistry so the gas – grain reactions are incorporated. Recent gas – phase models (Lee et al. 1996, Millar et al. 1997) contain nearly 4000 gas – phase reactions between 400 species containing up to 13 atoms. Uncertainty of basic importance is introduced by the existence of multiple solutions of the chemical networks (Pineau des Forets et al. 1992, Le Bourlot et al. 1993, 1995a, 1995b, Shalabiea & Greenberg 1995, Lee et al. 1996, Millar et al. 1997). However, the final models will mostly depend on a particular object studied.

Gas – phase models are generally either i) steady – state, depth – dependent or ii) time – dependent, depth – independent models (van Dishoeck 1998). Models of diffuse and translucent clouds and dense photon – dominated regions (PDRs) are usually steady – state models, where the molecular abundances do not change with time, but are functions of a cloud's depth. The short time scale for photoprocesses (a few hundred years) justifies the steady – state assumption. Input parameters in these models are: the elemental abundances of C, N, O, S, and other metals..., the cosmic ray ionization rate, ζ_0 in s^{-1}, the geometry (e.g., plane – parallel, spherical, cylindrical...), the $n_H = n(H) + 2n(H_2)$ density as a function of position, the incident radiation field specified by a factor $I_{UV} \times I_{ISRF}$ (ISRF stands for the standard interstellar radiation field) and the dust parameters (the extinction curve, albedo and scattering function). A model can include one additional input parameter, constrained from the observa-

tions - the temperature of the gas and dust as a function of position in the cloud. However, the uncertainty of the most input parameters can be large. As an example, recent calculations and observations gave a range for the cosmic ionization rate of $10^{-18} \leq \zeta \leq 10^{-16}$ (Caselli 2000), larger then previously thought. The cosmic ionization rate can be determined from the relative electron abundances, $x(e)$, as (Caselli et al. 1998, 2000)

$$x(e) = \frac{2.7 \times 10^{-8}}{[\mathrm{DCO^+}]/[\mathrm{HCO^+}]} - \frac{1.2 \times 10^{-6}}{f_\mathrm{D}}, \tag{5.9}$$

where f_D is the depletion factor, and $1/f_\mathrm{D}$ is defined as the fraction of CO and O frozen onto dust grains; $[\mathrm{HCO^+}]$ and $[\mathrm{DCO^+}]$ are relative abundances. Then the cosmic ionization rate is

$$\zeta = \left[7.5 \times 10^{-4}\, x(e) + \frac{4.6 \times 10^{-10}}{f_\mathrm{D}}\right] x(e)\, n(\mathrm{H_2})\, \frac{[\mathrm{HCO^+}]}{[\mathrm{CO}]}. \tag{5.10}$$

The determination of the electron abundance is tedious: one needs measurements of the $[\mathrm{DCO^+}]/[\mathrm{HCO^+}]$ and $[\mathrm{HCO^+}]/[\mathrm{CO}]$ abundance ratios; CO depletion can be obtained from e.g., $[\mathrm{HC_3N}]/[\mathrm{CO}]$ abundance ratio (Caselli et al. 1998, Anderson et al. 1999); density and temperature structure of the core must be known. This implies accounting for the optical depth of observed lines and self–absorption effects. One approach is to observe rare isotopomers (e.g., $\mathrm{C^{17}O}$, $\mathrm{HC^{18}O^+}$, $\mathrm{D^{13}CO^+}$) in selected positions and then to use radiative transfer models to deduce physical parameters in the rest of the observed core. Typical values found for low mass dark cores are $10^{-8} \leq x(e) \leq 10^{-6}$ (Caselli 2000). Apart of the uncertainty introduced by the poorly known cosmic ray flux and metal depletion within the cores, the penetration of UV radiation deep into regions of high visual extinction due to cloud inhomogeneities and the ionization rate increase in the proximity of YSOs which may be strong X–ray emitters must be considered (Caselli 2000).

On the other side, time–dependent models are usually constructed for dark and dense molecular clouds, where the concentrations are computed as function of time at a single position deep into the cloud. In these models input parameters are: the elemental abundances of carbon, oxygen, nitrogen, sulphur and metals; the cosmic ray ionization rate ζ_0; the density (in so–called pseudo time–dependent models usually taken to be constant with time) and the visual extinction A_V at the position in the cloud. The temperature can be obtained from the thermal balance, but is usually set at 10 K for both gas and dust, temperature typical of a dark cloud shielded from UV radiation and heated by cosmic rays only. Usual assumption is that at $t = 0$ in molecular form only hydrogen appears, while the trace elements are in atomic form.

Gas–grain models consider both gas–phase and grain–surface processes (see Herbst 2000 and references therein). For gas densities larger then $10^4\,\mathrm{cm^{-3}}$, all the gas phase molecules (except $\mathrm{H_2}$, CO, $\mathrm{H_3^+}$, $\mathrm{N_2}$ and few other weakly polar molecules) should accrete onto grain surfaces in 10^5 yr, a time scale short compared to the ages of molecular clouds (Langer et al. 2000). The accretion time is defined as $\sim 2\times10^9/n_\mathrm{H} y_S$, where the sticking coefficient y_S is thought to lie between 0.1 and 1.0 (Williams 1993).

Therefore, mechanisms for returning molecules into the gas phase are an important parameter in gas – grain models. The most effective desorption mechanisms in cold molecular gas are likely to be cosmic–ray spot heating and explosive desorption caused by cosmic–rays or triggered by grain – grain collisions at velocities larger then $\sim 0.1\,\mathrm{km\,s^{-1}}$ (van Dishoeck 1998).

There are two different approaches to the modeling here (Tielens & Whittet 1997): an 'accretion limited' and a 'reaction limited' regime. In the accretion limited regime the chemistry is limited by the rate at which species are "delivered" to the grain surface, where they rapidly migrate over the surface and react. In the reaction limited regime, many reactive species are present on a grain surface and reactions are controlled by surface concentration and kinetic parameters. Most of the models have been formulated in the reaction limited regime using rate equations which mirror those used for gas – phase chemistry (e.g., Hasegawa & Herbst 1993, Shalabiea & Greenberg 1995). However, in interstellar clouds the accretion times are long, grains are small, and reactions are (usually) fast, so at most one reactive species is present on a grain at any time. The grain surface chemistry is therefore in the accretion limited regime and can be properly treated only by a Monte – Carlo method, which determines the likelihood of two such species arriving from the gas in succession onto a particular grain in a steady – state model (e.g., Langer et al. 2000).

According to the models of cold molecular clouds which include collapse (e.g., Shalabiea & Greenberg 1995, Bergin & Langer 1997), HCO^+ and N_2H^+ are good tracers of the molecular clouds' envelopes because their abundances remain high owing to the increase in the H_3^+ abundance when its main removal partners (CO, O...) are depleted onto grains. Additionally, the two molecules trace different regions: N_2H^+ traces better the outer envelope, avoiding the inner, warmer envelopes where its main partners have been returned to the gas – phase; HCO^+ being primarily destroyed by electrons, traces better the inner envelope of the cloud.

Gas – grain interactions and formation of ices can also be significant in regions recently subjected to shocks due to outflows from young stars. Bergin et al. (1998) predicted that large quantities of water vapor are produced in shocked gas. *ISO* observations of strong emission from gaseous water towards Orion BN–KL (Harwit et al. 1998) supported this result. After brief time–interval, in the cold postshock gas the abundant H_2O will condense onto the dust grain surface productions a water–dominated mantle (Bergin et al. 1998).

5.3. CHEMICAL EVOLUTION OF PROTOSTARS

Based on theoretical considerations, the chemistry around embedded young stellar objects (YSOs) is expected to be governed by the interplay between gas – phase reactions, condensations of molecules onto dust grains, grain surface reactions and evaporation of altered ice mantles near the star and in the outflow (see e.g., van Dishoeck & Blake 1998). In cold molecular cloud cores prior to star formation chemistry is dominated by low – temperature gas – phase ion – molecule and neutral – neutral reactions leading to the formation of small radicals and unsaturated molecules (e.g., CH, OH, CN, C_2H,...). During the cold collapse phase, the density becomes so

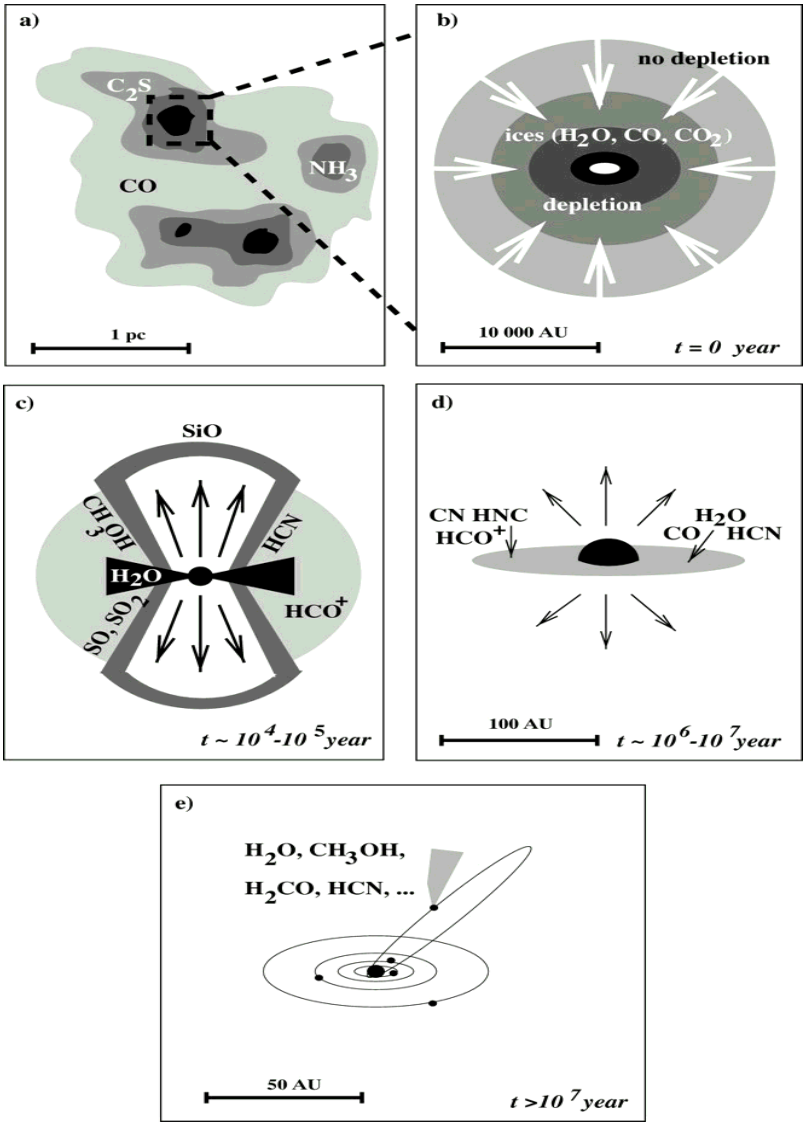

Figure 5.1: Adopted Figure 1. from van Dishoeck & Blake (1998): a schematic view of low-mass star formation. (a) Dark cloud cores, roughly 1 pc in size, gradually contract until (b) magnetic support is overcomed and inside-out collapse begins at t = 0. (c) For $\sim 10^4$-10^5 years, a phase of both high accretion and supersonic outflow occurs in deeply embedded protostars (young stellar objects or YSOs). (d) Gradual clearing by the outflow leaves only the young T Tauri star and a residual protoplanetary accretion disk, which, on time scales of 10^6-10^7 years, leads to the formation of a mature planetary system (e). Characteristic molecules at each of these stages are indicated.

high that most molecules accrete onto the grains and form an icy mantle. The chemistry is probably actively modified by grain – surface reactions through processing by UV photons, X – rays and cosmic rays. After a new star forms, its radiation begins to heat up the surrounding gas and dust and molecules evaporate back into the gas phase, with the most volatile species (CO and N_2, with the sublimation temperatures of $\sim 20\,\mathrm{K}$ and $\sim 16\,\mathrm{K}$, respectively) returned first. In addition, the outflows from the YSO(s) penetrate the surrounding envelope, creating high–temperature shocks and lower temperature turbulent regions in which the icy mantles and more refractory material containing silicon can be returned to gas. These freshly evaporated molecules can drive a rich and complex chemistry in the gas for a period of $\sim 10^5$ years until finally, the envelope is dispersed by stellar winds (van Dishoeck & Blake 1998). Figure 5.1 presents an overview of the scenario developed for the formation of a single, isolated low mass star from the collapse of a molecular cloud. However, the majority of stars are born in environments that are considerably more complex then the outlined.

One of the main long–term goals of astrochemistry is to use certain molecules as "signposts" of the evolutionary state of an object, where enhancements and decreases of their abundances compared with those in pre–star–forming clouds act as temporal indicators. This 'chemical diagnostics' can be then compared with more traditional indicators of an age, such as the development of an H II region or the size and time–scale of the outflow. Note that 'chemical age' does not necessarily measure the true age, but rather indicates the time since some dynamical–event produced an atomic–carbon rich phase, when the 'clock' was reset (e.g., van Dishoeck & Hogerheijde 1999).

The chemical evolution of star – forming region starts with the dark and dense clouds out of which new stars are born. Most of our knowledge about the chemistry is based on a detailed study (observational and theoretical/modeling) of only a few nearby ($\sim 100 - 200\,\mathrm{pc}$) dark cloud cores: TMC–1, a small ($\sim 0.6 \times 0.06\,\mathrm{pc}$) elongated dense ridge in Taurus, L 134 N (e.g., Dickens et al. 2000 and references therein), and the quiescent core L 1498 (see, e.g., van Dishoeck & Hogerheijde 1999). Suzuki et al. (1992) and Benson et al. (1998) have performed a systematic study of few characteristic molecules (C_2S, HC_3N, HC_5N, N_2H^+, NH_3) in the large set of dark cores identified by Myers & Benson (1983). The abundances of the carbon chains are found to correlate well with each other, but not with NH_3 or N_2H^+, consistent with the case of TMC–1. Ammonia was found to be more abundant in 'older cores' i.e. in cores where stars have already formed. The observed C_2S/NH_3 abundances can be reproduced quantitatively in models which start from diffuse gas and form dense cores over a period of 10^5 to $2 \times 10^6\,\mathrm{yr}$. Thus, this ratio was suggested as a particularly useful tracer of cloud evolution. The chemically differentiated onion–shell structure is very well seen in the case of, also, pre – stellar core, L 1498, where the unsaturated carbon chain molecules C_2S and CS are more abundant in the atomic–rich outer part, and NH_3 peaks in the inner region of the core (Kuiper et al. 1996, Wolkovitch et al. 1997).

Ice mantles have been observed in quiescent dark clouds through observations of field stars in Taurus and Serpens (e.g., Whittet et al. 1998). Water, carbon–monoxide and carbon–dioxide were clearly detected at abundances which indicate that up to 40% of the heavy elements may be frozen out at densities of a few $\times\ 10^4\,\mathrm{cm}^{-3}$. The

amount of solid CO is comparable to that of gas – phase CO.

Pre – stellar cores have a relatively flat density distribution on scales up to a few hundreds of parsecs. As the evolution proceeds, after the onset of the gravitational collapse, the core becomes centrally concentrated. Such cores have been recently observed in the Taurus and Ophiuchus regions (e.g., Ward–Thompson et al. 1994, Motte et al. 1998). Once collapse occurs, the increasing density and decreasing temperatures accelerate the gas – phase depletion molecules onto grain mantles, while the radiative heating and outflow from the central star act to return molecules into gas phase. Freezing out of the molecules is difficult to prove observationally, since every collapsing core has an outer envelope in which the abundances are normal and effectively mask any depletion inside (e.g., van Dishoeck & Blake 1998). Since at this deeply embedded stages the obscuration is so high that the sources are not visible even at mid–infrared wavelengths, the only probe of abundances appears to be careful modeling of the line and dust continuum data. In this way, depletion factors in different objects are estimated to be of several to more then 20 (see, e.g., van Dishoeck & Blake 1998 and references therein). Line profiles of HCO^+, CS and H_2CO were suggested to be good tracers of the collapsing envelope i.e. the evidence of infall in the earliest stages (Zhou et al. 1993, Choi et al. 1995, Gregersen et al. 1997, Mardones et al. 1997).

A combination of single dish and interferometric data is necessary to probe deeply the envelopes of more evolved embedded objects (e.g., Hogerheijde et al. 1997, 1998). The HCO^+ abundance is an excellent tracer of the inner envelope structure and mass, and in some cases it appears to be influenced by the outflow. N_2H^+, on the other hand, seems to trace preferentially the outer envelope gas in low–mass YSOs (e.g., Mardones et al. 1997). This ion may be destroyed by proton transfer to CO in dense regions where CO is not significantly condensed onto the grains (van Dishoeck & Blake 1998). Langer et al. (1996) showed that HCO^+ traces an extended circumstellar disk, whereas HCN seems to avoid the inner part. A tool for even finest distinction between the stages of the YSO evolution was suggested by Yun et al. (1999) and Park et al. (1999). The survey of 37 star-forming and quiescent dense clouds indicated that the HCN (1–0) emission strength is well correlated with the YSO's class, Class 0 and Class I being detected preferentially.

When a young star begins to heat the inner surrounding envelope by radiation and/or shocks above ∼100 K, various distinct chemical regions occur, including the so–called 'hot region', the region of interaction of the outflow with the surrounding envelope and the more extended radiatively–heated warm envelope (e.g., van Dishoeck & Hogerheijde 1999). Van der Tak et al. (1999) derived for a $\sim 10^5\,L_\odot$ source that the region where $T_{dust} \approx T_{\rm gas} > 90$ K extends to $\sim 5 - 10000$ AU, resulting in evaporation of water and methanol ices and an enhancement of the gas – phase abundances of these species by a factor of 100–1000. The region where $T > 20$ K extends to ~ 50000 AU, and while an increase in the temperature from 10 to 100 K does not have significant effects on the gas – phase chemistry, it does result in evaporation of volatile species like CO (e.g., van Dishoeck & Hogerheijde 1999). The hot gas contains high abundances of C_2H_2, HCN and CH_4 (e.g. Lahuis & van Dishoeck 2000) which are enhanced by at least 1–2 orders of magnitude compared with the outer,

colder envelope.

The chemical manifestations of the outflow generated shocks can be substantial and depend on whether the shocks are of the $J-$ or $C-$ (or jump and continuum type, respectively, see, e.g., the review Draine & McKee 1993). The type of shock that will develop depends on the shock velocity, the magnetic field strength and the fractional ionization in the pre–shocked gas. For typical ionization fraction in dense cores, at $v_s \leq 40 - 50\,\mathrm{km\,s^{-1}}$, $C-$shocks will occur. Their peak temperature of typically few thousand Kelvins is too low to dissociate molecules. However, some reactions with low energy barriers such as $O+H_2 \rightarrow OH \rightarrow H_2O$ and $S+H_2 \rightarrow SH \rightarrow H_2S$, would proceed rapidly, driving all available oxygen and sulphur into H_2O and H_2S (see, e.g., van Dishoeck & Blake 1998). In $J-$shocks the temperatures increase to several $10^5\,\mathrm{K}$, and all molecules are dissociated. In addition, UV radiation is produced, which may photodissociate molecules both in and ahead of the shocks. The molecules then reform slowly in a lengthy, warm zone in the wake of the shock. Once substantial H_2 has been reformed, the chemistry resembles that of the $C-$shocks (see, e.g., van Dishoeck & Blake 1998). Apart of the gas, grain cores and their mantles are affected by the shocks. A variety of both refractory and volatile species can be ejected into the gas phase. Enhancements of species such as OH, H_2O, SiO and SiO_2 have been observed (e.g., Blake et al. 1995). SiO is particularly increased because of the large depletion of silicon in the pre–shocked gas, making it as a good tracer of the outflows influence on the surrounding gas.

Hot–core regions have been mostly observed in the regions of high – mass star formation, where they appear to have high abundances of fully hydrogenate molecules such as H_2O, NH_3 and H_2S, along with a rich variety of complex organic molecules ranging from CH_3OH and C_2H_4, to $(CH_3)_2O$, $HCOOCH_3$ and C_2H_5CN (see the review van Dishoeck & Blake 1998 and references therein).

Finally, masers have been also widely observed to be associated with star–forming regions (see, e.g., Menten 1997 for review). H_2O masers most likely originate in outflows since they require densities of 10^7–$10^9\,\mathrm{cm^{-3}}$ and temperatures of $\sim$500 K to be excited. In contrast, the OH and class II CH_3OH masers can be generated in regions where their abundances are enhanced owing to evaporation of methanol and water from icy mantles.

Chapter 6
STARLESS DARK CLOUDS: L 1274 AND Kh 15

L 1274 is a small dark cloud with estimated area, opacity and center coordinates of $0.032\,\mathrm{deg}^2$, 4 and $\alpha = 23^h55^m$, $\delta = +70°40'$ (1950.0), respectively (Lynds 1962). Cloud no. 454 in Taylor et al. (1987) was identified as L 1274. In the ^{13}CO survey of this region by Yonekura et al. (1997) L 1274 is listed as cloud number 109 and is referred to as the 118.1+08.8 cloud. The cloud was also detected in the all–sky ^{12}CO survey of Dame et al. (1987) as one of many small clouds in the region $115° \leq l \leq 125°$, $5° \leq b \leq 15°$. Grenier et al. (1989) show a composite map of the nearby CO emission in Cassiopeia and Cepheus from the all–sky survey integrated from -8 to $+8\,\mathrm{kms}^{-1}$, where L 1274 is part of a fairly large cloud complex at $115° \leq l \leq 123°$, $6° \leq b \leq 12°$. The projected location of L 1274 is close to the peak of excess soft X–ray emission in this area (Grenier et al. 1989), possibly indicating that a shock front, associated with a supernova explosion, has passed L 1274. The orientation of the shock passage then depends on the relative distance between L 1274 and the supernova; if large it would be nearly face–on.

Kh 15 (Khavtassi 1955), located at $\ell = 122.7°$ and $b = +9.6°$ on the POSS image appears as an elongated opaque spot with size of $40' \times 20'$ near another dark cloud L 1308 (Lynds 1962). In the Atlas of Galactic Dark Clouds (Khavtassi 1960) cloud no. 216 is an E–W elongated banjo–shaped feature which includes both L 1308 and Kh 15. We investigated the most opaque western part, and the catalogue number, 15, is used accordingly. This cloud is also visible in the all–sky ^{12}CO survey of Dame et al. (1987) as a small "bright" spot, and is listed as cloud no. 473 in the ^{12}CO and ^{13}CO survey of Taylor et al. (1987). In the ^{13}CO survey of this region by Yonekura et al. (1997) Kh 15 is listed as cloud number 137. The Catalogue of Infrared Excess Clouds (Désert et al. 1988) list Kh 15 as a cold core under number 169.

6.1. DISTANCE DETERMINATION

In order to get the distance to the clouds, objective prism images of the region centered at L 1274 and Kh 15 were made with the 60/90/180 cm Schmidt telescope of the Konkoly Observatory (Piszkéstető mountain station) equipped with an UV transmitting objective prism with a refracting angle of 5° and 580 Å/mm linear dispersion at H_γ.

Classifications of the objective prism spectra were made by eye using the set of criteria of the Bonner Spectral Atlas II (Seitter 1975), by comparing our observed

spectra with the spectra set of the MK standards presented in the Atlas made with a prism that had a linear dispersion at H_γ of 645 Å/mm. Errors are estimated to ± 2 spectral subclasses, which is equivalent to $\pm 0.4^{\rm mag}$ in the distance modulus for A – type stars. In case of L 1274 we have classified total of 508 stars (B, A, F spectral type), and in case of Kh 15 768 stars, and consider our sample to be complete down to V=12 $^{\rm mag}$ (for A type stars). We assumed all stars to be main – sequence objects. Visual magnitudes of all the classified stars were taken from the HST Guide Star Catalogue CD-ROM Version 1.1. The stars were identified in the GSC using the SKYMAP software (version 2.7). We assigned absolute magnitudes, M_V, to all the classified stars using values listed by Lang (1992), and then calculated the corresponding apparent distance moduli, $\rho = m_V - M_V$.

We derive a distance of 200 ± 30 pc to L 1274 and a distance of 250 ± 25 pc to Kh 15.

6.2. DUST CONTENT

To investigate the dust properties of L 1274, we used plates extracted from the final Atlas of Sky images[6] (Infrared Survey Sky Atlas, ISSA, Wheelock et al. 1994) created from the IRAS data. IPAC (Infrared Processing and Analyzing Center) has processed these, on–line available, images to a uniform standard, with a pixel size close to 1.′5.

The L 1274 cloud has moderate Far Infrared (FIR) emission at 100μm, but lacks significant emission at 60μm, a property indicative of dense (dark) clouds (Laureijs et al. 1991, Abergel et al. 1994). Comparative analysis of the FIR, ^{13}CO and ^{12}CO data for dark cloud regions (see, e.g. Abergel et al. 1994) shows that the 100 μm excess emission, calculated as $\Delta I_{100} = I_{100} - 5 \times I_{60}$ (see Boulanger et al. 1998), is well correlated with the ^{13}CO emission. The L 1274 100 μm excess emission is spatially

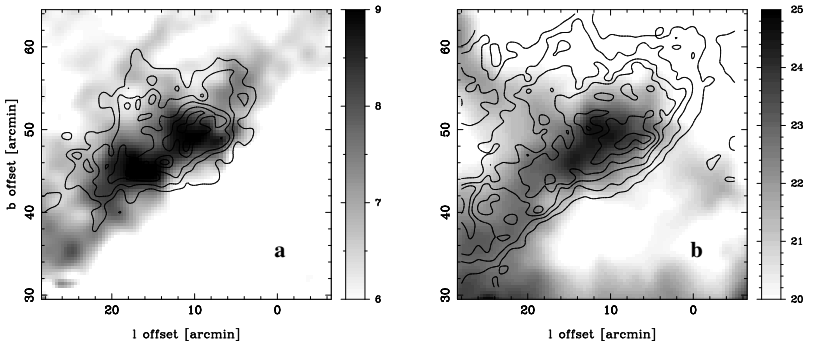

Figure 6.1: (a) The 100μm excess emission (greyscale) towards L 1274 overlayed with the ^{13}CO (1–0) contours. **(b)** The 100 μm emission (greyscale) overlayed with the ^{12}CO (2–1) contours. Greyscale is in MJy sr^{-1} units. The contour plots show the total integrated CO emission from 20% level in steps of 20%.

[6]Downloaded from the SkyView, Web version: v4.1, `http://skyview.gsfc.nasa.gov/`.

very well correlated with the ^{13}CO emission, as shown in Fig. 6.1 a. However, due to the insignificant 60 μm emission, there is also a good correlation between the ^{12}CO and the 100 μm emission, as seen in Fig. 6.1 b. The 100 μm excess emission is likely due to a decrease of the emission at 60μm, rather than the increased emission at 100 μm. This implies that the dust is composed mainly of the large grains with the radius $a \geq 0.1$ μm (Mathis 1996), with a decrease of the abundance of very small particles ($a \leq 3$ Å) stochastically heated in the densest part of the cloud.

Kh 15 was not detected at 12 and 25 μm, but at 100 μm is well resolved and shows a clumpy structure. Too study dust properties of this cloud we constructed and used a "cold dust" map, $I_{\rm cold} = 1.67 \times \Delta I_{100}$, ($\Delta I_{100}$ defined as above). The scaling factor corrects for the assumed fraction of the 100 μm emission lost in the background subtraction. $I_{\rm cold}$ is free of the radiation coming from smaller sized grains (the "cirrus component"). Therefore one can assume that the total IR emission comes from only one grain family, the big grains, with one dust temperature. As it was the case with L 1274, the Kh 15 $I_{\rm cold}$ emission is spatially very well correlated with the ^{13}CO emission, the three subcores in both maps closely following the contours of each other.

6.3. MOLECULAR GAS

Molecular gas was traced by the submillimeter radio emission. The observations were conducted at the Onsala Space Observatory's (OSO) 20–m telescope, the University of Cologne's KOSMA 3–m telescope (Kramer et al. 1998) for L 1274. For Kh 15 both listed telescopes have been used with the addition of Nagoya University's 4–m (Ogawa et al. 1990). For L 1274 we made maps on an 1′ grid in the following CO transitions: ^{12}CO 1 $\rightarrow$ 0 and ^{13}CO 1 $\rightarrow$ 0 at OSO, and ^{12}CO 2 $\rightarrow$ 1 with KOSMA. Some positions were observed in C^{18}O 1 $\rightarrow$ 0, CS 2 $\rightarrow$ 1 and HCN 1 $\rightarrow$ 0 (OSO) and ^{12}CO 3 $\rightarrow$ 2, ^{13}CO 2 $\rightarrow$ 1 and C^{18}O 2 $\rightarrow$ 1 (KOSMA). The ^{13}CO 1 $\rightarrow$ 0 map of Kh 15 was made at Nagoya with the 2′ step. Selected positions were observed also in ^{12}CO 1 $\rightarrow$ 0 (Nagoya), ^{13}CO 1 $\rightarrow$ 0 and C^{18}O 1 $\rightarrow$ 0 (OSO) and ^{12}CO 2 $\rightarrow$ 1 and ^{12}CO 3 $\rightarrow$ 2 (KOSMA).

6.3.1. CO DISTRIBUTIONS

The L 1274 CO channel maps in Fig. 6.2 and Fig. 6.3 show two distinct structures: the "main body" of the cloud emitting within the velocity range –5 to –2.5 km s^{-1} and the "ridge" seen between –2 and 0 km s^{-1}. The two structures seem to have a common origin: the channel maps in Fig. 6.2 show that the ridge follows closely the edge of the main body and the main body seems to turn gradually into the ridge, spatially as well as kinematically. This is also apparent in Fig. 6.3 which shows similar distributions for all the three CO transitions observed. Those of ^{12}CO (1–0) and (2–1) are remarkably similar with approximately the same extents. At a distance of 200 pc the linear extent of the main body is 1.5 to 2 pc as defined by the lowest (10%) contours in Fig. 6.3. In ^{13}CO(1–0) the main body is well defined while the ridge has barely any emission, indicating that the ridge consists of more diffuse gas.

In the ^{13}CO map Kh 15 appears as a 20′ $\times$ 15′ sized, NE–SW elongated cloud. At the distance of 250 pc the linear extent of the cloud is 1.0 to 1.5 pc, slightly smaller

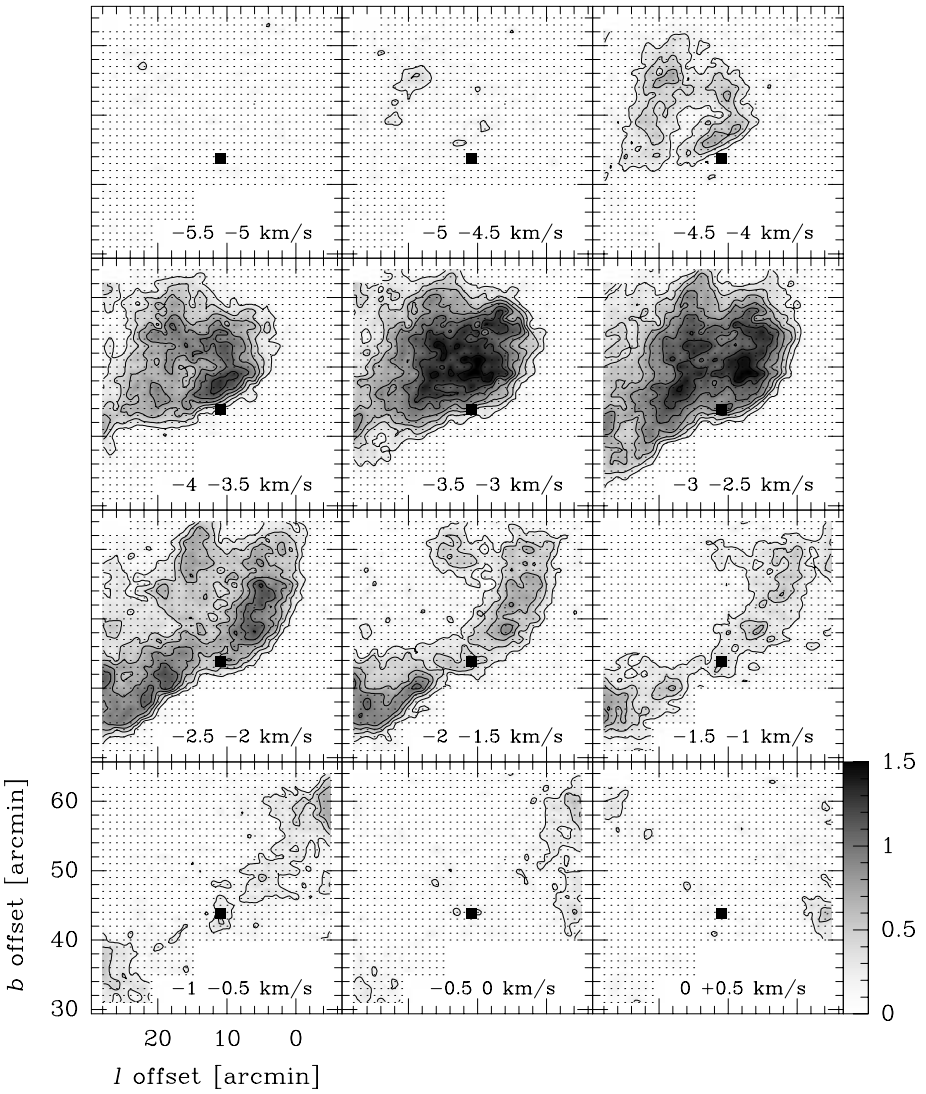

Figure 6.2: ^{12}CO (2–1) channel maps. The velocity ranges are indicated in the lower right corner of each panel. The observed positions are indicated by dots. The intensity scale is in $T_A^*\ dv$ [K km s^{-1}]. Offsets are relative to $\ell = 118.^\circ00, b = 8.^\circ00$. The square marks the position of the IRAS PS classified as a cold clump.

than L 1274. The peak $v_{\rm LSR}$ velocities show a gradient of about $0.5\,{\rm km\,s^{-1}\,pc^{-1}}$, from $3.3\,{\rm km\,s^{-1}}$ in the NE ("head front") to $2.8\,{\rm km\,s^{-1}}$ in the SW part of the cloud ("back"). Due to poorer spatial resolution of the Nagoya map (2.7′ versus OSO's 35″) and more coarse spectral resolution, channel maps could not show any distinct substructure of the total emission.

6.3.2. PHYSICS OF THE GAS

To estimate physical properties of the gas in L 1274 we mapped the central part of the cloud in the 3–2 transitions of ^{12}CO and the ^{13}CO and 2–1 transitions of ^{13}CO and C^{18}O.

Table 6.1: LTE and MEP solutions for the L 1274 observed data. R_{nk} are the ^{12}CO integrated intensity ratios of the transitions with upper levels n and k. The listed uncertainties in the derived parameters correspond to χ^2 - numbers twice those of the best fits.

		observed	LTE [1)]	MEP [2)]
$T\,(^{12}{\rm CO}1 \rightarrow 0)$	[K]	7.1 ± 0.5	6.5	7.5
$I(^{12}{\rm CO})\,/\,I(^{13}{\rm CO})$				
$1 \rightarrow 0$		3.8 ± 0.3	3.7	3.8
$2 \rightarrow 1$		3.3 ± 0.4	2.9	3.8
$3 \rightarrow 2$		10.0 ± 2	6.0	10.0
R_{21}		0.70	0.78	0.80
R_{31}		0.65	0.57	0.54
$N(^{13}{\rm CO})\,/\,N({\rm C}^{18}{\rm O})$				
$1-0$		9.4 [2)]	10.9	10.4
$2-1$		7.8 [2)]	9.6	8.5
$N(^{12}{\rm CO})$ [4)]	$[10^{17}{\rm cm^{-2}}]$		4 ± 1	2.5 ± 0.5

[1)] T_{ex}=10 ±2 K, $\langle\tau_{13}\rangle$ = 0.32; 0.43; 0.19 for the (1–0), (2–1) and (3–2) transitions, respectively; [2)] $T_K = 11 \pm 1\,{\rm K}$, $n_{\rm H_2} = 5^{+5}_{-2} \times 10^3\,{\rm cm^{-3}}$; [3)] Integrated intensity ratio; [4)] $N(^{12}{\rm CO})/N(^{13}{\rm CO}) = 75$ assumed.

In Table 6.1 we present the results of an LTE and a non-LTE analysis of our data. The latter analysis uses a statistical-equilibrium excitation and radiative transfer (mean escape probability approximation, MEP) code assuming a spherical cloud with constant temperature and density (a model developed by J.H. Black and described in e.g., Jansen et al. 1994). In the LTE assumption we have used the following relations:

$$T = \eta[J(T_{ex}) - J(T_{\rm bg})](1 - e^{-\tau}), \tag{6.1}$$

where η is the beam efficiency, τ the optical depth, T_{ex} is the excitation temperature, $T_{\rm bg}$ is the cosmic background radiation (2.73 K) and

$$J(T) = \frac{h\nu}{k}(e^{\frac{h\nu}{kT}} - 1)^{-1}, \tag{6.2}$$

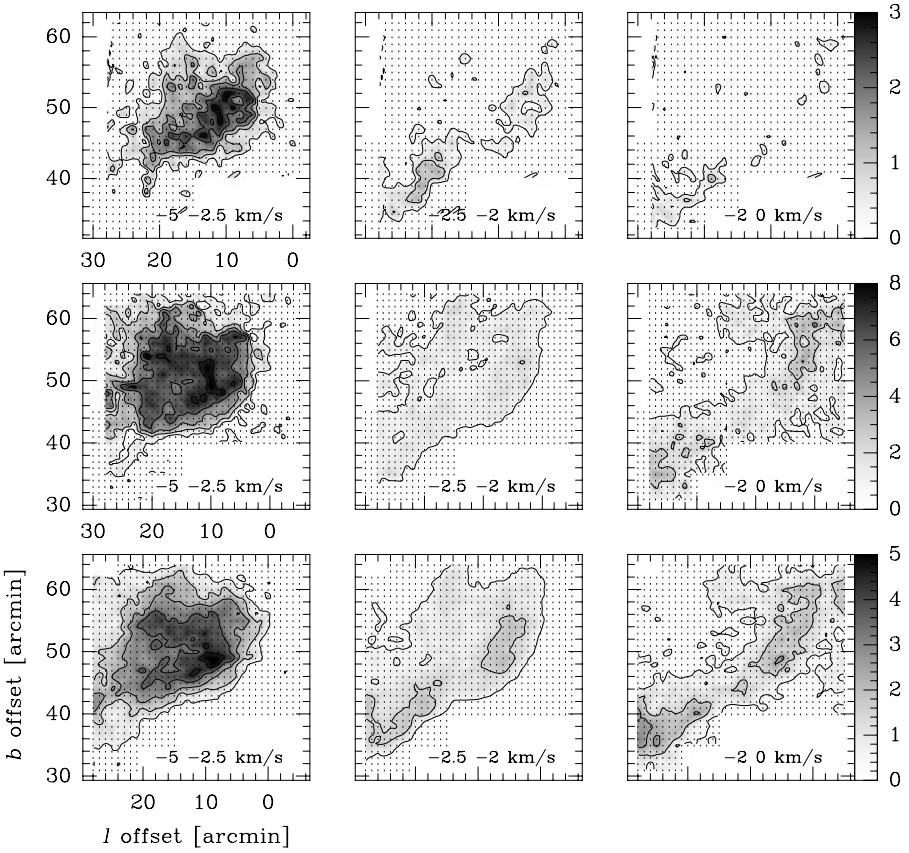

Figure 6.3: CO channel maps. The velocity ranges are indicated in the lower right corner of each panel. **First row**: ^{13}CO (1–0) maps, contours from 0.3 by 0.6 to 3.0 K km s^{-1}; **second row**: ^{12}CO (1–0) maps, contours from 0.8 by 1.6 to 8.0 K km s^{-1}; **third row**: ^{12}CO (2–1) maps, contours from 0.5 by 1.0 to 5.0 K km s^{-1}. The observed positions are indicated by dots. The intensity scale is in T_A^* dv [K km s^{-1}]. Offsets are in arcminutes relative to $\ell = 118^\circ 00, b = 8.^\circ 00$.

where h is the Planck and k is the Boltzmann constant, and ν is the frequency of the transition. For the ^{13}CO column density, N_{13}, we have used the LTE formula for linear rotors (see e.g. Heikkilä et al. 1999) corrected by the optical depth

$$N_{13}[\mathrm{cm}^{-2}] = 4.72 \times 10^{13} \, \frac{T_{ex} e^{5.3/T_{ex}}}{1 - \frac{J(T_{\mathrm{bg}})}{J(T_{ex})}} \, \frac{\langle \tau_{13} \rangle}{1 - e^{-\langle \tau_{13} \rangle}} I_{13}, \tag{6.3}$$

I_{13} is the integrated antenna temperature [K km s^{-1}] divided by the beam efficiency and $\langle \tau_{13} \rangle$ is the optical depth in the ^{13}CO line, determined from the ratio of the

observed ^{12}CO and ^{13}CO integrated intensities. In this sense, $\langle\tau_{13}\rangle$ is a weighted average over the line profiles and thus more appropriate than the peak value when calculating column densities. To derive $\langle\tau_{13}\rangle$ and T_{ex}, we assume that the excitation temperatures are equal for ^{12}CO and ^{13}CO.

The MEP - solution for CO gives $n_{\rm H_2} \sim 5{\times}10^3\,{\rm cm^{-3}}$. However, in surveying the cloud we have detected some high density gas tracers - CS and HCN, indicating gas densities $> 10^4\,{\rm cm^{-3}}$. The MEP solution for HCN, assuming $T_{\rm kin}$=10 K, gives $n_{\rm H_2} \approx 5{\times}10^4\,{\rm cm^{-3}}$ and an HCN column density of $10^{12}\,{\rm cm^{-2}}$.

Kh 15 data were analyzed in more simple way. Using only the LTE approximation, with assumed uniform excitation temperature throughout the cloud, kinetic temperatures and ^{13}CO column densities were estimated. Setting the clouds boundary at the 6σ level i.e., the contour of the ^{13}CO integrated intensity emission of $0.5\,{\rm km\,s^{-1}}$, the average ^{13}CO column density is $N_{13} = 0.8 \times 10^{15}\,{\rm cm^{-2}}$, and corresponding hydrogen column density, using the $N_{\rm H_2}/N_{13} = 1.2 \times 10^6$ conversion factor (Tóth et al. 1995, Harjunpää & Mattila 1996), $N_{\rm H_2} = 0.96 \times 10^{21}\,{\rm cm^{-2}}$. The average CO column density and molecular hydrogen column density in the core are $2.3 \times 10^{15}\,{\rm cm^{-2}}$ and $2.76 \times 10^{21}\,{\rm cm^{-2}}$, respectively. An average number density was derived by dividing the peak column density value with the geometrical mean of the major and minor diameters of the cloud/core. The resulted values place Kh 15 among dark clouds: the average number density of hydrogen molecules for the whole cloud is $0.3 \times 10^3\,{\rm cm^{-3}}$, and for the core alone $n_{\rm H_2} = 1.3 \times 10^3\,{\rm cm^{-3}}$, with peak density of $7 \times 10^3\,{\rm cm^{-3}}$.

6.3.3. MASS ESTIMATES

In Table 6.2 we present mass estimates for L 1274 resulting from different methods.

`A.` The virial mass estimates are based on the relation (Johansson et al. 1998)

$$M_{\rm vir} = 150\; d\; \Delta v^2\; [M_\odot] \tag{6.4}$$

where d [pc] is the diameter of the cloud as defined by the half intensity contour of the CO emission and Δv [km s^{-1}] is the full halfwidth of the global line profile of the cloud. More specifically, the diameter is determined by fitting a two-dimensional Gaussian function to the observed intensity distribution and use the resulting harmonic mean of the major and minor axis extents.

`B.` With a CO-to-H_2 conversion factor of $1.9 \times 10^{20}\,{\rm cm^{-2}}\ ({\rm K\,km\,s^{-1}})^{-1}$ (Strong & Mattox 1996) and a correction for helium of 36% by mass, the total gas mass estimated from the CO(1–0) data is

$$M_{\rm x} = 4.35\; L_{\rm CO}\ [M_\odot] \tag{6.5}$$

where $L_{\rm CO}$ is the CO – luminosity in units of ${\rm K\,km\,s^{-1}\,pc^2}$.

`C.` A third estimate, from the ^{13}CO emission, uses the ratio $[{\rm H_2}]/[^{13}{\rm CO}] = 4.8{\times}10^5$ (Dickman & Clemens 1983).

As seen in Table 6.2 the virial masses derived are a factor of 3 – 17 higher than other mass estimates. A similar difference between virial masses and masses derived from the CO-to-H_2 conversion factor is typical for high-latitude molecular clouds (HLCs), a fact explained in terms of deviations from gravitational virial equilibrium (see e.g. Heithausen 1996). Analysis has shown that the main body has properties more similar

Table 6.2: Estimates of distance and mass of the main body in L 1274. The distance derived from the Wolf (Wolf 1923) diagram is 200 pc, which we have adopted for all mass estimates. At this distance, $10'$ corresponds to a linear size of 0.58 pc. The error estimates are formal 1σ uncertainties. For the virial masses the uncertainties in the diameters and linewidths contribute roughly equally. In the other mass estimates, the absolute intensity scale uncertainty is the dominant factor.

		$CO(1-0)$	$^{13}CO(1-0)$	$CO(2-1)$
Δv	[km s^{-1}]	1.51	1.12	1.65
d [1)]	[arcmin]	18.6	12.0	17.7
r [2)]	[arcmin]	14	10	13
D [3)]	[pc]	190	160	230
M_{vir}	[$M_\odot$]	370 ± 30	130 ± 8	420 ± 35
M_x [4)]	[$M_\odot$]	45 ± 4		
M_{13} [5)]	[$M_\odot$]		25 ± 2	
n_{H_2} [6)]	[cm^{-3}]	320	460	

[1)] Diameter of the emission (50% contour); [2)] Radius of the emission (10% contour); [3)] Distance determined from the size – line width relation by Solomon et al. (1987); [4)] Mass estimate using a CO – to – H_2 conversion factor of 1.9×10^{20} cm^{-2}(K km s^{-1})$^{-1}$ (Strong & Mattox 1996); [5)] Mass estimate assuming $[H_2]/[^{13}CO] = 4.8 \times 10^5$ (Dickman & Clemens 1983); [6)] Mean density in a volume of radius r.

to ordinary dark cloud cores e.g., the mean density of H_2 within a volume of radius r is at least an order of magnitude larger than typical for HLCs (Heithausen 1996); the volume filling factor of the molecular gas larger by a magnitude than observed in HLCs i.e., about 10% for L 1274 and less than 1% for HLCs (Heithausen 1996).

We have also estimated the mass of the ridge component from the ^{12}CO and ^{13}CO luminosities in the same way as for the main body. We find $25\,M_\odot$ and $3.5\,M_\odot$ from the CO-to-H_2 conversion factor and the $[H_2]/[^{13}CO]$ ratio, respectively. Although highly uncertain due to the weak ridge emission and blending by the main body component, this large difference in the two mass estimates might be a result of isotope selective photodissociation of the CO gas, provided that the density in the ridge is low. Support for low gas densities in the ridge comes from the weak CO emission itself, as well as high $^{12}CO/^{13}CO$ intensity ratios (a factor of 2 higher than in the main body). Thus, our data indicate that the ridge has different properties, notably more dilute gas, than the main body.

Again, more simpler analysis/mass estimate was done in the case of Kh 15 cloud: using the derived average molecular hydrogen number density and the predefined extent of the ^{13}CO emission, knowing the distance to the cloud, the total gas mass of the cloud is 34 $M_\odot$, and for the core alone 16 $M_\odot$. If we assume that the full halfwidth of the global line profile of the cloud is similar to the average full halfwidth of the ^{13}CO emission area, than virial masses can be estimated to be 2–4 times larger than the CO-derived masses.

6.3.4. UNCERTAINTIES ON THE DERIVED MASSES

As noted in the previous section, the large virial masses relative to other mass estimates for the main body of L 1274 point to an object with properties similar to HLCs while the mean density is more in accordance with that of dark cloud cores. This mass difference can be removed by assigning a larger distance to the cloud, since the virial mass is proportional to the distance while the other mass estimates relate to the distance squared. Thus, a distance larger by a factor of 5 (^{13}CO data) or about 9 (^{12}CO) would result in similar masses and a mean density closer to what is observed in HLCs. At such distances, however, the cloud would not be detectable by star counts. Another possibility is of course that we underestimate the mass derived from the ^{12}CO and ^{13}CO data by an order of magnitude. For example, Boulanger et al. 1998) find such deviations between masses calculated from the CO–to–H_2 conversion factor and those derived from 100 μm data, for some small clouds in the Chamaelon complex, although the two mass estimates agree satisfactorily in the region as a whole. They attribute the differences to a CO deficient gas component, characterized by 100 μm emission with warm IRAS color (excess of 60 μm emission), while clouds with low 60/100 μm flux ratios are better traced by CO. With respect to IRAS colors, L 1274 resembles the latter category, possibly indicating that our mass estimate from ^{12}CO suffers from an error less than an order of magnitude.

Our mass estimate from the ^{13}CO data relies on an [H_2]/[^{13}CO] ratio of 4.8×10^5 (Dickman & Clemens 1983), determined from a relatively large sample of local dark clouds (Dickman 1978) taken from the Lynds (1962) catalog. Their sizes, opacity classes and kinetic temperatures (Dickman 1978) are similar to those of L 1274. In this sense, the applied [H_2]/[^{13}CO] ratio should be quite reliable. Whether L 1274 is an extreme case in any other properties, like e.g. CO depletion or line saturation, is harder to decide. In an attempt to reveal such effects we have used the ratio of the H_2 column densities as derived by the CO–to–H_2 conversion factor (Strong & Mattox 1996) and a [$C^{18}O$]/[H_2] ratio of 1.7×10^{-7} (Frerking et al. 1982):

$$\frac{N(\mathrm{H_2})_{\mathrm{CO}}}{N(\mathrm{H_2})_{\mathrm{C^{18}O}}} = \frac{1.9\times10^{20}\,I_{\mathrm{CO}}}{5.9\times10^{6}\,N_{18}} = 0.32\times10^{14}\,\frac{I_{\mathrm{CO}}}{N_{18}}, \tag{6.6}$$

where I_{CO} is the velocity integrated ^{12}CO emission in K km s^{-1} and N_{18} is the $C^{18}O$ column density in cm^{-2}. Since this ratio, in most cases, involves an optically thick and thin line, it should be sensitive to physical and chemical (e.g. CO depletion or isotope selective processes) properties deviating from the "typical" case. To isolate a few cases (assuming that the CO isotopic ratios remain constant): i) if the CO gas is depleted, the $C^{18}O$ column density scales directly with the depletion while the saturated ^{12}CO emission ($\sim 1-e^{-\tau_{\mathrm{CO}}}$) is less affected, implying a ratio > 1 and, (ii) if the ^{12}CO line is saturated to an extraordinary level, some fraction of the gas is missed in ^{12}CO giving a ratio < 1. Applying formula (6.6) to the observed ^{12}CO (1–0) and $C^{18}O$ (1–0) data in the center position of L1274 (Table 6.1) we find a factor of 1.2, i.e., a close agreement between the two H_2 column density estimates. To compare, we have chosen a well–studied dark cloud where several tracers indicate more extreme conditions: the dense, starless and collapsing core of L 1544 (see, e.g., Tafalla et al. 1998, Caselli et al. 1999). High density tracers, e.g. the CS(2–1) line, show the typical double-peaked line shapes

indicative of matter infall (note that the CS(2–1) line observed towards L1274 lacks any tendency of a secondary peak). The ^{12}CO (1–0) line is extremely saturated with an estimated optical depth of ∼400 (Tafalla et al. 1998); the corresponding optical depth in L 1274 is an order of magnitude lower (Table 6.1). Using the CO isotope data in Tafalla et al. (1998), formula (6.6) gives a ratio of 0.3 for L 1544, at least an indication to question the mass estimates. It is interesting to note that Caselli et al. (1999) estimate from C^{17}O and 1.3 mm continuum observations, that the CO gas is depleted by a factor of 10 in L 1544. If so, the CO–to–H_2 conversion factor underestimates the H_2 content by a factor of 30 in this core. Note, however, that this is likely not due to the suggested CO gas depletion but to the extreme saturation of the ^{12}CO line.

The discussion above indicates that the L1274 cloud has similar properties as the cloud sample for which the [^{13}CO]/[H_2] ratio is defined. Furthermore, all CO isotopes observed here give H_2 column densities which agree closely, lending support to our mass estimates.

6.4. L 1274: A SHOCK – CLOUD CLOSE ENCOUNTER

From the ^{13}CO survey of the Cep – Cas region Yonekura et al. (1997) also find high $M_{\rm vir}/M_{13}$ ratios for clouds with $M_{13} \leq 100\,{\rm M}_\odot$. They estimated the external pressure in this region to $P_{\rm ext}/\,k \sim 10^5\,{\rm K\,cm^{-3}}$. This pressure is high enough to bind most of the clouds in their sample, except maybe the smallest ones. For L 1274, using the M_{13} mass estimate, we find that the pressure required to bind the main body is $\sim 10^{4.5}\,{\rm K\,cm^{-3}}$. This indicates that the main body might be pressure confined.

In any case, L 1274 and other clouds of similar properties are apparently not gravitationally bound. This suggests that they are, either, formed by another process than gravitation, or, disturbed by some internal or external process. Both cases might be explained by the passage of a shock front. In the former case, the shock front triggers the formation of a cloud, which, if gravitation does not take over, eventually evaporates. In the latter case, the shock front injects energy to the cloud, which may be seen, e.g., in form of increased turbulence. Support for a passage of a shock front comes from the channel maps in Fig. 6.2 and Fig. 6.3 which indicate that the main body and the ridge component are related. In this scenario the ridge is an expanding low density feature that comes from the outer layers of the main body.

The question is, also, whether an external disturbance such as a shock wave is consistent with the observed IRAS colors. In the warm diffuse interstellar medium high speed shocks ($50 < v_s < 200\,{\rm km\,s^{-1}}$) change the grain size distribution towards smaller grains (e.g., Jones et al. 1996), which should decrease the 100 μm/60 μm ratio. The situation is less clear for dense clouds and slow shocks. Draine et al. (1983) have studied MHD shocks in molecular clouds with preshock densities $n_{\rm H} \approx 10^4 - 10^6\,{\rm cm^{-3}}$ and speeds in the range 5–50 $\rm km\,s^{-1}$. Magnetic fields enhance the sputtering of grain mantles, thus requiring shock waves of only $v_s \geq 25\,{\rm km\,s^{-1}}$ for H_2O ice mantles to be substantially eroded. Refractory grain cores, however, have binding energies an order of magnitude larger than H_2O and will be almost unaffected by sputtering at these shock speeds (Draine et al. 1983). This model does not include grain-grain

collisions which could change the size distribution of the grains. Observationally, one possible example of a dense cloud//slow shock collision is the ρ Ophiuchi cloud where two distinct regions are found: a low-density, less depleted, predominantly atomic preshock gas and a predominantly molecular, more depleted postshock gas (Meyers et al. 1985). On the basis of UV and optical studies they inferred the presence of a shock wave with a velocity of about $10\,\mathrm{km\,s^{-1}}$ and traced the origin to a $\sim 10^6$ yr old SNR (Sancisi 1974). The age of the SNR is sufficient for grain enlargement to occur in the postshock gas (Meyers et al. 1985). They concluded that a low – velocity shock enhances grain growth in the postshock gas probably through some combination of accretion and coagulation, resulting in a grain distribution in which there is an excess of large grains and a deficiency of very small grains. Thus, a low velocity shock seems to be consistent with the observed $100\,\mu$m excess emission in L 1274.

The projected position of L 1274 is in a region of two cataloged FIR loops: inside GIRL 116+10 and at the periphery of GIRL 120+11 (abbreviation "GIRL" stands for Galactic (F)IR Loop; Kiss et al. 2003, in preparation). Such loops are thought to trace dust and gas swept out by supernova explosions or strong stellar winds. If any of these loops has affected L 1274, the latter is the better candidate for geometrical reasons, provided that the ridge is an extension of the main body. This is, however, very speculative. On the other hand, L 1274 seems to be in a rather violent area as indicated by soft X – ray excess radiation, lack of CO emission and presence of radio-continuum loops. A scenario where a shock front from an old supernova explosion has already passed L 1274 is possible. For example, the center and the estimated distance to the center of Loop III (Berkhuijsen 1971, 1973) and the position and distance of L 1274 are consistent with passage of a SN-induced shock front during the last 10^6 years. Assuming that the ridge has been swept away, the relative motions of the main body and the ridge in the radial direction are also consistent with this scenario (i.e. the ridge has gained some positive peculiar velocity relative to the main body).

Indications of internal disturbances are harder to find. Our data show that the main body is cold with no optical or IR signs of strong activity. No large-scale motions like contraction or rotation are evident. There is a weak IR source at the edge of the main body (see Fig. 6.2), classified as a cold clump. However, the location of this source seems to correlate more with the ridge properties than those of the main body: the weakest CO emission (Fig. 6.3), the highest ^{12}CO (1–0)/^{13}CO (1–0) and the lowest ^{12}CO (2–1)/^{12}CO (1–0) ratios of the ridge are found close to the IR source. The geometry of the ridge combined with the location of the IR source resembles a bipolar flow. As noted is also, possibly, a small velocity gradient along the ridge, consistent with an almost face – on flow. Interpreted in this way, the ridge emission might then be the result of low mass star formation at the edge of the main body. Anyway, the main point of this discussion is that any internal activity (core collapse or star formation), which could explain the difference between our mass estimates, seems to be absent.

If we consider all the collected data, from the optical to the radio domain, we find that an external disturbance, e.g. interaction with a shock front induced by supernova explosion(s), which, either, disturbed an existing cloud, or, triggered the formation of it, is plausible. The ridge might be a consequence of such a passage.

6.5. KH 15: YET ANOTHER SURVIVOR?

The large-scale structure of the interstellar dust in the direction of Kh 15 suggested that this cloud might be associated with a $\sim 7^\circ$ diameter loop/shell GIRL 126+10 (Kiss et al. 2003, in preparation). On the 100 μm image of the Kh 15 region this loop appears to run through Kh 15 on the south–western side, Kh 19 in the west–northwest, L 1333 (north–northeast) and Kh 20 in the south. Moreover, the line that connects Kh 15 and the neighboring dark cloud L 1308 points straight to the center of this hypothetical loop $\ell \approx 126^\circ$, $b \approx 10^\circ$.

The question is whether this FIR loop is a real structure, and if it is, is Kh 15 physically connected to it or the apparent connection is only due to the clouds' projection on the sky. To answer the first question we have looked at the H I velocity channel maps from Hartman & Burton (1997). The principal component analysis shows that this loop is the most significant structure in the velocity interval $1\,\mathrm{km\,s^{-1}} \leq v_{\mathrm{LSR}}(\mathrm{H\,I}) \leq 5\,\mathrm{km\,s^{-1}}$. The 21 cm radiation is well correlated with the 100 μm FIR emission (Kiss et al. 2003, in preparation). With this we may safely accept that the GIRL 126+10 is a real structure.

An answer to the second question may be established through precisely estimated distances to the various parts of the loop. From the Schmidt plates we were able to determine the distance to the NW–part of the loop, Kh 19 and L 1308. The distance to L 1308 is estimated to around 150 pc, and to the NW part of the GIRL 126+10 and at the same time Kh 19 the estimated distance is 200 ± 20 pc (Kiss et al. 2000). Furthermore, the distance to L 1333 is 180 pc (Obayashi et al. 1998). The first possibility is that Kh 15 is a background cloud, only projected on the loops's periphery but in reality about 25–50 pc away from it. On the other side, if Kh 15 is part of the FIR loop, than the loop is tilted projection of a shell, whose closest part is at the distance of about 180 pc and the furthest part at the distance of around 250 pc (with 25 pc uncertainty). In this case, Kh 15 has probably collided with a shock front some time in the past. Support for this may come from the dust properties of the cloud and the argument runs along the very same lines as it was the case in L 1274. However, contrary to L 1274, there were no large discrepancies in mass estimates for Kh 15.

Assuming the microturbulent velocity field to be homogenous and isotropic and to have Gaussian distribution, the three–dimensional velocity dispersion of the mean gas particle in the ^{13}CO cloud area is:

$$\sigma_{\mathrm{obs}} = \sqrt{\sigma^2_{\mathrm{therm}} + \sigma^2_{\mathrm{turb}}} = \sqrt{3\Big[\frac{kT}{\bar{m}} + \Big(\frac{\Delta v^2}{8\ln 2} - \frac{k\,T}{m}\Big)\Big]}, \tag{6.7}$$

where k is the Boltzmann constant, $\bar{m}$ is the mean gas particle mass, Δv is the observed full width half maximum ^{13}CO line width corrected for instrumental and opacity line broadening and m is the mass of the ^{13}CO molecule. On the other hand, we can also determine the velocity dispersion of the gas which corresponds to the virial theorem. If the molecular gas motions of the cloud are governed solely by gravitation, than the virial theorem for a stationary cloud is

$$M\,\sigma^2_{\mathrm{vir}} = A\,\frac{G\,M^2}{R}, \tag{6.8}$$

where M is the cloud mass, G is the gravity constant, R is the (effective) cloud radius and A is a constant dependent on the cloud geometry and density structure. Our data give $\sigma_{\rm vir} = 0.37\,{\rm km\,s^{-1}}$ and $0.48\,{\rm km\,s^{-1}}$ for a homogeneous and centrally condensed ($\rho \propto R^{-2}$) sphere, respectively. The typical observed ^{13}CO line width in the core is $\Delta v = 0.80\,{\rm km\,s^{-1}}$, or corrected for the opacity effects $\Delta v = 0.65\,{\rm km\,s^{-1}}$, thus giving $\sigma_{\rm obs} = 0.55\,{\rm km\,s^{-1}}$. The ratio $\sigma_{\rm obs}/\sigma_{\rm vir}$ is close enogh to 1 to imply that the cloud is probably in gravitational virial equilibrium.

If we take into account the external pressure, the analysis can be repeated following e.g., Spitzer (1978). We assumed spherical symmetry and uniform external pressure. Magnetic fields or rotation of the cloud were neglected. The dynamical "temperature" of a ^{13}CO core is the Doppler temperature corresponding to the line width of the ^{13}CO emission at the peak:

$$T_D = \frac{\bar{m}\,\Delta v^2}{k\,8\ln 2}, \tag{6.9}$$

where $\bar{m}$, Δv and k are defined in the previous paragraph. The full virial theorem is then written as

$$4\,\pi\,R^3\,P_{\rm ext} = 3\,k\,\frac{M\,T_D}{\bar{m}} - 3\,G\,\frac{M^2}{5\,R}, \tag{6.10}$$

where M is the mass (here of the ^{13}CO core). The external pressure $P_{\rm ext}$ is given for the ideal gas as follows:

$$P_{\rm ext} = n_{\rm ext}\,k\,T_{\rm ext}, \tag{6.11}$$

where $n_{\rm ext}$ and $T_{\rm ext}$ are the number density and temperature at the edge of a ^{13}CO core, respectively. We assumed $n_{\rm ext} \approx n_{\rm cloud} = 300\,{\rm cm^{-3}}$ and $T_{\rm ext} \approx T_D = 39\,{\rm K}$. With the derived $P_{\rm max} = 1.9 \times 10^{-12}\,{\rm N\,m^{-2}}$ and $P_{\rm ext} = 3.4 \times 10^{-13}\,{\rm N\,m^{-2}}$, and $R > R_{\rm min} = 0.16\,{\rm pc}$ we conclude that Kh 15 is in stable equilibrium. However, if we consider the average external pressure in the Cep – Cas region estimated by Yonekura et al. (1997) of $P_{\rm ext}/k \sim 10^5\,{\rm K\,cm^{-3}}$ to be valid for Kh 15 as well, the cloud appears to be in unstable equilibrium.

New line measurements of different transitions and maps with better spatial and velocity resolution are necessary to distinguish whether Kh 15 has been subjected to a shock front of unknown origin with very weak legacy of the collision.

Chapter 7
L1251: A DARK LOW–MASS STAR FORMING CLOUD

The dark cloud L 1251 (Lynds 1962) has an estimated SFE[7] as high as 30% (Kun & Prusti 1993; KP). Both location and cloud morphology suggest that external trigger(s) contributed to the on – going star formation. This cometary – shaped cloud, at a distance of 300 pc (KP), lies on the Eastern boundary of the Cepheus cloud complex, with the "head" turned towards the center of the Cep – Cas Void (Grenier et al. 1989). At least two supernovas have exploded in this area within the last $\sim 10^6$ years, as indicated by the presence of a major radio – continuum loop, Loop III (Berkhuijsen 1971) and a runaway star HD203854, whose space velocity suggests that it might have been a companion of a supernova some $5 \times 10^5 - 10^6$ years ago (Kun et al. 2000). The Cep – Cas Void is suggested to be created by a third SN (Grenier et al. 1989). However, the estimated age of 10^4 yr means that this SN is much too young to have affected the star forming processes observed now.

Detected Hα stars in the vicinity of the cloud (Kun 1982) and seven embedded YSO candidates (KP) indicate that the cloud is an active low – mass star formation site. Summary of the embedded YSOs and PMS stars in L 1251 is given in Table 7.1. Of the YSOs, IRAS 22376+7455 and IRAS 22343+7501, classified as Class I YSOs (Mardones et al. 1997) apparently power two detected CO outflows (Schwartz et al. 1988, Sato & Fukui 1989, Sato et al. 1994). Herbig–Haro objects (Balázs et al. 1992, Alten et al.1997, Eiroa et al. 1995) and H_2 masers (Tóth & Walmsley 1994, Wilking et al. 1994, Xiang & Turner 1995, Claussen et al. 1996, Tóth & Kun 1997) are observed in their vicinity.

NH_3 and CS are among the most commonly used tracers of dense and cold molecular material. Tóth & Walmsley (1996; TW) surveyed the $C^{18}O$ cores areas defined by Sato et al. (1994) in L 1251. The $C^{18}O$ cores are named from "A" to "E" in increasing RA direction, while TW identified three core groups, "head", "north" and "tail", following the morphology of the cloud. The ammonia "head" group of cores corresponds to "core E", group "north" to "core C" and the "tail" group to "core A".

Apart of ammonia and CS, good tracers of the dense gas in molecular clouds are the isomeric molecules, HCN and HNC, whose J=1–0 transitions have critical densities as high as $10^6\,\mathrm{cm}^{-3}$. Both molecules are commonly observed in interstellar clouds.

[7]Star Forming Efficiency, SFE, is defined as $M_{star/YSO}/(M_{star/YSO}+M_{gas})$, where M_{gas} is total gas mass of the molecular cloud.

Moreover, a recent survey of 37 star-forming and quiescent dense clouds indicated that the HCN (1–0) emission strength is well correlated with the YSO class (Yun et al. 1999).

7.1. OBSERVATIONS

We used the Onsala Space Observatory's (OSO) 20–m telescope over five observing sessions in 1998, 1999 and 2000 to map the cloud in the HCN (1–0), HNC (1–0), CS (2–1) and HCO^+ (1–0) transitions. Selected positions were subsequently observed in ^{13}CO (1–0), $C^{18}O$ (1–0), $H^{13}CN$ (1–0), $HN^{13}C$ (1–0), $H^{15}NC$ (1–0), $C^{34}S$ (2–1), SO ($2_1 - 1_1$), CH_3CCH ($5_K - 4_K$), $H^{13}CO^+$ (1–0) and $HC^{18}O^+$ (1–0). The receiver was a SIS mixer with a typical T_{rec}=100 K (SSB) in the frequency range used. We used a 1600–channel correlator with 20 MHz bandwidth (i.e a velocity resolution of 0.04 km s^{-1} at 90 GHz). The HPBW of the telescope at 90 GHz is 45″ and the main beam efficiency is 0.6. The pointing was checked by observing several SiO maser sources and we estimate the pointing uncertainty to be about 3″ r.m.s. in Az and El. The observations were made in frequency (the main isotopes) and double beam switching mode (the rarer isotopes). The chopper–wheel method was used for the calibration, and the intensity scale is given in terms of T_A^*. We used mostly a grid point spacing of 30″, however, occasionally 60″ step was used. The data were reduced using the XS[8] package.

Table 7.1: YSOs and T Tau candidates in L 1251 (see Fig. 7.1). Compiled from Kun & Prusti (1993) and Kun (1998).

No.	Name IRAS	F_{12} [Jy]	F_{25} [Jy]	F_{60} [Jy]	F_{100} [Jy]	$L_{\rm IRAS}$ $L_\odot$	$L_{\rm bol}$ $L_\odot$	Classification
4	22290+7458	<0.277	0.375	0.734	<9.090	>0.20		YSO
5		<0.060	<0.050	0.84				YSO?
6		<0.060	<0.040	0.79				YSO?
8	22343+7501	4.970	26.100	66.300	80.000	23.60	27.98	Class I YSO
9	22350+7502	0.362	0.655	<0.400	<80.000	>0.39		H_α
13		<0.270	0.510	<9.210				?
14	22376+7455	0.799	5.550	32.300	66.800	10.28	13.93	Class I YSO
15		0.16	0.50	<8.23				YSO?
16		0.12	0.26	<7.110				H_α
17	22385+7457	0.309	0.330	<1.034	<29.290	>0.28		H_α

7.2. THE MAPS

The HCN and HNC (1–0) integrated intensity maps are shown in Fig. 7.1, and the corresponding CS (2–1) and HCO^+ (1–0) maps are shown in Figs. 7.2 and 7.3, respectively. The area mapped in HNC and HCN covers the two ammonia cores in the "head" designated as "H1" and "H2" by TW, the northern part of L 1251, and the cores "T1", "T2" and "T3" in the tail. All these ammonia cores are associated with

[8]The program is developed by P. Bergman, OSO.

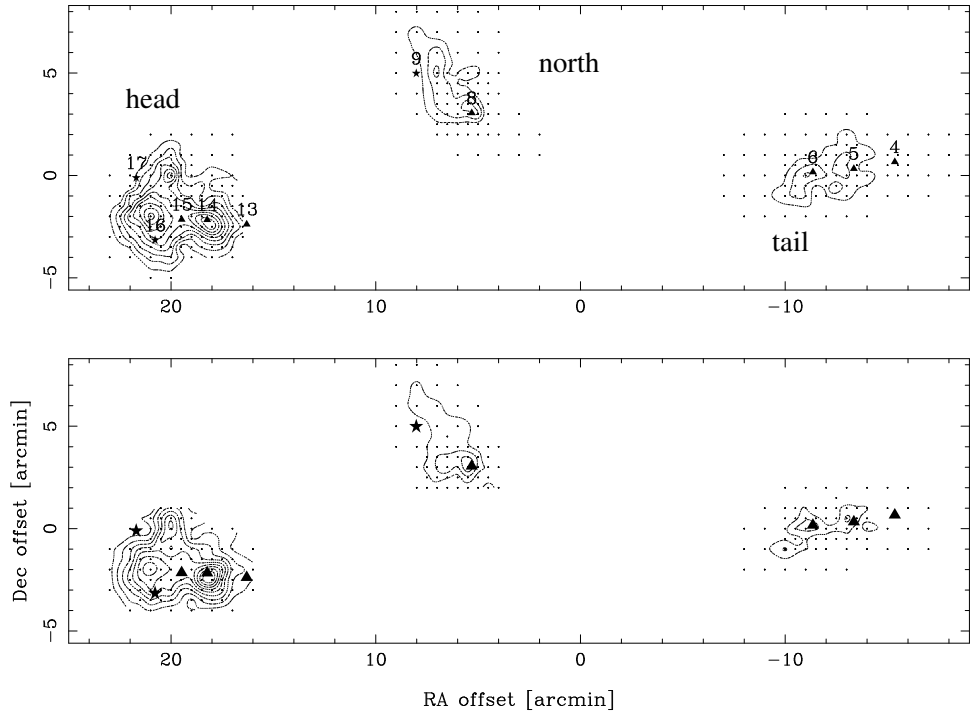

Figure 7.1: HNC (upper) and HCN (lower panel) integrated intensity maps of the (–2,–6.5) km s^{-1} velocity range (for HCN the velocity range of the main 2–1 component). The center position is R.A.=22^h33^m Dec.=$74^\circ58'$ (1950) and the observed positions are indicated by dots. The intensity scale is in $T_A^* dv$ [K km s^{-1}] and contours start from 0.9 and increase by 0.45 increments to 4.5 for HNC and from 0.8 with 0.4 increment to 4.0 K km s^{-1} for HCN. The stars denote the FIR point sources classified as T Tau stars, and the triangles those classified as embedded YSOs.

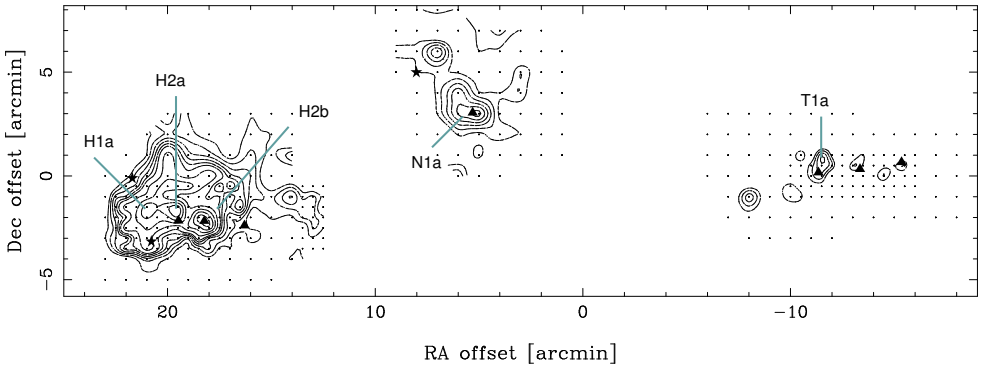

Figure 7.2: The CS (2–1) integrated intensity map of L 1251. The velocity range of the emission, the center position, the intensity scale and markers as in the previous figure. Contours start from 0.65 to 1.3 by 0.13 K km s^{-1} and from 1.3 to 2.34 by 0.26 K km s^{-1}.

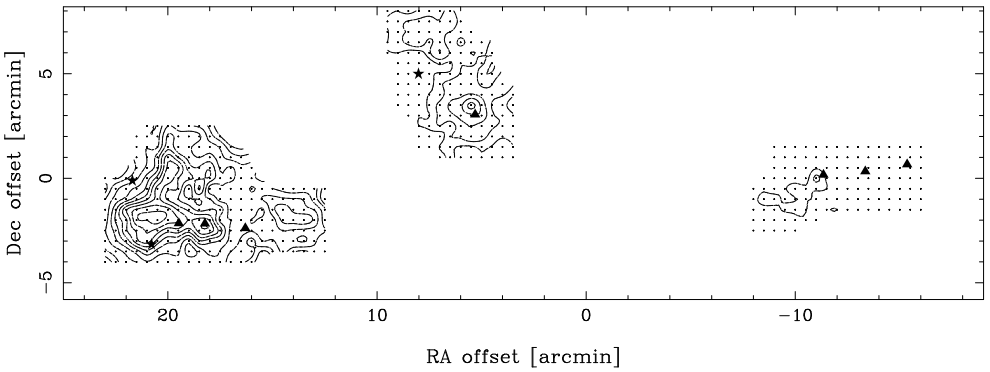

Figure 7.3: The HCO^+ (1−0) integrated intensity emission map of L 1251 for the (−2,−8) $km\,s^{-1}$ velocity range. The center position, markers and the intensity scale as in Fig. 1. Contours start from 0.8 by 0.45 $K\,km\,s^{-1}$.

newly born stars or protostars. The maps in CS and HCO^+ include also the starless core "H3" on the western side of the head core group. Locations of YSOs and T Tau stars probably associated with the cloud, with labeling that follows Tab. 3 of KP (the same as in column 1 of Table 7.1) are indicated in the upper panel of Fig. 7.1.

7.2.1. IDENTIFICATION OF CORES

The maps show local maxima which roughly correspond to the ammonia cores detected by TW. Because of the denser sampling and the higher spectral resolution available in the present study we see, however, more structure than discernible in the previous NH_3 maps. Using the spatial – velocity information available, we have identified altogether 15 cores in the mapped region, most of which can be seen in all four lines. Some of the NH_3 cores of TW divide in our maps into two components. Following the nomenclature of TW we label the five cores studied in more details as H 1a, H 2a, H 2b, N 1a and T 1a, where "a" and "b" stress either the existence of a secondary peak or a separate velocity component compared with the NH_3 defined core.

Table 7.2 lists the identified cores in order of decreasing R.A. offset (i.e., in head-to-tail direction). The columns are: (1) identification number; (2) line center velocity; (3, 4) core center in the R.A. and Dec. offsets with respect to the center of the map; (5) full half intensity width of the integrated emission corrected for the beam size; (6) the full halfwidth of the global line profile of the core; (7) virial masses; (8) masses calculated from $C^{18}O$ and (9) association with YSOs or T Tau stars *and* core designation following TW. The core size, D, is estimated from the extent of the half power intensity contour deconvolved with the beam assuming Gaussian shapes of the beam as well as the source. In most cases cores are elliptical, and we use the geometrical mean of the major and minor axes to define the size. Virial masses are derived using the formula $M_{\rm vir} = 150\,D\,\Delta v^2$ (see Johansson et al. 1998). For 5 cores independent mass estimates are derived from the $C^{18}O$ observations as $M = 1.456 \times 10^{-13}\,N_{\rm C^{18}O}$

Table 7.2: Derived parameters from the CS (2–1) observations. Sizes and masses assume a distance of 300 pc.

Core	$v_{\rm LSR}$ [1] [km s^{-1}]	$\Delta\alpha$ [′]	$\Delta\delta$ [′]	D [pc]	Δv [km s^{-1}]	$M_{\rm vir}$ [2] [M$_\odot$]	$M_{\rm CO}$ [3] [M$_\odot$]	Comments [4]
1	−4.8	21.0	−1.5	0.26	1.30	66	16	T Tau (H_α) #16; H 1a
2	−4.2	20.0	−0.5	0.16	0.75	14		
3	−3.3	19.5	−1.5	0.14	0.74	11	11	T Tau candidate #15; H 2a
4	−4.3	18.5	−2.0	0.16	1.68	70	8	embedded YSO #14, H 2b compact outflow
5 [a]	−3.6	14.0	−1.5	0.13	1.15	26		H 3
6 [b]	−4.6	7.0	6.0	0.16	0.98	23		N 2
7	−5.0	5.5	3.5	0.25	1.21	55	36	embedded YSO #8; N1 a extended outflow
8 [c]	−4.4	−8.0	−1.0	0.13	0.66	8		
9	−4.4	−10.0	−1.0	0.13	0.76	11		
10 [d]	−4.1	−10.5	1.0	0.09	0.93	12		
11	−4.3	−11.5	0.0	0.15	0.97	18	4	embedded YSO #6; T 1a
12 [d]	−4.2	−12.5	−0.5	0.07	0.75	6		
13 [b]	−4.0	−13.0	0.5	0.08	0.76	7		embedded YSO #5; T 2
14 [d]	−4.3	−14.5	0.0	0.09	1.12	14		
15 [d]	−4.4	−15.5	0.5	0.08	0.97	11		embedded YSO #4; T 3

[1] Gaussian fitted line center velocity at the peak position of the core.
[2] $M_{\rm vir} = 150\, D\, \Delta\, v^2$ (Johansson et al. 1998).
[3] $M = 1.456 \times 10^{-13}\, N_{\rm C^{18}O}\, (D_s^2 + D_b^2)$.
[4] Association with YSO candidates and selected positions observed in the rarer isotopomers.
[a] Surveyed only in CS and HCO^+. [b] Not detected in HCO^+. [c] Not detected in HCN. [d] Detected only in CS.

$(D_s^2 + D_b^2)$, where D_s and D_b are source diameter and beam size at the corresponding frequency, respectively (see Nikolić et al. 2001).

We have calculated standard deviation of the cores' radii for all available molecules to be 0.02–0.07 pc. For the first seven cores the emission extents of observed molecules agree, in most cases, within $\pm 1\sigma$ of the arithmetical mean.

All but three cores have virial masses of about or less than 20 M$_\odot$. An "excess" value of virial mass for H 1a, H 2b and N 1 cores may possibly be linked to the presence of T Tau stars, compact and extended outflows, respectively.

7.2.2. CLOUD KINEMATICS AND CHANNEL MAPS

The observed emission in the head covers the range from –6 to –2 km s^{-1}, while the northern area and the tail are seen only in the ranges (–6, –4) and (–5, –3) km s^{-1}, respectively. This is consistent with the dominant velocity components of the ^{13}CO emission according to Sato et al. (1994).

Figure 7.4 shows the HNC (1–0) line emission of the head region in four velocity channels. The other observed lines show similar features in the corresponding channel maps. Two velocity components, centered at ≈ -3.5 km s^{-1} and at ≈ -4.5 km s^{-1} are clearly seen in the maps. These two velocity components are also discernible in the HN^{13}C spectra of H 1a, H 2a and H 2b.

The two velocity component seen in the head region are easy to distinguish if the spectral resolution is high and map coverage good. If the velocity resolution of spec-

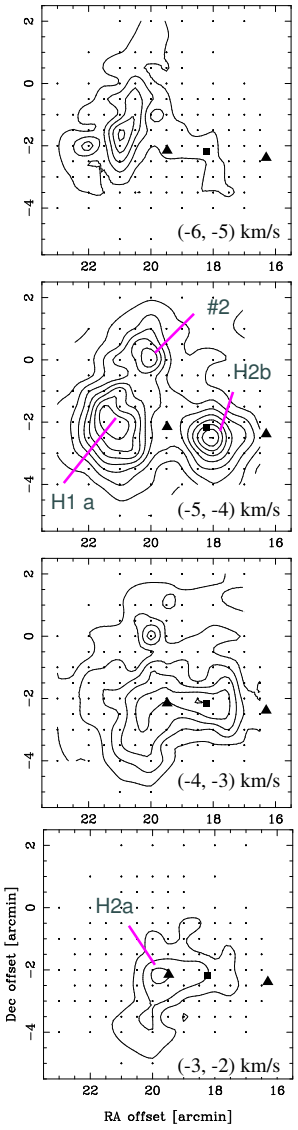

Figure 7.4: The HNC channel velocity maps of the "head" region, the observed positions are indicated by dots. The intensity scale is in $T_A^* dv$ [K km s^{-1}] and the contours start from 0.15 and are increasing by 0.3 K km s^{-1}. The velocity ranges are from –6 km s^{-1} (a) to –2 km s^{-1} (d), with 1 km s^{-1} wide range. The FIR point sources, in increasing RA, are 13, 14 (IRAS 22376+7455), and 15 (notification is according to Kun & Prusti (1993)). Embedded YSOs are marked with triangles and the embedded YSO suspected to be driving the compact outflow is marked by a dot.

tra is low, mapping of such close velocity components may be interpreted as a velocity gradient. Based on their ammonia maps TW suggested a velocity gradient of $\sim 1.3\,\mathrm{km\,s^{-1}\,pc^{-1}}$ in the head region. Assuming *only one* velocity component i.e., fitting a single Gaussian over the HNC map we arrive at "velocity gradient" in the head of $\approx 3.3\,\mathrm{km\,s^{-1}\,pc^{-1}}$. Such gradients are seen across the whole L 1251.

On the other side, if only selected positions are sampled, e.g. the IRAS PSs locations, close velocity components may mimic the line profile typical of infall candidates. Mardones et al. (1997) have identified the IRAS 22376+7455 source as an infall candidate on the basis of their CS(2–1) and H_2CO line profiles which exhibited blue–shoulder and double peaked profiles, respectively. Such profiles could arise from local self–absorption, but also if there is a foreground layer of dense gas with the systematic velocity of the source. Our interpretation is that a superposition of two dense gas velocity sheets contributes to the observed line asymmetry significantly, yet not ruling out a possible infall of the dense gas.

7.2.3. COMPARISON WITH THE NH_3 MAP

A survey of the L 1251 dense cores in ammonia of Tóth & Walmsley (1996) was made with a similar beam and double–beam grid–point spacing. The NH_3 observations suffer from low spectral resolution ($0.15\,\mathrm{km\,s^{-1}}$) which makes it difficult to distinguish the different velocity components. If the slightly different definition of cores is accounted for, all diameters fall within the errors. However, comparing our maps and the NH_3 map we see two important differences: in the northern part of L 1251 no NH_3 core is detected around IRAS 22343+7501, and the emission intensities in both head and tail part are approximately of the same order in the NH_3 line, in contrast to our data (note the contour levels in Figs.7.1,2,3). This applies to the total integrated emission. However, peak intensities from individual cores are similar all over L 1251. The difference is the density of cores, which is highest in the head region.

7.3. AN HCO^+ "DISK" OF IRAS 22343+7501?

Close inspection of the HCO^+ spectra in the N1 a core area reveals an apparent influence of the CO outflow (Sato & Fukui 1989) on the HCO^+ line shapes up to about $2'$ from the IRAS 22343+7501 source. At the distance of the cloud this equals to 36000 AU. The structure presented in Fig. 7.5 mimics a rotating HCO^+ "disk" around the protostar. The orientation of this disk to the outflow axes is difficult to determine due to the large opening angle of the CO outflow. The dashed line in Fig. 7.5 gives roughly the orientation of the outflow axes. Defined by the peak of the emission in the blue and the red shifted lobes, the mean disk radius is $\approx 50''$ i.e. 12000 AU (corrected for the beam dilution).

Based on IRAS and submilimmeter continuum observations Mardones et al. (1997) derived a source bolometric temperature of $T_{\mathrm{bol}} \leq 108\,\mathrm{K}$. According to the classification scheme of Chen et al. (1995) IRAS 22343+7501 should, then, be a Class I YSO. Kun (1998) derived envelope mass and a mass of hypothetical central star to be $M_{\mathrm{env}} = 0.12\,M_\odot$ and $M_* = 2.35\,M_\odot$, respectively. The ratio of $M_{\mathrm{env}}/M_* \ll 1$ defines IRAS 22343+7501 as a more evolved Class I YSO. Using Chen et al. (1995) empirical

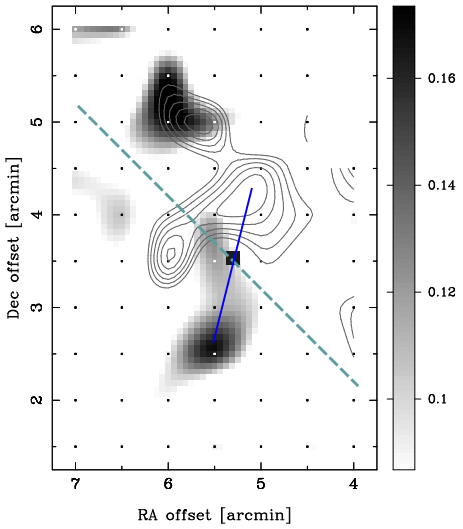

Figure 7.5: Integrated intensity map of the blue– (greyscale) and the red-shifted (contours) HCO^+ emission of the N1a core. The velocity ranges are (–7,–8) and (–2,–3) $km\,s^{-1}$ for the blue and the red wings, respectively. The intensity scale is in $T_A^* dv$ [$K\,km\,s^{-1}$] with contours from 0.09 by an increment of 0.01 $K\,km\,s^{-1}$. The filled square marks the position of IRAS 22343+7501, the solid line marks the proposed disk and the dashed line shows the orientation of the corresponding CO outflow.

relation between age and bolometric temperature for YSOs with $T_{\rm bol} \leq 1000\,K$, we estimate IRAS 22343+7501 to be $(1.3\pm0.1)\times10^4$ years old. This age would classify the source as a very young Class I YSO. Near – infrared images (Rosvick & Davidge 1995) and recent 3.6 cm and 6 cm VLA continuum observations (Grissom Meehan et al. 1998, Beltrán et al. 2001) show that this IRAS source consists of several central protostellar objects. The near – IR images exhibit a 20 to 30″ large nebulosity corresponding to a maximum size of 9000 AU. VLA continuum measurements revealed two sources, separated by 7″, i.e., around 2000 AU. Both continuum sources have a spectral index consistent with thermal emission, and any of them could be the CO outflow driving source (Beltrán et al. 2001).

We derived a total mass of molecular gas in the HCO^+ "disk" as $M = 5.67 \times 10^{-12}\,N_{\rm HCO^+}\,(D_s^2 + D_b^2)$, where D_s and D_b are source diameter and beam size at the corresponding frequency, respectively. Velocity intervals for blue– and redshifted emission are defined as in Fig. 7.5. The "disk" contains in total $\approx 4.5\,M_\odot$ of molecular gas, almost evenly distributed among the approaching ($2.53\,M_\odot$) and receding ($1.99\,M_\odot$) emission regions. Sato et al. (1994) derived the dynamical timescale of the CO outflow to 9.2×10^4 and 1.8×10^5 years for the blue– and the red–wing, respectively. Providing that IRAS 22343+7501 is the CO outflow driving source, the difference in the age estimates implies that the flow plane is close to the plane of sky, i.e., tilted by 4–8°.

The "disk" stability may be tested assuming that this "disk" rotates as a solid body with velocity of $v_{\rm rot} = 2.25\,{\rm km\,s^{-1}}$ ($v_{\rm rot}$ is equal to the half of the absolute value of the sum of the maximum velocity shift of the HCO^+ blue– and red–wing emission from the $v_{\rm LSR}$ of the core). We calculate the centrifugal force of such a disk to be 30× larger than the gravitational force of a central object with mass $M_\star = 2.35\,M_\odot$. This would indicate that the central star(s) is not able to support the disk, and that, in fact, this "disk" may be in the process of dissipation.

7.4. MASS FRACTION OF DENSE GAS AND SFE ESTIMATES

From the $C^{18}O$ data, Sato et al. (1994) derived a total gas mass in the head region of $65\,M_\odot$. Adding up our estimates of core masses in the same region, we arrive at $\sim 50\,M_\odot$ (column 8 of Table 7.2 with exception of core 2), i.e. some 75% of the total mass is concentrated in the dense cores. For the northern region of L 1251 Sato et al. (1994) estimate a total gas mass of $56\,M_\odot$. We derive a mass of $36\,M_\odot$ for core 7 i.e. the N1 a core, implying that for this region at least 65% of the total mass is in the form of dense gas.

Five out of six proposed embedded YSOs by KP in the region we surveyed are probably still deeply embedded in the dense gas of the cloud: sources #4, #5 and #6 in the tail area (associated with the cores 15, 13 and 11 in Table 7.2, respectively), source #8, i.e., IRAS 22343+7501, in the northern area (core 7, N 1a) and source no. #14, i.e., IRAS 22376+7455, embedded in core 4 (H 2b). Additionally, based on their projection onto the dense areas, three T Tau stars are probably associated with the cloud: sources #16 and #17 in the topmost part of the head area and source #7 in the N 2 core are all coincident with detected H α emission stars. Sources #13 and #15 are both blended by the strong IR emission from IRAS 22376+7455, and have ill defined uncertainty ellipses. Probably they are faint, low – mass embedded stars (Kun, private communication). Position of source #15 correlates well with the center of core 3 (see Fig. 4), where the HCN peak integrated emission is $\sim 2.5\,{\rm K\,km\,s^{-1}}$. Yun et al. (1999) used a criteria for a molecular cloud core with an embedded YSO to have a total integrated HCN intensity emission $> 1\,{\rm K\,km\,s^{-1}}$. They derived an 80% likelihood of tracing an embedded Class 0 YSO if the detected emission is stronger than $3\,{\rm K\,km\,s^{-1}}$. Thus, source #15 would fit well into an embedded Class 0/I YSO object class.

To derive SFE of the cores we assume that a protostar has $M_* \sim 1\,M_\odot$ for all the embedded YSOs and T Tau stars with unknown masses, i.e., sources #6, #15, #16 and #17. IRAS 22376+7455 and IRAS 22343+7501 have estimated masses of $1.78\,M_\odot$ and $2.35\,M_\odot$, respectively (Kun 1998). If we use masses of the cores listed in Table 7.2, SFEs for the H1 a, H2 a, H2 b, N1 a and T1 a cores are 11%, 9%, 18%, 6% and 20%, respectively. On average, SFE of the observed cores would be $\sim$ 13%, almost 3 times lower than the previously estimated SFE for the whole cloud, but still 5–6 times higher than the overall SFE for the Galaxy[9]. Low SFEs are typical for dark clouds where low – mass stars are born. However, there are clouds with much higher – than – average SFE what indicates that apart of spontaneous there is a contribution from externally

[9]Overall star forming efficiency for the Galaxy is estimated to be only ∼2% (Myers et al. 1986).

induced/stimulated star formation. Such external events e.g., supernova shock fronts, ionization fronts, stellar winds, spiral density waves or cloud collisions, speed up the spontaneous star formation by changing the initial or boundary conditions. 'Collision' of a shock front and dense molecular gas is bound to increase the density of the gas on small scales through compression, enhance turbulency and increase kinetic temperature of the gas, eventually change the ionization fraction and thus also alter the chemistry of the dark core/cloud. Thus, the observed high SFE in L 1251 may be considered as an evidence of a cloud–shock 'collision'.

Chapter 8
DETERMINING A MOLECULAR GAS KINETIC TEMPERATURE

The gas kinetic temperature, $T_{\rm kin}$, is established by the balance between heating and cooling rates, and is in principle a key datum required to understand the processes in the molecular clouds. Both, the heating and cooling processes depend on several parameters: gas density and kinetic temperature, dust opacity and surface properties, the spectrum and intensity of the radiation field, the cosmic ray flux and the atomic and molecular abundances of both ions and neutral species in the gas. Many of these parameters vary as function of position or depth into a cloud, thus a single temperature along the line of sight in most molecular clouds should not be expected.

In practice, a mean value of $T_{\rm kin}$ is estimated in molecular clouds from the excitation temperature, T_{ex} of a particular molecular transition whose level populations are believed to be in thermal equilibrium. The most widely used molecule for this purpose is carbon monoxide, $^{12}C^{16}O$ whose lowest rotation transition is generally optically thick. The level populations are assumed to be in thermal equilibrium due to the long radiative lifetime relative to typical collision rates leading to $T_{ex} = T_{\rm kin}$. Another temperature probe frequently used is ammonia. The rotation temperature of the two inversion transitions $J, K = 2, 2$ and $1, 1$, T_{21}, can be calculated from the relative intensities of the observed lines and the usual assumption is that $T_{21} = T_{\rm kin}$. A comparison between the excitation temperature of the $J = 1 - 0$ transition of CO and the rotation temperature of ammonia inversion transitions in many clouds shows that $T_{ex}({\rm CO}) \approx T_{21}({\rm NH_3})$ in dark clouds where $n \sim 10^4\,{\rm cm^{-3}}$ and $T_{\rm kin} \leq 15\,{\rm K}$ (e.g. Churchwell & Holis 1983). A serious problem with the CO use is the tendency for the $J = 1 - 0$ line to be self–absorbed by the overlaying cooler gas, which may result in a severe underestimation of $T_{\rm kin}$.

Another potential gas kinetic temperature probe in molecular clouds are symmetric top molecules methyl cyanide, CH_3CN, and methyl acetylene, CH_3CCH / CH_3C_2H (Churchwell & Hollis 1983, Kuiper et al. 1984, Askne et al. 1984, Bergin et al. 1994, Anderson et al. 1999). Symmetric top molecular rotational energy levels are described by two quantum numbers: J, the total angular momentum, and K, the component of J along the axis of symmetry. The rotational energy levels of a symmetric top molecule are given by $E = h\,B\,J\,(J{+}1){+}h\,(A{-}B)\,K^2$, where A and B are rotational constants. The energy levels are then grouped according to the K quantum number into separate ladders, with the lowest energy level having $J = K$. Radiative transitions between

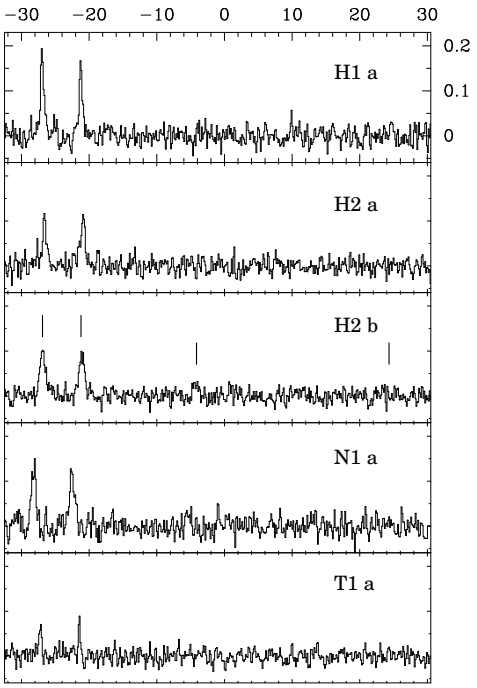

Figure 8.1: The observed CH_3CCH $5-4$ spectra smoothed to a velocity resolution of $0.12\,\mathrm{km\,s^{-1}}$. Core designation is given in the upper right corner and the observed $K = 0, 1, 2, 3$ transitions are marked with solid lines. The intensity scale is T_A^* [K], and the velocity scale v_{LSR} [$\mathrm{km\,s^{-1}}$].

the K–ladders are forbidden by the radiative selection rules $\Delta J = 0, \pm 1$ and $\Delta K = 0$. Therefore, the relative populations of the K–ladder depend primarily on the kinetic temperature of the colliding particles. Generally, symmetric top molecules make good temperature probes because each K–component of a given J rotational transition has a different excitation energy and being relatively close in frequencies, all K components can be observed simultaneously, avoiding calibration problems. The effects of nuclear spin divide methyl acetylene into two distinct species, depending on the relative orientation of the spins of the hydrogen atoms. This, so called torsional symmetry states are labeled A and E. A species have $K = 3\,n$ ($n = 0, 1, 2, ...$), and E species are those with $K = 3\,n + 1$, $3\,n + 2$. The two species are independent since both collisional and radiative transitions between them are forbidden. The formation process is unlikely to discriminate between the two, and we assume their equal abundances in the molecular gas. CH_3CCH is a prolate symmetric top, with low dipole moment (0.78 D) and no dipole moment perpendicular to the symmetry axis and is more easily thermalized than other symmetric rotors (CH_3CN has a dipole moment of 3.9 D). This suggests that the data may be analyzed assuming LTE. Furthermore, the relatively weak lines observed in interstellar clouds suggest that the (usual) simplifying assumption of low optical depth may be valid.

Table 8.1: The results of the CH_3CCH rotational diagram method weighted with observational errors plus E, A species uncertainties (case I) and using the $K = 1$ and $K = 2$ lines only (case II). Ammonia temperatures are from TW.

	H 1a	H 2a	H 2b	N 1	T 1a
case I					
$T_{\rm rot}$ [K]	27 ± 6	16 ± 5	18 ± 2	23 ± 2	22 ± 7
$N_{\rm tot}$ $[10^{12}\,{\rm cm}^{-2}]$	31 ± 8	16 ± 8	21 ± 4	27 ± 5	8 ± 3
case II					
$T_{\rm rot}$ [K]	15 ± 4	8 ± 2	15 ± 2	16 ± 3	10 ± 5
$N_{\rm tot}$ $[10^{12}\,{\rm cm}^{-2}]$	25 ± 2	27 ± 5	23 ± 1	28 ± 2	8 ± 1
$T_{21}^{\rm NH_3}$ [K]	11	12	14	–	10

The $J = 5 - 4$ and $J = 6 - 5$, $K = 0, 1, 2, 3$ transitions of methyl acetylene were observed towards the 5 previously selected cores in L 1251, H1 a, H2 a, H2 b,N1 a and T1 a (see Table 7.2 for reference positions). Figure 8.1 shows the detected 5–4 spectra.

To estimate kinetic temperatures we have used the rotational diagram method (see, e.g., Anderson et al. 1999) which assumes LTE conditions and optically thin emission. Assuming optically thin emission, the integrated brightness temperature of a spectral line component as a function of the column density of the molecules in the upper transition level, N_u, is

$$\int T_B(v)\,dv \equiv \frac{1}{\eta}\int T_A^*(v)\,dv = \frac{2\pi^2}{3}\,\frac{\nu\mu^2}{k\varepsilon_0}\,\frac{S_{J,K}}{2J+1}\left[1 - \frac{F(T_{\rm bg})}{F(T_{\rm ex})}\right] N_u\,, \tag{8.1}$$

where η is the beam–source coupling efficiency, ν is the line rest frequency, μ is the permanent dipole moment of the molecule, k is the Boltzmann constant, ε_0 is the vacuum permittivity, $T_{\rm bg}$ is the cosmic background radiation temperature and $T_{\rm ex}$ is the excitation temperature of the transition being observed. $S_{J,K}$ is the so called line strength of the transition $(J, K) \rightarrow (J - 1, K)$ defined as

$$S_{J,K} \equiv \frac{J^2 - K^2}{J}. \tag{8.2}$$

The function $F(T)$ is defined by

$$F(T) \equiv \frac{1}{e^{\,h\,\nu/k\,T} - 1}, \tag{8.3}$$

where h is the Planck constant.

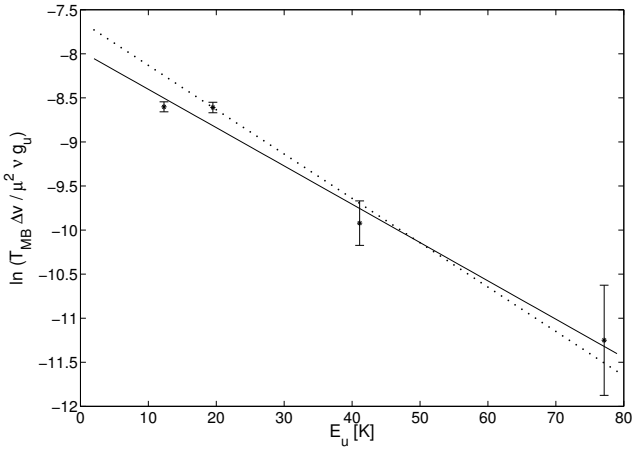

Figure 8.2: Rotation diagram of the CH_3CCH 5–4 transition for core N1 a. For definition of case I and case II see text and Table 8.1. The error bars refer to the observational uncertainties only.

Now, assuming rotational equilibrium at a temperature $T_{\rm rot}$, the column density N_u can be obtained from the total column density of the molecule N according to

$$N_u = g_J\, g_K\, g_I\, \frac{e^{\,E_u\,/\,k\,T_{\rm rot}}}{Q}\, N, \tag{8.4}$$

where g_J and g_K are the statistical weights due to angular momentum and its projection onto a given axis, respectively ($g_J = 2J + 1$; $g_K = 1$ when $K = 0$ and $g_K = 2$ when $K \neq 0$). The statistical weight g_I takes account of the spins of the three hydrogen nuclei (each having $I = \frac{1}{2}$ and takes the value 4 when $K = 0, 3, 6, ...$ and 2 when $K = 1, 2, 4, 5, ...$). The partition function, Q, is given by

$$Q = \sum_{J=0}^{\infty} \sum_{K=0}^{J} g_J\, g_K\, g_I\, e^{\,E(J,K)\,/\,k\,T_{\rm rot}} \tag{8.5}$$

Than, if $F(T_{\rm bg}) \ll F(T_{ex})$, it can be shown that

$$\ln\left(\frac{\int T_A^*\, dv}{\eta\, \nu\, S_{J,K}\, g_I\, g_K}\right) = \ln\left(\frac{2\,\pi^2}{3k}\,\frac{\mu^2}{\varepsilon_0}\,\frac{N}{Q}\right) - \frac{1}{T_{\rm rot}}\,\frac{E_u}{k} \tag{8.6}$$

where E_u is the upper energy level of the transition.

The unknowns in the equation are the total column density and the rotational temperature. By observing several transitions belonging to different K–ladders, one is able to obtain both $T_{\rm rot}$ and N/Q. The slope of the line is determined by the reciprocal of $T_{\rm rot}$, and its intersection with the $E_u/k = 0$ axis gives the ratio N/Q.

Rotational temperatures derived in this way are unexpectedly high as are the associated errors. The reason for this can be traced back to the intensity of the $K = 0$ relative to $K = 1$ transition; with the exception of the region H 1a, the observed ratios all indicate $T_{\rm rot} > 50\,{\rm K}$. Such results can be explained in terms of non – LTE excitation *or* that the total abundances of the A ($K = 0$) and E ($K = 1$) species are not equal. Assuming $T_{\rm rot} = 15\,{\rm K}$, the E/A population ratio would be about 1.5 based on the observed $K = 0$ and 1 transitions.

Askne et al. (1984) find that statistical equilibrium and rotational diagram calculations agree, with the exception of cold regions. Their analysis indicates that the total abundances of the A and E species are equal, however, defined by different partition functions at low kinetic temperatures. For TMC – 1, their observations show an intensity ratio of ~ 1 between the $K = 0$ and 1, $J = 5 - 4$ transitions, while the statistical equilibrium analysis indicates $T_K \sim 10\,{\rm K}$ and $T_{\rm rot} \sim 6\,{\rm K}$. Observationally, this is very similar to our sample, with the exception of H 1a, possibly indicating that this head core is warmer than the rest of the regions observed here.

To proceed we have introduced an uncertainty in the A and E species populations of 30%. The results are given as "case I" in Table 8.1, and clearly show smaller errors in the derived parameters in spite of larger total errors in the input data, a reflection of the inconsistent intensities of the $K = 0$ and 1 transitions. Fig. 8.2 visualizes this inconsistency common for all our cores with the exception of H1 a. These are indicators that the partition function of the A and E species deviate at low temperatures and, in our sample analysis, overestimate the temperatures. This effect would than apply to all our cores except H1 a.

In "Case II" we have only used the $K = 1$ and 2 transitions (i.e. the E–species) to estimate the rotation temperatures. The CH_3CCH results favor a kinetic temperature in excess of $\sim 25\,{\rm K}$ for H1 a and less or significantly less than $\sim 20\,{\rm K}$ for the rest of the cores. Note, however, that this is not consistent with the NH_3 observations. The discrepancies might be due to ammonia freezing on the dust grains, when molecular gas temperature is still not high enough to enable significant NH_3 evaporation.

Chapter 9
STAR FORMATION AND CHEMISTRY IN L 1251

Our choice of molecules used for studies of L 1251 was determined by two requirements: that a molecule traces the dense gas in a cloud and that molecules belong to different 'families' according to present chemical networks. Based on the production pathways via ion–molecule or neutral–neutral reactions, and their dependence on neutral carbon (C I), some molecules are classified either as 'early–time', or 'late–time' species. 'Early–time' molecules reach their peak abundances early on, $10^4 - 10^6$ years after the onset of chemistry. On the other side, the 'late-time' species slowly build up their abundances in time and reach the maximum abundances later, when a core has $10^6 - 10^8$ years of 'chemical age' (e.g. Herbst & Leung 1989). HCO^+ and SO are usually considered as late-time molecules; CS belongs to the 'early–time' species, and HNC and HCN are usually assumed to fit into the latter family.

Figure 9.1 shows integrated intensity channel maps of the L 1251 head region. Velocity range was selected so that the two different components of molecular gas in this area are clearly seen. Close inspection of the figures confirms our earlier (Sec. 7.2) decision to define the IRAS PS #15, in spite insufficient data, as an embedded YSO. Being always close to the dense core center, yet invisible, it can possibly be defined as a Class 0/I young stellar object. Comparing the extent of the CS and HCO^+ emission suggests indeed that these molecules belong to different families — the CS emission is more extended, while HCO^+ is concentrated toward the center of a dense core. Since both molecules have similar critical densities of the observed transitions, these differences are not likely to be due to the gas density.

9.1. COLUMN DENSITIES AND RELATIVE FRACTIONAL ABUNDANCES

Table 9.1 gives column densities towards selected positions, derived assuming LTE conditions and optically thin emission. In addition, it was assumed that the excitation temperature, $T_{\rm ex}$, is 10 K for ^{13}CO and $C^{18}O$, and 6 K for other species, which are likely to be subthermally excited (see e.g., Caselli et al. 2002). The column densities of $C^{34}S$ and $HN^{13}C$ show the largest variations across the cloud. The $C^{34}S$ column density has a minimum towards H1a in the head, whereas $HN^{13}C$ peaks towards T1a in the tail. The column densities of the other molecules change less than by a factor of three. A comparison between different molecules brings forth some pairs with large

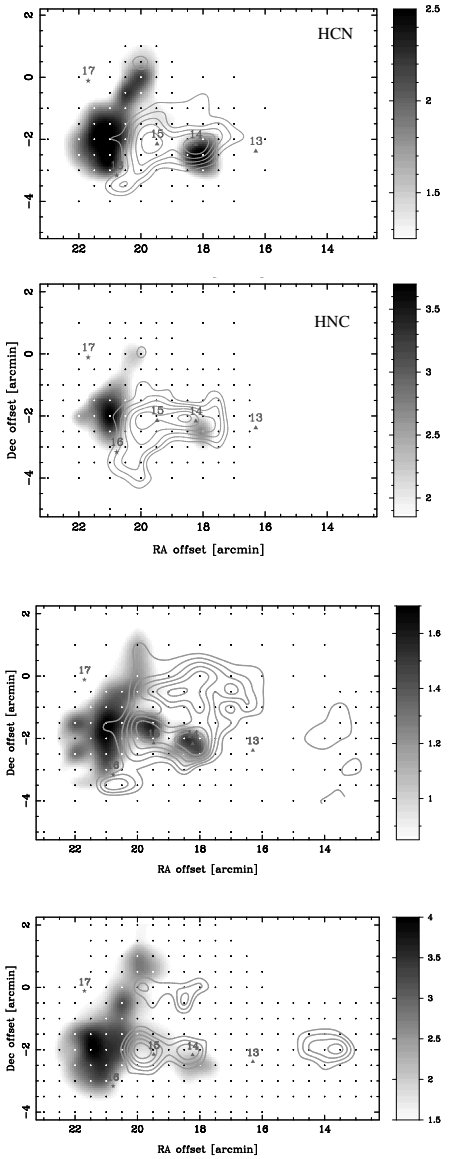

Figure 9.1: The HCN, HNC, CS and HCO^+ channel intensity maps of the L 1251 "head". The greyscale maps are integrated intensities for the (–6,–4) $km\,s^{-1}$ velocity interval. The overlayed contour maps are integrated in the (–4,–2) $km\,s^{-1}$ interval. Contours start from 1.5 an increase by 0.2 $K\,km\,s^{-1}$ for HCN and HNC; for CS contours start from 0.5 and increase by 0.5 $K\,km\,s^{-1}$; for HCO^+ contours start from 2 and increase by 0.5 $K\,km\,s^{-1}$. The stars mark the FIR point sources classified as T Tau stars, and the triangles those classified as embedded YSOs (annotations are from Kun & Prusti 1993).

Table 9.1: LTE–derived total column densities. For the three cores in the "head" appropriate velocity components of the cores were used (see Table 7.2). CO column densities, as defined by noise fluctuations only, have error of 1–2%, while for the other molecules these errors are ∼5–10%.

Molecule	[cm^{-2}]	H 1a	H 2a	H 2b	N 1	T 1a
^{13}CO	[10^{15}]	6.1	5.9	7.5	13.9	7.9
C^{18}O	[10^{15}]	1.2	1.9	1.6	2.7	1.1
C^{34}S	[10^{11}]	4.3	7.7	11.5	14.0	11.2
H^{13}CN	[10^{11}]	2.5	5.4	3.7	2.1	6.6
HN^{13}C	[10^{11}]	4.4	7.6	6.3	5.5	13.8
H^{15}NC	[10^{11}]	0.9	1.3	0.8	1.5	3.0
H^{13}CO$^+$	[10^{11}]	4.0	5.8	3.7	8.6	4.6
HC^{18}O$^+$	[10^{11}]	0.20	–	0.17	–	–
SO	[10^{13}]	1.8	1.0	1.0	0.7	1.0
NH$_3$ [a]	[10^{14}]	18	–	9.9	–	22

[a] From TW, velocity components of the cores in the head are not resolved.

variations in the column density ratios, and others with little changes. For example, H^{13}CO$^+$/C^{18}O and HN^{13}C/H^{13}CN are roughly constant ($\sim 3 \pm 1 \times 10^{-4}$ and $\sim$ 2 ± 0.5, respectively), C^{34}S/SO has by far the lowest value towards H1a, and HN^{13}C/C^{18}O is clearly largest towards T1a.

We have also estimated the H_2 column densities, $N(H_2)$, with the aid of C^{18}O and the conversion factor [C^{18}O]/[H$_2$]=1.7×10^{-7} determined by Frerking et al. (1982). The $N(H_2)$ values have been then used to derive the fractional abundances of other observed molecules. In the conversion to the main isotopomer fractional abundances the following isotopic ratios characteristic of the local ISM have been used: ^{12}C/^{13}C = 77, ^{32}S/^{34}S = 22, ^{16}O/^{18}O = 560 and ^{14}N/^{15}N = 450 (Wilson & Rood 1994). The H_2 column density estimates and the fractional abundances are given in Table 9.2. According to this Table the position H 1a has the lowest CS abundance and the largest SO abundance. The fractional HCN and HNC abundances seem to peak towards T1a. N1a, with the highest H_2 (in fact C^{18}O) column density, has the lowest SO abundance. In the other molecules the changes are less marked. It should be noted that the fractional abundances derived here reflect column densities relative to C^{18}O, and do not represent the true relative abundances with respect to H_2 in case the C^{18}O/H_2 column density ratio changes e.g. due to freezing–out. As comparison we list in the Table also the H_2 column density value determined from ^{13}CO using the conversion factor of [H$_2$]/[^{13}CO]=4.8 × 10^5 (Dickman & Clemens 1983).

Hirota et al. (1998) obtained for a large dark cloud sample fractional abundances of $X(\mathrm{HNC}) = 1.2 - 33 \times 10^{-9}$ and $X(\mathrm{HCN}) = 1.4 - 24 \times 10^{-9}$ relative to H_2. In OMC–1, Sgr B2 and TMC–1 dark cloud cores Blake et al. (1987) got relative fractional abundances of hydrogen cyanide of 5×10^{-9}, 3×10^{-9} and 1.2×10^{-8}, respectively. Our results fit well into these ranges.

Table 9.2: The H_2 total column density obtained from ^{13}CO using conversion factor of $N\ (H_2)/N\ (^{13}CO) = 4.8 \times 10^5$ (Dickman & Clemens 1983) and $C^{18}O$ using the ratio $[C^{18}O]/[[H_2]=1.7\times10^{-7}$ (Frerking et al. 1982) in $[10^{21}\,cm^{-2}]$; and the calculated fractional abundances of the main isotopomers with respect to $[H_2]$ derived from $[C^{18}O]$.

		H 1a	H 2a	H 2b	N 1	T 1a
$[^{13}CO] \Rightarrow [H_2]$		2.93	2.84	3.58	6.67	3.77
$[C^{18}O] \Rightarrow [H_2]$		6.76	11.41	9.65	16.06	7.12
CS	$[10^{-9}]$	1.4	1.5	2.6	1.9	3.4
HCN	$[10^{-9}]$	2.9	3.6	2.9	1.0	7.1
HNC [a]	$[10^{-9}]$	5.0	5.2	5.0	2.6	14.9
HNC [b]	$[10^{-9}]$	0.6	4.4	4.0	4.4	21.0
HCO^+ [a]	$[10^{-9}]$	4.6	3.9	3.0	4.1	4.9
HCO^+ [c]	$[10^{-9}]$	> 1.7	–	> 1.0	–	–
SO	$[10^{-9}]$	2.8	0.7	1.0	0.5	1.3
NH_3	$[10^{-7}]$	2.6	–	1.0	–	3.1

[a]The main isotopomer column density obtained from ^{13}C– isomeric specie; [b]The main isotopomer column density obtained from ^{15}N– isomeric specie; [c]The main isotopomer column density obtained from ^{18}O–isomeric specie.

9.2. CHEMISTRY

9.2.1. HNC AND HCN PRODUCTION AND DESTRUCTION

The observed abundance ratio in dark clouds of HNC/HCN > 1 (Irvine & Schloerb 1984, Churchwell et al. 1984, Harju 1989) was the main point to consider in discussing possible network of chemical reactions that produce both molecules. In an environment with a cold and dense gas chemistry should be able to produce slightly more HNC. According to gas – phase chemical models the main route for production of hydorgencyanide and hydrogenisocyanide is the dissociative recombination reaction (e.g. Hirota et al. 1998):

$$HCNH^+ + e^- \rightarrow HNC + H,\ \ HCN + H. \tag{9.1}$$

Another possible production reaction is a dissociative recombination reaction (Allen et al. 1980)

$$H_2NC^+ + e^- \rightarrow HNC + H, \tag{9.2}$$

where only HNC is produced. The neutral–neutral reactions can produce preferably HNC (Nejad et al. 1990, Herbst et al. 2000)

$$C + NH_2 \rightarrow HNC + H, \tag{9.3}$$

or analogously HCN

$$N + CH_2 \rightarrow HCN + H. \tag{9.4}$$

In cirrus and CB translucent cores the neutral – neutral reactions dominate (Turner et al. 1997), while their importance in dark clouds is not clear yet. The metastable ion H_2NC^+ is initially produced in the reaction between C^+ and NH_3, but the subsequent isomerization leaves $HCNH^+$ as the overwhelmingly dominant product ruling out the (9.2) production route (Talbi & Herbst 1998). Based on their observations of starless and star forming cores Hirota et al. (1998) derived a branching ratio of the reaction (9.1) of 0.4 and 0.6 in favor of HNC production.

Both molecules are destroyed in reactions with ions

$$HCO^+ + HNC,\ HCN \rightarrow HCNH^+ + CO, \tag{9.5}$$

and

$$H_3^+ + HCN,\ HNC \rightarrow HNCH^+ + H_2. \tag{9.6}$$

At low temperatures the evaporation process of HNC and HCN from dust grains is probably inhibited. Once the temperature exceeds the critical temperature of 24 K (Hirota et al. 1998) the evaporation from grains starts and the ratio HNC/HCN drops, mostly because there are more energetically favorable paths for destruction of HNC. The reaction

$$HNC + H \rightarrow HCN + H \tag{9.7}$$

has an activation barrier estimated to either 190 K (Hirota et al. 1998), or ∼1700 K (Talbi et al. 1996). However, there are many alternative pathways for the HNC destruction, e.g., HNC+O→ HN+CO, HNC+OH→ NH_2+CO (Herbst et al. 2000).

Nejad et al. (1990) suggested that around outflows, in the post – shock region, high concentrations of H^+ can drive the isomerization reaction

$$H^+ + HNC \rightarrow H^+ + HCN, \tag{9.8}$$

while the high gas temperatures open another route for the HCN production

$$H_2 + CN \rightarrow HCN + H. \tag{9.9}$$

Chemical isotope fractionation in cold interstellar clouds is mostly caused by a thermodynamic effect in which the exchange of isotopic atoms between molecules in pairs of forward and reverse reactions has a preferred direction owing to exothermicity (Terzieva & Herbst 2000). These authors used the statistical mechanical approach to calculate rate coefficients for 8 specific reactions and found out that the most N – fractionation is caused in the

$$^{15}N + HCNH^+ \rightleftarrows N + HC^{15}NH^+ \tag{9.10}$$

reaction which has an exothermicity of ∼36 K. In a dissociative recombination with electrons the $HC^{15}NH^+$ ion can produce both $H^{15}NC$ and $HC^{15}N$, with so far not studied branching ratios. In the temperature range of 10–40 K, in general, no matter how small, N–isotope fractionation is more discernable the lower the temperature (Terzieva & Herbst 2000).

Assuming the local ISM isotopic values, the ratio $HN^{13}C/H^{15}NC$ is equal to 5.8. This ratio of the column densities in L 1251, is in the range 3.6–7.4. However, due to the large noise in the $H^{15}NC$ data, the result is inconclusive of possible chemical isotope fractionation of HNC.

9.2.2. CHEMICAL NETWORKS FOR CS, HCO^+ AND NH_3

Considering pure gas–phase reactions the main destruction route for SO goes through (e.g. Nilsson et al. 2000):

$$\mathrm{SO + C \rightarrow CO + S}, \tag{9.11}$$

and

$$\mathrm{SO + C \rightarrow CS + O}. \tag{9.12}$$

As long as the C abundance is high the loss reactions are efficient and the SO abundance is low. CS on the other side is produced in ion–molecule reactions (e.g. Taylor et al. 1996)

$$\mathrm{CS^+ + H_2 \rightarrow HCS^+ + H} \tag{9.13}$$

$$\mathrm{HCS^+ + e^- \rightarrow CS + H}, \tag{9.14}$$

and is destroyed either in the reactions of dissociative charge exchange or neutral–neutral molecular reactions, none of which includes C atoms.

The widely accepted synthetic scheme for ammonia starts from N^+ ions in a reaction sequence of successive hydrogen abstraction, followed by recombination (e.g. Taylor et al. 1998):

$$\mathrm{N^+ \overset{H_2}{\rightarrow} NH^+ \overset{H_2}{\rightarrow} NH_2^+ \overset{H_2}{\rightarrow} NH_3^+ \overset{H_2}{\rightarrow} NH_4^+} \tag{9.15}$$

$$\mathrm{NH_4^+ + \mathit{e}^- \rightarrow NH_3 + H}. \tag{9.16}$$

The first reaction in the sequence (9.15) is slightly endothermic (for about 1734 $\mathrm{J\,mol^{-1}}$), however the current consensus is that this reaction is sufficiently fast under interstellar conditions in order to maintain an acceptable rate of production of NH_3 at temperatures down to 10 K. The last reaction in the sequence (9.15) has a small activation barrier, is slow at room temperatures and the rate coefficient decreases as T decreases. However, at even lower temperatures the rate coefficient increases due to tunneling under the activation barrier (Herbst et al. 1991). Given the high relative abundance of H_2 in dense cores, this reaction seems to remain sufficiently fast so not to act as an impedance to ammonia production (Scott et al. 1997).

An alternative synthesis of ammonia initiated by the reaction between H_3^+ and N atoms which bypasses the first two reactions in (9.15), proposed by Dalgarno (1975):

$$\mathrm{H_3^+ + N \rightarrow NH_2^+ + H}, \tag{9.17}$$

was largely discounted due to supposedly large activation barrier obtained from *ab initio* quantum calculations. The detection of H_3^+ in interstellar space and later observations of this ion in several dense molecular clouds indicated that the significancy of this reaction may have been underestimated. Unlike most molecules, H_3^+ has a constant number density in molecular clouds independent of total H_2 number density, and the derived high number densities of $n(\mathrm{H_3^+}) \sim 1 \times 10^{-4}\,\mathrm{cm^{-3}}$ (McCall et al. 1999) stress the likelihood of the proposed initialization reaction for ammonia production. Additionally, recent first laboratory measurements show that the reaction (9.17) is sufficiently fast (the rate coefficient is $k = 4.5 \times 10^{-10}\,\mathrm{cm^3\,s^{-1}}$ at 300 K) to provide

a larger source of NH_3 in dense interstellar clouds at 10 K. If the observed rate coefficient does not change substantially with temperature, the relative rates of the first reaction in (9.15) and reaction (9.17) indicate that the later NH_3 production route may be a major source at temperatures around 10 K with both routes having equal roles at around 50 K (Scott et al. 1997).

9.2.3. "EARLY–" AND "LATE–TIME MOLECULES

HCO^+, SO and NH_3 are usually considered as late–time molecules; HCO^+ because it is formed from CO, and the latter two because their formation mechanisms involve relatively slow neutral–neutral reactions. SO is furthermore destroyed primarily by C I which at later stages is locked up in CO (e.g. Nilsson et al. 2000). CS forms early, but its abundance remains roughly constant because of recycling via HCS^+ (Nejad & Wagenblast 1999). The situation of HCN and HNC is less clear in this picture. The precursor ion, $HCNH^+$, is produced mainly via a reaction between NH_3 and the C^+ ion, thus involving both a typical 'late-time' molecule and an ion characteristic of young chemistry.

Usual assumption in all chemical networks is that almost all hydrogen is initially in form of H_2. However, the hydrogen atom number density in the coldest parts of a dark cloud may be more than one order of magnitude higher than expected for a cosmic rays induced ionization rate of $10^{-17}\,s^{-1}$ and an H/H_2 equilibrium obtained. In the recent models of Rawlings et al. (2002) it is shown that in an 'H-rich' environment the nitrogen chemistry is initiated at an early stage, and because of the less effective destruction of He^+ (due to a low CO abundance) NH_3 forms quickly thereafter. Under these circumstances also HNC is produced at early times via C + NH_2. NH_2 forms from a dissociative recombination of NH_3^+, which is one of the precursors of ammonia. In the 'H-poor' models of Rawlings et al., on the other hand, the formation of HCN is efficient via N + CH_2 or N + CH_3 at early times. From these results one can expect that at early stages of chemical evolution the HCN/HNC abundance ratio depends strongly on the initial H content.

9.2.4. IMPLICATION FOR THE CHEMISTRY OF THE ON–GOING STAR FORMATION

This division of molecules into two different families eventually holds only until a protostar is formed in the central part of a core. In YSOs heated molecular gas grain mantle material is returned to the gas, elemental depletion is controlled and we are able to observe characteristically 'young' chemistry (e.g., Nejad et al. 1990). X – ray surveys of star forming regions prove that YSOs of Class I–III have significant X – ray emission (e.g., Getman et al. 2002, Casanova et al. 1995). While X – ray emission from YSOs significantly heats only a very small fraction of the molecular core volume (e.g., Lepp & McCray 1983), X – ray ionization affects the whole core/cloud. Casanova et al. (1995) derived X – ray induced ionization rate throughout the ρ Oph cloud core to be comparable with the usually assumed cosmic rays ionization rate of $\sim 10^{17}\,s^{-1}$. A paradox situation may occur that a dynamically older core, with a central Class 0 embedded YSO is chemically younger than a preprotostellar core (Kontinen et al. 2000).

Table 9.3: Ratios of column densities, based on Table. 9.2. Relative errors of the ratios are in the range of 5–15%, for SO, CS, HCO^+ and HNC. For ratios that include ammonia, errors are in the range 20–25%.

	$\frac{[SO]}{[CS]}$	$\frac{[HCO^+]}{[CS]}$	$\frac{[NH_3]}{[CS]}$	$\frac{[SO]}{[HNC]}$	$\frac{[HCO^+]}{[HNC]}$	$\frac{[NH_3]}{[HNC]}$
H 1a	2.0	3.2	186	0.6	0.9	53
H 2a	0.5	2.6	–	0.1	0.8	–
H 2b	0.4	1.1	39	0.2	0.6	20
N 1	0.2	2.1	–	0.2	1.6	–
T 1a	0.4	1.4	90	0.1	0.3	20

Considering L 1251, the presence of T Tau stars in H1 a would indicate a dynamical age $\geq 10^6 - 10^7$ years for this core. The embedded YSOs (#6, #8, #14 and #15) in the remaining 4 cores point to ages of $10^4 - 10^5$ years, with the tail cores the youngest. The fractional abundances given in Table 9.2 lack clear trends with respect to the adopted dynamical ages of the cores. A high SO/CS ratio observed in H 1a indicates an evolved chemical stage of this core, yet close-by T Tau star (source #16) should have altered the chemistry and made the core look 'younger'. High HNC fractional abundance observed in T 1a (the coldest core) indicates that hydrogen–isocyanide belongs to the molecules which are resistive to freezing-out. The $NH_3/C^{18}O$ ratio observed in this core indicates CO depletion.

To possibly isolate trends suggested by chemical modeling, we have taken the naive approach to form the abundance ratios of 'late' – time relative to 'early' – time molecules. We assumed that HNC belongs to the later. Those data are presented in Table 9.3 (we used the relative fractional abundances of HNC and HCO^+ calculated from the ^{13}C – isotopomers), and should accordingly show decreasing ratios in the sequence H1 a, H2 a and the rest of the cores. Core H 1a shows the highest ratios (with one exception) indicating the most evolved dynamical stage in the sample and, thus, consistent with the adapted dynamical ages. However, as discussed above one would possibly expect the presence of T Tau star to alter the chemistry towards 'younger' stages. This suggests that the influence of the T Tau star is hardly significant, provided that present chemical networks of dense and cold clouds predict the evolution of molecular abundances in a rather accurate way. For the rest of the cores, Table 9.3 shows no definite trends which allow age sequencing. At the very best, our analysis indicates a possibility to discriminate cores with dynamical ages $\leq 10^5$ years from those older than $\geq 10^6$ years. However, to fully establish such a conclusion, a considerably larger sample of cores is needed.

9.3. CHEMICAL AGE VS. DYNAMICAL AGE

Chemistry in dark clouds and cold molecular cores changes during the star formation processes: prior to star formation, chemistry is dominated by low–temperature gas–phase reactions and grain surface reactions. As soon as the new star starts to warm

Table 9.4: Abundances relative to H_2. Both IRAS 22376+7455 and IRAS 22343+7501 are defined as Class I protostars, in spite of the very different outflow morphologies. Powering source of the compact outflow in L 1157, IRAS 20386+6751, is classified as a Class 0 protostar (Bachiller & Pérez Gutiérrez 1997).

Molecule	IRAS22376 + 7455	IRAS22343 + 7501	IRAS20386 + 6751
CS	2.6×10^{-9}	1.9×10^{-9}	6.4×10^{-9}
SO	1.0×10^{-9}	0.5×10^{-9}	8.0×10^{-9}

the surroundings, the ices are heated and molecules evaporate back to gas phase. Furthermore, shocks from protostellar outflows can change the environment significantly. While the abundances of some molecules (e.g. SiO, HCN, SO) are found to be larger by an order of magnitude along the axis of the outflow, the chemical composition of a dense core around the protostar may not change significantly (Bachiller & Pérez Guitérrez 1997). Therefore, chemical evolution of such dense cores can be described with gas–grain chemical models (e.g., Bergin & Langer 1997) or even pure gas-phase models, without need to incorporate shock-chemistry.

The L 1251 cores associated to the two CO outflows are H 2b and N 1. The embedded sources IRAS 22376+7455 and IRAS 2343+7501 are suggested to be powering the detected outflows (Sato et al. 1994). These CO outflows have different morphology indicating different ages (see Chapter 4.2.1): the IRAS 22376+7455 outflow is compact and highly collimated and has an estimated dynamical timescale[10] of 2×10^4 yr, while the IRAS 22343+7501 outflow is extended with the dynamical timescale estimated to be $\sim 1 \times 10^5$ yr (Sato et al. 1994). At the distance of L 1251, the spatial resolution achieved with the Onsala 20-m telescope is about 15 000 AU. The cores are of about the same size in all molecular lines mapped (see Chapter 7). Assuming spherical or elliptical shape, the 50% integrated intensity contour levels of the cores have diameters of about 20–35 000 AU.

Main isotope molecules *often* show that *strong saturation effects* are present and are thus not useful for abundance estimates. This is a general trend in both cores. The CS and SO fractional abundances relative to H_2 of the quiescent gas of the outflow cores are listed in Table 9.4. We have also included data from Bachiller & Pérez Gutiérrez (1997) of an IRAS source associated with a compact outflow in L1157 (Lynds 1962). Their fractional abundances have been recalculated using the isotopic abundance ratios of the Local ISM.

The fractional abundance variations we see cannot by certainty be attributed to chemical evolution. This applies to the gas within about 5 – 10 000 AU from the central objects. As indicated by the difference in the estimated dynamical ages of the outflows, ages of the two L 1251 cores might differ by about 10^5 years. This SO/CS ratio is expected to be low at 'early times' and high at 'late times', as demonstrated

[10]The dynamical timescale is determined as $\tau_{\rm dyn} = L/v$, where L is maximum separation, along the axes of the outflow, from the driving source to a point the peak wing intensity and v is maximum velocity shift of the ^{12}CO–wing emission from the $v_{\rm LSR}$ of the core/cloud. No correction for the unknown inclination is made.

by time–dependent chemical models (e.g. Bergin & Langer 1997). There are a number of reasons that might explain our results, e.g.:
• the drastic changes of the SO/CS abundance ratio only apply to the very dense parts of the cores, beyond the Onsala 20-m telescope spatial resolution;
• uncertainties in the sulfur chemistry in cold dark clouds, coupled with the oxygen chemistry;
• the *physical* ages of the cores studied are not within the relatively short time interval when significant changes of the SO/CS abundance ratio occur and
• the estimated dynamical ages of the outflows might be too crude, since the morphology of the outflow partly depends on the ambient ISM. Thus the sample cores may actually be of similar ages.

IRAS 20386+6751 in L 1157 powers a compact outflow; so far the best studied outflow from a chemical point of view (Bachiller & Pérez Gutiérrez 1997). Since the IRAS 22376+7455 outflow in L 1251 is also compact, the ages of the two sources may be similar. However, the comparison of fractional abundances in these two cores is not straightforward. The dark clouds L1157 and L1251 are not in the same region of the sky, implying that initial elemental abundances and physical environments are not necessarily the same. Thus different fractional abundances may be expected, e.g., the HCO^+ fractional abundances in both outflow cores in L 1251 are approximately the same, while in the L 1157 outflow core the HCO^+ is $\sim$4 times less abundant.

The best explanation in this case seems to be the last argument put forward, namely that the morphology of an outflow may be very different for powering sources of about the same age. IRAS 22376+7455 cannot be a Class 0 protostar, because it was observed at 12 μm, and even at 2.2 μm (Kun, 2001, priv. com.). Class 0 sources are not seen in NIR. The SEDs of the L 1157 protostar and IRAS 22376+7455 are very different, suggesting age difference. Moreover, having the Class I SED, IRAS 22376+7455 may be of about the same age as IRAS 22343+7501. The different morphologies of the outflows could be due to either different ambient ISM or, since the IRAS 22343+7501 "source" apparently consist of several YSOs, due to more energetic outflow and/or multiple outflows in different directions. If this is true, using the SO/CS ratio as a chemical clock actually may be quite reliable.

Chapter 10
STAR FORMATION IN L 1217/L 1219 I.

The double designation of the L 1217/L 1219 dark cloud is the result of an eye–estimate of the area and opacities of the clouds in the Lynds' catalog: L 1217 is a less opaque (opacity 3, on the scale 1–5 increasing opacity), more extended 'background molecular cloud', while L 1219 is the more opaque (opacity 5), central part of the cloud. The cloud lies at a distance of 400 pc (Kun 1998), at the southernmost edge of the Cepheus cloud complex. It is surrounded by Hα emission stars, stars having far–infrared excesses and a few Herbig Ae/Be stars (Kun et al. 2000a). All these young and PMS stars can be regarded as signposts of star formation in the recent past.

10.1. THE τ_{100} TRACED DUST

The IRAS 100 μm image of L 1217 indicates a "head – tail" structure (Kun et al. 2000b). The two clumps around cold far – infrared point sources, the IRAS 22129+7000 core (spatially well correlated with L 1219) and the IRAS 22127+7014 core may be sites of more recent star formation in L 1219. The brightest feature on the 100 μm image is the reflection nebula VDB 152, embedded in the "head" of L 1217 and illuminated by the young B9–type star BD+69°1231.

It is known (see, e.g., Langer at at. 1989) that, except along the line of sight toward embedded heat sources, the amount of dust associated with molecular clouds is reliably traced by the IRAS 100 μm optical depth images. Starting points of the procedure for construction such an image are the 60 μm and 100 μm ISSA images with the zodiacal light removed. For clouds with $\ell \geq 10°$, i.e., lying far from the Galactic plane, the diffuse Galactic FIR background can be approximated by a plane fitted on the intensity minima of the 100 μm image. Defined in this way, the Galactic background emission was subtracted from both images. The optical depth image was derived assuming a λ^{-1} dust emissivity law. Fig. 10.1 shows the L 1217 τ_{100} map (Nikolić & Kun 2003). The threshold value for dust cores is usually assumed to be $2-3\times10^{-4}$, the levels represented by the 2nd and 3rd contour, respectively. Thus, for the more strict core definition, L 1217 would have two "dust cores". The estimated center coordinates, the median optical depth, area and total mass of each core are given in Table 10.1. As usual in dark clouds, we assumed the dust – to – gas ratio to be 1:100.

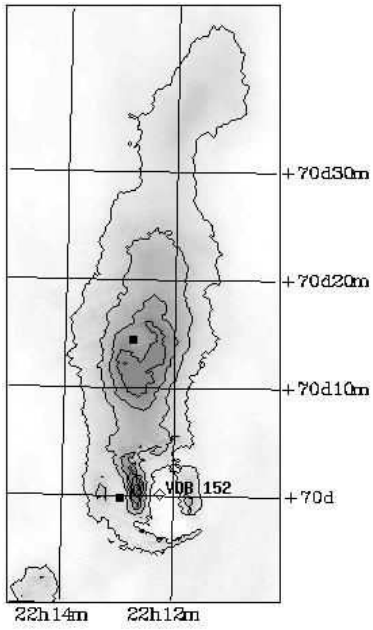

Figure 10.1: L 1217 IRAS 100 μm optical depth image. Contours start from 1.0×10^{-4} (which corresponds to $A_V \approx 2.0^{\rm mag}$) and increase by 1.0×10^{-4} to 6.0×10^{-4}. Filled squares denote IRAS 22129+7000 (in the southern area) and IRAS 22127+7014 (towards the north of the cloud). The VDB 152 reflection nebula is marked by open diamond.

Table 10.1: Dust cores in L 1217/L 1219.

N	RA(1950)			D(1950)			τ_{100}	A(pc^2)	$M/M_\odot$
1	22	12	49.3	70	0	43	2.65×10^{-4}	0.16	5
2	22	12	31.1	70	11	30	3.83×10^{-4}	1.27	59

10.2. MOLECULAR GAS

To trace the molecular gas content of L 1217 the 2×10^{-4} 100 μm optical depth defined area was selected for large–scale CO mapping. Using the Onsala Space Observatory 20-m telescope we made maps of L 1217/L 1219 in the ^{12}CO (1–0), ^{13}CO (1–0) and C^{18}O (1–0) lines during three observing sessions in 2000-2002. The telescope receiver was a SIS mixer with a typical $T_{\rm rec} = 100$ K (SSB) in the frequency range used. We used a 1600-channel correlator with 20 MHz bandwidth which yielded a spectral resolution of 0.034 km s^{-1} at 110 GHz. The HPBW of the telescope at this frequency is 35″. We estimate the pointing uncertainty to be $\approx 3''$ rms in Az and El. The observations were made in frequency switching mode, and calibration was done using the chopper–wheel method.

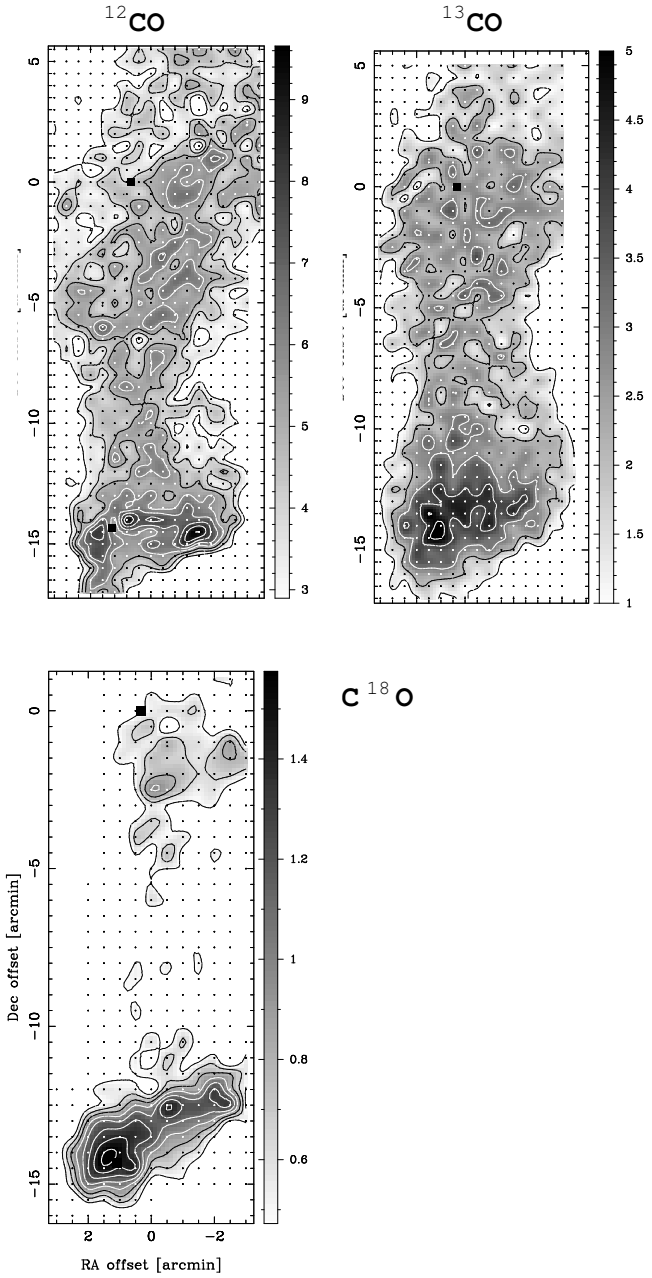

Figure 10.2: ^{12}CO,^{13}CO and C^{18}O integrated intensity ($\int T_A^* dv$) maps of L 1219. The offsets are relative to $22^h12^m31^s$, $70°14'30''$ (epoch 1950.0). Velocity ranges and contours are: for ^{12}CO - [–3,–7.5] km s^{-1}, 2.85(0.95)9.5 K km s^{-1}; for ^{13}CO- [–3.5,–6.5] km s^{-1}, 1.0(1.0)5.0 K km s^{-1} and for C^{18}O - [–4,–6] km s^{-1}, 0.45(0.15)1.5 K km s^{-1}, respectively. Filled squares denote the embedded FIR point sources.

Figure 10.2 shows the obtained maps (Nikolić & Kun 2003). The optical and IR structure of a comet shaped, characteristics of shocked clouds, is visible in the CO maps as well. The ^{12}CO and ^{13}CO line emissions are more extended than the C^{18}O line emission. This difference arises because the ^{12}CO and ^{13}CO lines emission trace the outer envelope of a dark cloud, while the C^{18}O line traces a higher column density gas. Assuming that the high column density gas is a high density gas, L 1217 would have one prominent dense core - the L 1219 cloud/core, with the embedded cold FIR point source IRAS 22129+7000.

To estimate the physical state of the gas we followed the procedure of Nikolić et al. (2001). The excitation temperature $T_{\rm ex}$ was assumed to be equal for the three CO isotopes. It was estimated from the peak intensity of the ^{12}CO (1–0) emission. Assuming optically thick ^{12}CO emission the excitation temperature of the 1–0 transition is calculated as

$$T_{\rm ex} = \frac{5.53}{\log[1 + \frac{5.53}{\eta T_A^* + 0.819}]}, \qquad (10.1)$$

where T_A^* is the measured ^{12}CO antenna temperature and η is the main beam efficiency of the telescope. For the L 1219 core the resulted $T_{\rm ex} = 12 \pm 1$ K, while in the norther part of L 1217 the excitation temperature was somewhat lower, $T_{\rm ex} = 10 \pm 1$ K. We adopted an excitation temperature of 10 K to be valid throughout the cloud.

The total gas mass (including He) of the cloud and the H_2 number density were derived from the ^{13}CO column densities, assuming an optically thin line and the LTE approximation, as $M = 10.5 \times I_{\rm mb}^{^{13}{\rm CO}}$ area. $I_{\rm mb}^{^{13}{\rm CO}}$ is the main beam integrated intensity of the ^{13}CO emission, and the derived mass is in $M_\odot$ if area is in [pc^2]. The whole cloud has around 62 $M_\odot$ gas mass, with almost half of the mass, 28 $M_\odot$, in L 1219 i.e., the "IRAS 22129+7000" core. Averaged across the cloud the hydrogen number density is 820 cm^{-3}. In the L 1219 core the higher average gas densities are found, $n_{\rm H_2} = 2.1 \times 10^3$ cm^{-3}. However, the peak hydrogen number density in this dense core is probably 10^{4-6} cm^{-3}, as revealed by CS (2–1) and HCN (1–0) observations (Nikolić & Kun, 2003, in preparation).

While the total mass estimates from the τ_{100} and the CO data for the whole cloud are in an agreement, there is a large discrepancy between mass estimates for L 1219 alone. This difference is most probably due to the VDB 152 reflection nebula. The nebula appears to heat up the outer layers of the cloud, raising the kinetic temperature of the gas from about 10 K in the periphery of the cloud to ~ 25 K in the reflection nebula adjacent gas layer. Assuming the ^{12}CO emission to be optically thick, Figure 10.4a shows the derived molecular gas kinetic temperature isolines overlayed on the clouds' optical image. Figure 10.4b presents the C^{18}O integrated emission contours. Thus, the heated up dust in the VDB 152 neighborhood has significantly lower emission in the 60–100 μm wavelength range.

10.2.1. DISCOVERY OF AN EXTENDED CO OUTFLOW

Fig. 10.3 shows the distribution of the ^{12}CO line integrated intensities between –6 and –8 km s^{-1}, and –2 and –4 km s^{-1}, the blue and the red emission wing component, respectively. The map displays an extended bipolar outflow with axes in the NE–SW

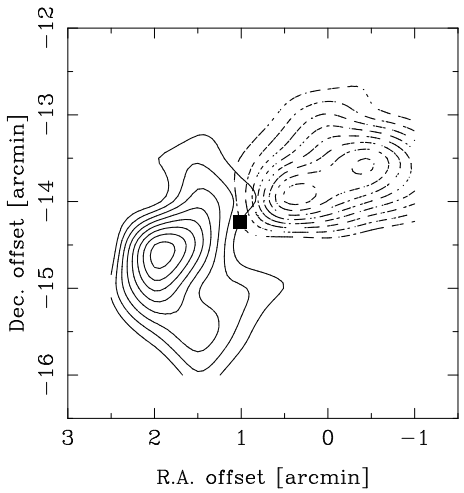

Figure 10.3: Integrated intensity map of the blue– (greyscale) and the red–shifted (contours) CO emission. The velocity ranges are (–6,–8) and (–2,–4) $\mathrm{km\,s^{-1}}$ for the blue and the red wings, respectively. The intensity scale is in $T_A^* dv$ [$\mathrm{K\,km\,s^{-1}}$] with contours from 0.3 by an increment of 0.15 $\mathrm{K\,km\,s^{-1}}$. The filled square marks the position of IRAS 22129+7000.

direction. Projected position of IRAS 22129+7000 suggests that it is the driving source of the CO outflow. Physical parameters of the outflow are presented in Table 10.2. The excitation temperature of the high–velocity gas was assumed to be the same as that of the quiescent gas, $T_{\mathrm{ex}} = 10\,\mathrm{K}$. We assumed an optical depth of 4 at all velocities of the outflowing gas. The column density of H_2 was estimated using the ratio $[H_2]/[^{12}\mathrm{CO}] = 1 \times 10^4$ (Frerking et al. 1982). In calculating momentum, kinetic energies and mechanical luminosities, we used characteristic velocities, listed in column (2) i.e., the maximum velocity shifts of the ^{12}CO emission from the $v_{\mathrm{LSR}} = -5.0\,\mathrm{km\,s^{-1}}$, the mean velocity of the quiescent gas. The radius was defined as the maximum separation, along the axes of the outflow, from the driving source to a point where the wing intensity falls to half the peak intensity. We assumed a distance to L 1219 of 400 pc (Kun 1998). The mechanical luminosity is calculated as $L_{\mathrm{CO}} = E_{\mathrm{kin}}/t_{\mathrm{dyn}}$. The dynamical timescale, on the other side is defined as $t_{\mathrm{dyn}} = L/v$, where L is the separation of the centers of the blue– and redshifted lobes, and v is the difference between the blue and the red characteristic velocities. No correction for the unknown inclination of the flow is taken into account, i.e. we assumed that $\sin i = 1$. The major uncertainties in the derived values are the CO optical depth, the excitation temperature of the gas and the inclination angle of the flow.

10.3. YSOS AND YOUNG PMS STARS

In the cloud region Kun (1998) has identified 9 YSO candidates. Table 10.3 is an excerpt from her Table 2. Columns 2–5 list the IRAS fluxes in given wavelengths. The dust temperature, T_d, given in column 6, is calculated from the 60 and 100 μm

Table 10.2: Physical parameters of the IRAS 22129+7000 CO outflow.

Outflow component	Velocity [km s^{-1}]	Mass [$M_\odot$]	Momentum [$M_\odot$ km s^{-1}]	$E_{\rm kin}$ [10^{43} erg]	r [pc]	$L_{\rm mech}$ [$L_\odot$]	$t_{\rm dyn}$ [yr]
Blue	4.0	0.04	0.18	0.7	0.20	1.1	4.9×10^4
Red	3.7	0.07	0.25	0.9	0.28	1.2	7.4×10^4

emission, assuming that the emitting radiation is optically thin and that standard interstellar grains (see, e.g., Hildebrand 1983) are responsible for the IR emission. Luminosities calculated over the 7–135 μm region are listed in column 7. The criteria which IRAS source should fulfill to be defined as a YSO were set up by Beichman et al. (1986): a source should have a 25 μm flux that is larger than the flux at 12 μm, $F_{25} > F_{12}$, or it should have definite detection of good quality (2 or 3 flag) at both longer wavelengths, 60 μm and 100 μm. Of the 9 sources, four sources coincide with $H\alpha$ emission stars, as revealed by photographic observations. Further two YSO candidates, IRAS 22129+7000 and IRAS 22144+6923, could possibly be associated with very faint stars. The rest of the embedded YSO candidates are invisible in the optical domain, that is, sources IRAS 22230+7112, IRAS 22150+7102 and IRAS 22127+7014.

Table 10.3: IRAS point sources adopted as YSO candidates in L 1217/L 1219.

Name IRAS	F_{12} (Jy)	F_{25} (Jy)	F_{60} (Jy)	F_{100} (Jy)	$T_d(100-60)$ (K)	$L_{\rm IRAS}$ ($L_\odot$)
22122+7000	2.190	3.690	28.800	74.19	-	21.15
22126+6947	0.144	0.302	0.732	<5.037	-	>0.54
22127+7014	<0.110	<0.100	0.576	8.60	20.0	>1.12
22129+7000	0.193	1.117	2.780	18.0	24.5	3.57
22144+6923	0.243	0.281	0.401	2.60	-	0.85
22150+7102	<0.100	<0.100	0.663	5.160	-	>0.76
22156+6948	<0.070	0.285	1.428	<1.7	-	>0.55
22230+7112	<0.100	0.210	0.284	3.600	-	>0.58
22233+6926	0.233	0.533	1.911	6.899	-	1.87

As discussed earlier (Sec. 10.1), IRAS 22129+7000 and IRAS 22127+7014 are apparently closely associated with the τ_{100} defined dust cores. Their estimated dust temperatures T_d are also listed in Table 10.3. Both sources show very cold dust emission indicative of an early evolutionary stage. IRAS sources classified as "embedded" YSOs usually have color indices of $[100-60] \leq 0.6$, corresponding to dust temperatures of $T_d > 27$ K. Sources of this class are found inside some well studied clouds of the Cepheus region (L1171, L1177, L1228, L1251 and L1262) and are powering molecular outflows and/or optical jets (see, e.g. Sato & Fukui 1989; Sato et al. 1994; Balázs et al. 1992). They are among the most luminous IRAS sources of the region,

and most of them proved to be multiple objects (Bally et al. 1995; Hodapp 1994; Yun 1996). All these objects are 'Class I' YSOs according to the empirical classification scheme (e.g. Lada 1987), i.e. they have already accreted most of their mass. IRAS 22127+7014, having lower dust temperature and projected within the area of a dense core might have been an accreting (Class 0) protostar, and thereby one of the youngest objects of the Cepheus Flare region, if it was not for the absence of any dense molecular gas (traced by e.g., $C^{18}O$, see Fig. 10.2) surrounding it. This may indicate that the source is only a foreground object, projected on the molecular cloud area. IRAS 22129+7000, however, coincides in position with a faint ($\approx 20^m$) star. The discovered CO outflow with IRAS 22129+7000 suspected to be the powering source, suggests on the other hand the existence of an invisible Class 0/I YSO. So does the discovery of the new Herbig – Haro (HH) object, HH 450 (Bally & Reipurth 2001), emerging from this cold source. These results all suggest that we are seeing the birth of a multiple, or at least a binary, stellar system.

The H_α emission stars, i.e. PMS stars, were subject of a follow up study by Kun et al. (2000a). Table 10.4 lists the results of the spectroscopic observations: name of the star is in column 1, IRAS source designation in column 2, $T_{\rm eff}$ and $v_{\rm LSR}$ derived from the H_α profile fit are in columns 3 and 4. The spectral type and luminosity class derived from their spectroscopy is shown in column 5, and the $E(B-V)$ color excess derived from the determined spectral types and published $B-V$ colors is in column 6. The distances, D, listed in column 7 are based on the absolute magnitudes and intrinsic colors corresponding to the derived spectral and luminosity classes.

Table 10.4: The results of the spectroscopic observations (from Table 3 of Kun et al. 2000a).

Name	IRAS	$T_{\rm eff}$ [K]	$v_{\rm LSR}$ [km s^{-1}]	SP.type	$E(B-V)$ [mag]	D [pc]
SAO19953	22127 + 6947	11000	−10(5)	B8.5 V	0.37(0.04)	450(50)
BOCep	22156 + 6948	–	−40(30)	F3 IVe	0.16(0.12)	540(50)
HD212826	22233 + 6025	10000	−4(5)	B9.5 V	0.19(0.04)	460(50)
BD + 69°1231	22122 + 7000	11000	0(10)	B9 V	0.22(0.04)	480(50)

These four stars may represent a loose group close to the L 1219 dark cloud. Taking a value of 10^7 yr for the ages of these stars, the dispersion of the radial velocities and the distances given in Table 10.4 do not contradict the assumption on their common birthplace (Kun et al. 2000a). Their spectral energy distribution (SED) was estimated from the unreddened B_0 and V_0 magnitudes together with the IRAS fluxes (Kun et al. 2000a). All stars showed the far – infrared excess emission, typical of stars still surrounded by the dust envelopes or disks. BO Cep has very peculiar SED, and there are indications that this star is an eclipsing binary. The spectral classification indicates that this Herbig Ae/Be star is above the main sequence, being a few times 10^7 yr old. SAO 19953 and HD 212826 both display SEDs resembling those of β Pic type stars. Their [12] – [25] colors indicate dust temperatures in the

160–330 K interval. The rising SED of HD 212826 in the 60–100 μm region is indicative of extended cold dust structures around the star. SAO 19953 exhibits a shallow H_α emission line. BD+69° 1231, a star associated with the VDB 152 reflection nebula, has a slope of the SED function that is characteristic of a geometrically thin, optically thick circumstellar disk, which derives its luminosity from re–radiating the absorbed star light. The star is still embedded in the large dust cloud, as shown by its reflection nebula.

10.4. THE REFLECTION NEBULA ENVIRONMENT

The optical appearance of L 1217/L 1219 cloud is dominated by the bright reflection nebula VDB 152/Ced 201. VdB 152 is a part of the molecular cloud illuminated by a B9 V star, BD+69°1231, (Kun et al. 2000a). Infrared Space Observatory (*ISO*) observations, combined with the ground based molecular line data, indicated presence of a small amount of very warm, with temperatures of ∼330 K, molecular gas, located in a thin layer at the illuminated edge of the cool PDR (Kemper et al. 1999).

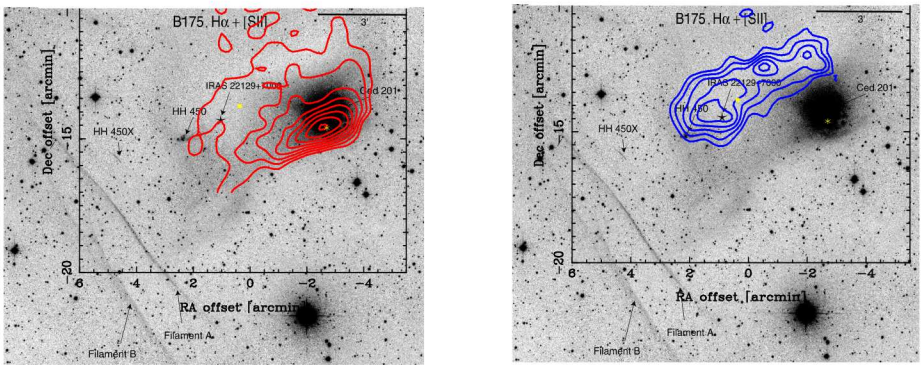

Figure 10.4: ^{12}CO estimated molecular gas kinetic temperature isolines (left) and C^{18}O integrated intensity contours (right) overlayed on the optical image of L 1219 (Barnard 175 globule) from Bally & Reipurth (2001). The nebulous star is the B9.5 V star BD +69°1231, surrounded by the reflection nebula VdB 152 (Ced 201). The new HH object, HH450, is identified, as is the location of its embedded driving source IRAS 22129+7000. Filaments of the new supernova remnant G110.3+11.3 are located southeast of the L 1219 (lower left corner). Assuming the optically thick ^{12}CO (1–0) line, contours are from 10 K increasing by 2 K. The C^{18}O intensity scale is in $T_A^* dv$ [K km s^{-1}] with contours from 0.45 by an increment of 0.15 K km s^{-1}. The star marks the position of IRAS 22129+7000.

Future mapping of the C^{18}O core area in appropriate high gas density and gas kinetic temperature tracers could reveal more about chemical effects of the reflection nebula on the molecular gas in L 1219 (Nikolić et al. 2004, in preparation).

Chapter 11
SUMMARY

Pre – protostellar and low – mass star – forming molecular clouds in the Cepheus and Cassiopeia region were studied in order to trace a SN induced shock legacy. The sample consists of the pre – protostellar clouds L 1274 (located at a distance of 200 pc, Nikolić et al. 2001) and Kh 15 (250 pc, Kiss et al. 2000) and protostellar L 1219 (400 pc, Kun 1998) and L 1251 (300 pc, Kun & Prusti 1993). We have considered dynamical (e.g. discrepancies in gas mass estimates) and chemical signposts (e.g. relative abundances of trace molecules in cores in supposedly different stages of evolution) of a shock – cloud interaction.

A prominent "banjo–shaped" structure in CO of Kh 15 indicates the possibility of a shock – cloud close encounter. ^{13}CO lines peak velocities vary systematically in the SW–NE direction, i.e., in the head–to–tail direction, thus giving a velocity gradient across the cloud of $0.3\,\mathrm{km\,s^{-1}\,pc^{-1}}$. The "head" of the cloud points toward the center of a $\sim 7^\circ$ diameter FIR loop/shell GIRL126+10. Such FIR loops are proposed to be traces of shocks of various origins (e.g., supernova induced or strong stellar winds) that have swept out the interstellar dust (and gas). However, dynamical stability analysis, with assumed external pressure and calculated for an ideal gas and with rotation and magnetic fields neglected, shows that Kh 15 may be in a stable equilibrium. If these assumptions hold, then the cloud might have collided with a shock front long time ago. The CO small velocity gradient seems to support this.

Apart of morphological and kinematical traces that a shock–cloud collision may leave, e.g., a cometary shaped cloud and large velocity gradient across a cloud, we have searched for dynamical legacy of such a collision in L1274. The cloud seems to be in a rather violent area as indicated by soft X – ray excess radiation, several detected Far–IR loops, lack of CO emission and presence of radio – continuum loops. Full CO maps of L 1274 indicated two distinct features: a "main body" and an adjacent filament, "ridge" . The main body virial mass is much larger than the CO – inferred gas mass which is a property usually attributed to HLCs. However, the derived mean density of H_2 is at least an order of magnitude larger than typical for HLCs, i.e. similar to ordinary dark cloud cores. No indications of extraordinary physical or chemical properties of the gas that would change significantly our mass estimates were found. Likewise, there were no obvious signs of an internal activity that could explain the difference between the virial masses and the CO mass estimates. An argument in favor of a slow–shock passage is the observed excess of the 100 micron

emission - a low – velocity shock would enhance grain growth in the postshock gas probably through some combination of accretion and coagulation, resulting in a grain distribution in which there is an excess of large grains and a deficiency of very small grains. From all available data, our analysis suggests that there is a high possibility of a supernova induced shock front passage which, either, disturbed an existing cloud, or, triggered the formation of it. The ridge might be a consequence of such a passage, i.e., it has gained some positive peculiar velocity relative to the main body.

The dark cloud L 1251 has an estimated SFE as high as 30% (Kun & Prusti 1993). Both location and cloud morphology suggest that apart of spontaneous there is a contribution from externally stimulated star formation. We have surveyed the ammonia defined dense cores areas in HCN, HNC, CS and HCO^+ and selected positions were observed in ^{13}CO, $C^{18}O$, $H^{13}CN$, $HN^{13}C$, $H^{15}NC$, $C^{34}S$, $H^{13}CO^+$, $HC^{18}O^+$, SO and CH_3CCH. The distribution of the cores in all molecules is divided into three groups - 'head', 'north' and 'tail', and follows the detected NH_3 cores from a comparable study. From the CH_3CCH observations we derived a molecular gas kinetic temperature "gradient" of around 15 K in head–to–tail direction. Although the temperature differences could be explained in terms of a slow shock passage, possibly the more extensive star formation in the head, with YSOs heating their surroundings are to blame. The high HNC fractional abundance observed in the coldest core of L 1251 indicates that hydrogen–isocyanide belongs to the molecules which are resistive to freezing–out and the observed $NH_3/C^{18}O$ ratio indicates possible CO depletion. Of the molecules we used HCO^+, SO and NH_3 are usually considered as "late–time" molecules. CS forms early, and its abundance remains roughly constant, and while the situation of HCN and HNC is less clear we assumed them to belong to the same "early–time" species. Assuming that the abundance ratios of "late–time" relative to "early – time" molecules can be used to follow the presumed "chemical" age, and that presence of YSO and PMS stars reflects the true dynamical age of the dense cores, from head–to–tail direction the ratios should show decreasing values. The core which has the most evolved chemistry has also the oldest adapted dynamical age. However, as discussed above one would possibly expect the presence of T Tau stars to alter the chemistry towards 'younger' stages. This suggests that the influence of a T Tau star is hardly significant, provided that present chemical networks of dense and cold clouds predict the evolution of molecular abundances in a rather accurate way. For the rest of the cores no definite trends which allow age sequencing are present. At the very best, our conclusion is that the observed chemical differences in L 1251 are probably due to combined effects of different gas density and, eventually, initial abundances of some elements/ions in the cloud and the extensive on–going star formation.

The low–mass star forming cloud L 1217/L 1219 is also a molecular cloud with a prominent cometary shape visible in all domains studied — optical, FIR and mm domain. The cloud has an extended low–density gas emission as traced by the ^{12}CO (1–0) and the ^{13}CO (1–0) lines, and one dense core, as indicated by the $C^{18}O$ (1–0) line emission. New stars have been born in the cloud during the last 10^7 years, and the star formation is still going on. We have detected an extended CO outflow, emerging from a deeply embedded companion of a faint star, what indicates that we are currently witnessing birth of a multiple solar system in L 1219.

The work presented here has shown that multiwavelength studies in as possible as broad range of the spectra are powerful tool in tracing kinematical and dynamical legacies of cloud – shock "collisions". For starless cores/clouds each of the optical, IR and radio spectroscopical data are necessary for proper estimate of the physical properties of the molecular gas and the associated dust. For star–forming clouds, morphology and kinematics of the cloud may be indicators of a close encounter with a shock front. However, we have chosen a new approach and made an attempt to evaluate importance of chemical signatures of a shock passage. It turned out that number of YSOs in different stages of evolution and their position in a cloud is more important indicator of a shock-triggered star formation than any chemical signatures such a shock might have left. As soon as a protostar reaches the Class I stage, it continously alters the chemistry via high–speed shocks, X-ray emission and thermal heating, thus undermining significance of a chemical age used for this purpose.

References

Abergel, A., Boulanger, F., Mizuno, A., Fukui, Y.: 1994, *Astrophys. J.* **423**, L59.

Ábrahám, P., Balázs, L.G., Kun, M.: 2000, *Astron. Astrophys.* **354**, 645.

Adams, F.C., Myers, P.C.: 2001, *Astrophys. J.* **553**, 744.

Alcála, J.M., Corvino, E., Sterzik, M.F. et al.: 2000, *Astron. Astrophys.* **355**, 629.

Alfvén, H.: 1947, *Mon. Not. Roy. Astron. Soc.* **107**, 211.

Allen, T.L., Goddard, J.D., Schaefer, H.F. III: 1980, *J.Ch.Ph.* **73**, 3255.

Alten, V.P., Bally, J., Devine, D., Miller, G.J.: 1997, in Low Mass star Formation - from Infall to Outflow, Poster Proc. of the IAU Symp. No. 182, eds Malbert F. & Castets A., p.51.

Alves, J., Lada, C.J., Lada, E.A., Kenyon, S., Phelps, R.: 1998, *Astrophys. J.* **506**, 292.

Alves, J., Lada, C.J., Lada, E.A.: 1999, *Astrophys. J.* **515**, 265.

Anderson, I.M., Caselli, P., Haikala, L.K., Harju, J.: 1999, *Astron. Astrophys.* **347**, 983.

André, P., Ward–Thompson, D., Barsony, M.: 1993, *Astrophys. J.* **406**, 122.

André, P., Montmerle, T.: 1994, *Astrophys. J.* **420**, 837.

André, P., Barsony, M., Ward–Thompson, D.: 2000, in Protostars and Planets IV, eds. Mannings V., Boss A., Russell S., Tucson: Univ. Arizona Press.

Anglada, G., Sepúlveda, I., Gómez, J.F.: 1997, *Astron. Astrophys. Suppl.* **121**, 255.

Anglada, G., Villuendas, E., Estalella, R. et al.: 1998, *Astron. J.* **116**, 2953.

Askne, J., Höglund, B., Hjalmarson, Å., Irvine W.M.: 1984, *Astron. Astrophys.* **130**, 311.

Bachiller, R., Martín–Pintado, J., Tafalla, M., Cernicharo, J., Lazarett, B.: 1990, *Astron. Astrophys.* **231**, 174.

Bachiller, R., Guillioteau, S., Dutrey, A., Planesas, P., Martín–Pintado, J.: 1995, *Astron. Astrophys.* **299**, 857.

Bachiller, R., Pérez Gutiérrez, M.: 1997, *Astrophys. J.* **487**, L93.

Bachiller, R., Tafalla, M.: 1999, in The Physics of Star Formation and Early Stellar Evolution, Kluwer: Dordrecht.

Balázs, L.G., Eisloeffel, J., Holl, A., Kelemen, J., Kun, M.: 1992, *Astron. Astrophys.* **255**, 281.

Bally, J.: 1982, *Astrophys. J.* **262**, 558.

Bally, J., Reipurth, B.: 2001, *Astrophys. J.* **552**, L159.

Bally, J., Devine, D., Fesen, R.A., Lane, A.P.: 1995, *Astrophys. J.* **454**, 345.

Bania, T.M.: 1977, *Astrophys. J.* **216**, 381.

Barlow, M.J., Silk, J.: 1976, *Astrophys. J.* **207**, 131.

Barnard, E.E.: 1927, in Photographic Atlas of Selected Regions of the Milky Way, ed. Frost E.B., Calvert M.L., Washington D.C.: Carnegie Inst.

Barnes, C.: 1979, *Astron. Astrophys.* **73**, 67.

Barsony, M., Kenyon, S.J.: 1992, *Astrophys. J.* **384**, L53.

Barsony, M., Ward–Thompson, D., André, P., O'Linger, J.: 1998, *Astrophys. J.* **509**, 733.

Bash, F.M., Peters, W.L.: 1976, *Astrophys. J.* **205**, 786.

Bate, M.R.: 1998, *Astrophys. J.* **508**, L95.

Beichman, C.A., Myers, P.C., Emerson, J.P., Harris, S., Mathieu, R., Benson, P., Jennings, R.E.: 1986, *Astrophys. J.* **307**, 337.

Beichman, C.A.: 1987, *Ann. Rev. Astron. Astrophys.* **25**, 603.

Bell, M.B.: 2000, *Astrophys. J.* **531**, 820.

Beltrán, M.T., Estalella, R., Anglada, G., Rodríguez, L.F., Torrelles, J.M.: 2001, *Astron. J.* **121**, 1556.

Benson, P.J., Myers, P.C.: 1989, *Astrophys. J. Suppl.* **71**, 89.

Benson, P.J., Daselli, P., Myers, P.C.: 1998, *Astrophys. J.* **506**, 743.

Bergin, E.A., Goldsmith, P.F., Snell, R.L., Ungerechts, H.: 1994, *Astrophys. J.* **431**, 674.

Bergin, E.A., Langer, W.D.: 1997, *Astrophys. J.* **486**, 316.

Bergin, E.A., Melnick, G.J., Neufeld, D.A.: 1998, *Astrophys. J.* **499**, 777.

Berkhuijsen, E.M., Haslam, C.G.T., Salter, C.J.: 1971, *Astron. Astrophys.* **14**, 252.

Berkhuijsen, E.M.: 1973, *Astron. Astrophys.* **24**, 143.
Bertout, C., Basri, G., Bouvier, J.: 1988, *Astrophys. J.* **330**, 350.
Bhattacharya, B.N., Gordy, W.: 1960, *Phys. Rev.* **119**, 144.
Black, J.H., Dalgarno, A.: 1973, *Astrophys. J.* **15**, L79.
Blake, G.A., Sutton, E.C., Masson, C.R., Phillips, T.G.: 1987, *Astrophys. J.* **315**, 621.
Blake, G.A., Sandell, G., van Dishoeck, E.F., Groesbeck, T.D., Mundy, L.G., Aspin, C., 1995, *Astrophys. J.* **441**, 689.
Blandford, R.D., Payne, D.G.: 1982, *Mon. Not. Roy. Astron. Soc.* **199**, 883.
Blitz, L., Shu, F.H.: 1980, *Astrophys. J.* **238**, 148.
Blitz, L., Magnani, L., Mundy, L.: 1984, *Astrophys. J.* **282**, L9.
Bok, B.J., Reilly, E.F.: 1947, *Astrophys. J.* **105**, 255.
Bonazzola, S., Heyvaerts, J., Falgarone, E., Perault, M., Puget, J.L.: 1987, *Astron. Astrophys.* **172**, 293.
Bontemps, S., André, P., Ward–Thompson, D.: 1995, *Astron. Astrophys.* **297**, 98.
Bontemps, S., André, P., Tereby, S., Cabit, S.: 1996, *Astron. Astrophys.* **311**, 858.
Boreiko, R.T., Betz, A.L.: 1995, *Astrophys. J.* **454**, 307.
Boss, A.P.: 1997, *Astrophys. J.* **483**, 309.
Boulanger, F., Bronfman, L., Dame, T.M., Thaddeus, P.: 1998, *Astron. Astrophys.* **332**, 273.
Bourke, T.L., Garay, G., Lehtinen, K.K., Koehnenkamp, I., Launhardt, R. et al.: 1997, *Astrophys. J.* **476**, 781.
Bouvier, J., Covino, E., Kovo, O., Martín, E.L., Matthews, J.M. et al.: 1995, *Astron. Astrophys.* **299**, 89.
Brand, P.W.J.L., Zealey, W.J.: 1975, *Astron. Astrophys.* **38**, 361.
Burton, W.B., Hartmann, D.: 1994, *Astrophys. Space Sci.* **217**, 189.
Bystrova, N.V.: 1998, in The Local Bubble and Beyond Lyman-Spitzer Colloquium, Proceedings of the IAU Colloquium No. 166, Lecture Notes in Physics, vol.506, Springer-Verlag Berlin Heidelberg New York, eds. Breitschwerdt D., Freyberg M.J., Truemper J.
Cabrit, S., Raga, A., Gueth, F.: 1997, in Herbig–Haro Flows and the Birth of Low Mass Stars, IAU Symp. 182, eds. Reipurth B., Bertout C.
Calvet, N., Basri, G., Kuhi, L.V.: 1984, *Astrophys. J.* **277**, 725.
Carruthers, G.P.: 1970, *Astrophys. J.* **161**, L81.
Casanova, S., Montmerle, T., Feigelson, E.D., André, P.: 1995, *Astrophys. J.* **439**, 752.
Caselli, P., Walmsley, C.M., Terzieva, R., Herbst, E.: 1998, *Astrophys. J.* **499**, 234.
Caselli, P., Walmsley, C.M., Tafalla, M., Dore, L., Myers, P.C.: 1999, *Astrophys. J.* **523**, L165.
Caselli, P.: 2000, in Astrochemistry: From Molecular Clouds to Planetary Systems, IAU Symp. 197, eds. Minh Y.C., van Dishoeck E.F., ASP Publ. pg. 41
Caselli, P., Benson, P.J., Myers, P.C., Tafalla, M.: 2002, *Astrophys. J.* **572**, 238.
Cernicharo, J., Castets, A., Duvert, G., Guilloteau, S.: 1984, *Astron. Astrophys.* **139**, L13.
Cernicharo, J., Guellin, M.: 1987, *Astron. Astrophys.* **176**, 299.
Cesarsky, D., Lequeux, J., Ryter, C., Gérin, M.: 2000, *Astron. Astrophys.* **354**, L87.
Chandrasekhar, S.: 1939, An Introduction to Stellar Structure, Chicago: Univ. Chicago Press.
Chandrasekhar, S., Fermi, E.: 1953, *Astrophys. J.* **118**, 116.
Charnley, S.B.: 1998, *Astrophys. J.* **508**, L121.
Chen, H., Myers, P.C., Ladd, E.F., Wood, D.O.S.: 1995, *Astrophys. J.* **445**, 377.
Chengalur, J.N., Braun, R., Butler Burton, W.: 1997, *Astron. Astrophys.* **318**, L35.
Cheung, A.C., Rank, D.M., Townes, C.H., Knowles, S.H., Sullivan, W.T.: 1969, *Astrophys. J.* **157**, L13.
Choi, M., Evans, N.J. II, Gregsen, E.M., Wang, Y.: 1995, *Astrophys. J.* **448**, 742.
Chou, W., Matsumoto, R., Tajima, T., Umekawa, M., Shibata, K.: 2000, *Astrophys. J.* **538**, 710.
Churchwell, E., Hollis, J.M.: 1983, *Astrophys. J.* **272**, 591.

Churchwell, E., Nash, A.G., Walsmley, C.M.: 1984, *Astrophys. J.* **287**, 681.
Ciolek, G.E., Mouschovias, T.Ch.: 1993, *Astrophys. J.* **418**, 774.
Claussen, M.J., Wilking, B.A., Benson, P.J. et al.: 1996, *ApJSS* **106**, 111.
Clemens, D.P., Sanders, D.B., Scoville, N.Z., Solomon, P.M.: 1986, *Astrophys. J. Suppl.* **60**, 297.
Clemens, D.P., Barvainis, R.: 1988, *Astrophys. J. Suppl.* **68**, 257.
Cohen, M.: 1984, *Phys. Rep.* **116(4)**, 173.
Combes, F.: 1991, *Ann. Rev. Astron. Astrophys.* **29**, 195.
Coppin, K.E.K., Greaves, J.S., Jenness, T., Holland, W.S.: 2000, *Astron. Astrophys.* **356**, 1031.
Cox, D.P., Raynolds, R.: 1987, *Ann. Rev. Astron. Astrophys.* **25**, 303.
Crutcher, R.M.: 1999, *Astrophys. J.* **520**, 706.
Dalgarno, A.: 1975, in Interaction between Ions and Molecules ed. Ausloos P., Plenum Press, New York, p. 341.
Dalgarno, A.: 2000, in Astrochemistry: From Molecular Clouds to Planetary Systems, IAU Symp. 197, eds. Minh Y.C., van Dishoeck E.F., Astr. Soc. of Pacific.
Dalgarno, A., Lepp, S.: 1984, *Astrophys. J.* **287**, L47.
Dame, T.M.: 1998, in The Physics and Chemistry of the Interstellar Medium, Proc. of the 3rd Cologne–Zermatt Symp. eds. Ossenkopf V., Stutzki J., Winnewisser G., GCA-Verlag.
Dame, T.M., Elmegreen, B.G., Cohen, R.S., Thaddeus, P.: 1986, *Astrophys. J.* **305**, 892.
Dame, T.M., Ungerechts, H., Cohen, R.S. et al.: 1987, *Astrophys. J.* **322**, 706.
Dame, T.M., Hartman, D., Thaddeus, P.: 2000, *Astrophys. J.* in prep.
De Boisanger, C., Helmich, F.P., van Dishoeck, E.F.: 1996, *Astron. Astrophys.* **310**, 315.
De Jong, T., Chu, S.-I., Dalgarno, A.: 1975, *Astrophys. J.* **199**, 69.
De Jong, T., Dalgarno, A., Boland, W.: 1980, *Astron. Astrophys.* **91**, 68.
De Zeeuw, P.T., Hoogerwerf, R., de Bruijne, H.J., Brown, A.G.A., Blaauw, A.: 1999, *Astron. J.* **117**, 354.
Désert, F.X., Bazell, D., Boulanger, F.: 1988, *Astrophys. J.* **334**, 815.
Désert, F.X., Boulanger, F., Puget, J.L.: 1990, *Astron. Astrophys.* **327**, 215.
Dickens, J.E., Irvine, W.M., Snell, R.L., Bergin, E.A., Schloerb, F.P., Pratap, P., Miralles, M.P.: 2000, *Astrophys. J.* **542**, 870.
Dickey, J.M., Lockman, F.J.: 1990, *Ann. Rev. Astron. Astrophys.* **28**, 215.
Dickman, R.L.: 1978, *Astrophys. J. Suppl.* **37**, 407.
Dickman, R.L., Clemens, D.P.: 1983, *Astrophys. J.* **271**, 143.
Dickman, R.L., Horvath, M.A., Margulis, M.: 1990, *Astrophys. J.* **365**, 568.
Digel, S.W., Grenier, I.A., Heithausen, A., Hunter, S.D., Thaddeus, P.: 1996, *Astrophys. J.* **463**, 609.
Douglas, A.E., Herzberg, G.: 1941, *Astrophys. J.* **94**, 381D.
Draine, B.T., Roberge, W.G., Dalgarno, A.: 1983, *Astrophys. J.* **264**, 485.
Drain, B.T., McKee, C.F.: 1993, *Ann. Rev. Astron. Astrophys.* **31**, 373.
Duley, W.W., Williams, D.A.: 1986, *Mon. Not. Roy. Astron. Soc.* **223**, 177.
Dunham, T.: 1937, *Publ. Astron. Soc. Pacific*, **49**, 26.
Dunham, T., Adams, W.S.: 1937, *Publ. Am. Astr. Soc.* **9**, 5.
Eiroa, C., Torrelles, J.M., Miranda, L.F., Anglada, G., Estalella, R.: 1994, *Astron. Astrophys. Suppl.* **108**, 73.
Elmegreen, B.G.: 1982, *Astrophys. J.* **253**, 634.
Elmegreen, B.G.: 1985, in Protostars and Planets II, eds. Black D.C., Matthews M.S., Tucson: Univ. Arizona Press.
Elmegreen, B.G.: 1987, in Interstellar Processes, eds. Hollenbach D.,J., Thornston H.A.Jr., Dordrecht: D.Reidel Publishing company.
Elmegreen, B.G.: 1987a, *Astrophys. J.* **312**, 626.
Elmegreen, B.G.: 1989, *Astrophys. J.* **342**, L67.

Elmegreen, B.G.: 1992, in Star Formation in Stellar Systems, III Canary Islands Winter School in Astrophysics, eds. Tenorio–Tagle G., Pieto M., Sánchez F., Cambridge Univ. Press.
Elmegreen, B.G., Lada, C.J.: 1977, *Astrophys. J.* **214**, 725.
Elmegreen, B.G., Clemens, C.: 1985, *Astrophys. J.* **294**, 523.
Elmegreen, B.G., Falgarone, E.: 1996, *Astron. J.* **471**, 816.
Elmegreen, B.G.: 1997, *Astrophys. J.* **477**, 196.
Evans, II N.J., *Ann. Rev. Astron. Astrophys.* **37**, 311.
Ewen, H.I., Purcell, E.M.: 1951, *Nature*, **168**, 356.
Falgarone, E., Puget, J.P.: 1988, in Galactic and Extragalactic Star Formation, eds. Pudritz R., Fich M., Dordrecht: Kluwer.
Falgarone, E., Phillips, T.G.: 1996, *Astrophys. J.* **472**, 191.
Falgarone, E., Phillips, T.G., Walker, C.K.: 1991, *Astrophys. J.* **378**, 186.
Fatuzzo, M., Adams, F.C.: 2002, *Astrophys. J.* **570**, 210.
Ferreira, J., Pelletier, G.: 1993, *Astron. Astrophys.* **276**, 625.
Fiege, J.D., Henriksen, R.N.: 1996, *Mon. Not. Roy. Astron. Soc.* **281**, 1038.
Fiegelson, E.D., Montmerle, T.: 1999, *Ann. Rev. Astron. Astrophys.* **37**, 363.
Field, G.B.: 1978, in Protostars and Planets, ed. Gehrels, Tucson: Univ. Arizona Press.
Fleck, R.C.Jr.: 1980, *Astrophys. J.* **242**, 1019.
Fleck, R.C.Jr.: 1981, *Astrophys. J.* **246**, L151.
Fleck, R.C.Jr.: 1989, *Astron. J.* **97**, 783.
Foster, P.N., Chevalier, R.A.: 1993, *Astrophys. J.* **416**, 303.
Frerking, M.A., Langer, W.D., Wilson, R.: 1979, *Astrophys. J.* **232**, L65.
Frerking, M.A., Langer, W.D., Wilson, R.W.: 1982, *Astrophys. J.* **262**, 590.
Fuller, G.A., Myers, P.C.: 1987, in NATO/ASI Physical Processes in Interstellar Clouds, ed. Scholer M., Dordrecht: Reidel.
Fukui, Y., Yonekura, Y.: 1997, in New Horizons from Multi–Wavelength Sky Surveys, IAU Symp. 179, eds.McLean B.J., Golombeck D.A., Hayes J.J.E., Payne H.E., Kluwer: Dordrecht.
Gammie, C.F., Ostriker, E.C.: 1996, *Astrophys. J.* **466**, 814.
Garay, G., Lizano, S., Gomez, Y., Brown, R.L.: 1998, *Astrophys. J.* **501**, 710.
Geballe, T., Oka, T.: 1996, *Nature*, **384**, 334.
Gensheimer, P.D., Snyder, L.E.: 1997 *Astrophys. J.* **490**, 819.
Gerin, M., Phillips, T.G., Keen, J., Betz, A.L., Boreiko, R.T.: 1998, *Astrophys. J.* **500**, 329.
Getman, K.V., Fiegelson, E.D., Townsley, L. et al.: 2002, *Astrophys. J.* **575**, 354.
Gibb, A.G.: 1999, *Mon. Not. Roy. Astron. Soc.* **304**, 1.
Goldreich, P., Kwan, J.: 1974, *Astrophys. J.* **189**, 441.
Goldsmith, P.F.: 1987, in Interstellar Processes, eds. Hollenbach D.,J., Thornston H.A.Jr., Dordrecht: D.Reidel Publishing company.
Goldsmith, P.F., Irvine, W.M., Hjalmarson, Å., Elldér, J.: 1986, *Astrophys. J.* **310**, 383.
Gonzáles-Alfonso, E., Cernicharo, J.: 1993, *Astron. Astrophys.* **279**, 506.
Goldreich, P., Kwan, J.: 1974, *Astrophys. J.* **189**, 441.
Goodman, A.A., Benson, P.J., Fuller, G.A., Myers, P.C.: 1993, *Astrophys. J.* **406**, 528.
Goodman, A.A., Barranco, J.A., Wilner, D.J., Heyer, M.H.: 1998, *Astrophys. J.* **504**, 223.
Grazziani, F.R., Black, D.C.: 1987, *Astrophys. J.* **25**, L235.
Gredel, R., Lepp, S., Dalgarno, A., Herbst, E.: 1989, *Astrophys. J.* **347**, 289.
Green, S.: 1975, *Astrophys. J.* **201**, 366.
Green, S.: 1986, *Astrophys. J.* **309**, 311.
Green, S.: 1994, *Astrophys. J.* **434**, 188.
Green, S., Thaddeus, P.: 1974, *Astrophys. J.* **191**, 653.
Green, S., Chapman, S.: 1978, *Astrophys. J. Suppl.* **37**, 169.
Gregersen, E.M., Evans, N.J.II, Zhou, S., Choi, M.: 1997, *Astrophys. J.* **484**, 256.
Gregersen, E.M., Evans, N.J.II, Mardones, D., Myers, P.C.: 2000, *Astrophys. J.* **533**, 440.
Grenier, I.A., Lebrun, F., Arnaud, M. et al.: 1989, *Astrophys. J.* **347**, 231.

Grissom Meehan, L.S., Wilking, B.A., Claussen, M.J., Mundy, L.G., Wootten, A.: 1998, *Astron. J.* **115**, 1599.
Guenther, E.W., Lehmann, H., Emerson, J.P., Staude, J.: 1999, *Astron. Astrophys.* **341**, 768.
Gueth, F., Guilloteau, S.: 1999, *Astron. Astrophys.* **343**, 571.
Gusten, R., Mezger, P.G.: 1982, *Vistas Astron.* **26**, 159.
Hanawa, T., Matsumoto, R., Shibata, K.: 1992, *Astrophys. J.* **393**, L71
Harju, J.: 1989, *Astron. Astrophys.* **219**, 293.
Harjunpaää, P., Mattila, K.: 1996, *Astron. Astrophys.* **305**, 920.
Haro, G.: 1952, *Astrophys. J.* **115**, 572.
Harris, A., Townes, C.H., Matsakis, D.N., Palmer, P.: 1983, *Astrophys. J.* **265**, L63.
Hartmann, L., Hewett, R., Stahler, S., Mathieu, R.D.: 1986, *Astrophys. J.* **309**, 275.
Hartmann, D., Burton, W.B.: 1997, The Leiden/Dwingelo Survey of H I in the Galaxy, Cambridge University Press.
Hartquist, T.W., Dyson, J.E.: 1987, *Mon. Not. Roy. Astron. Soc.* **228**, 957.
Harwit, M., Neufeld, D.A., Melnick, G.J., Kaufman, M.J.: 1998, *Astrophys. J.* **497**, L105.
Hasegawa, T.: 1997, in CO: Twenty-five Years of Millimeter-wave Spectroscopy, IAU Symp. 170, eds. Latter W.B., Radford S.J.E., Jewell P.R., Mangum J.G., Bally J., Kluwer: Dordrecht.
Hasegawa, T.I., Herbst, E.: 1993, *Mon. Not. Roy. Astron. Soc.* **261**, 83; **263**, 589.
Heikkilä, A., Johansson, L.E.B., Olofsson, H.: 1999, *Astron. Astrophys.* **344**, 817.
Heiles, C.: 1987 in NATO/ASI Physical Processes in Interstellar Clouds, ed. Scholer M., Dordrecht: Reidel.
Heiles, C.: 1990, *Astrophys. J.* **354**, 483.
Heiles, C., Habing, H.J.: 1974, *Astron. Astrophys. Suppl.* **14**, 1.
Heithausen, A.: 1996, *Astron. Astrophys.* **314**, 251.
Heithausen, A., Bensch, F., Stutzki, J., Falgarone, E., Panis, J.F.: 1998, *Astron. Astrophys.* **331**, 65.
Herbig, G.: 1951, *Astrophys. J.* **113**, 697.
Herbig, G.: 1962, *Adv. Astron. Astrophys.* **1**, 47.
Herbig, G.: 1977, *Astrophys. J.* **217**, 693.
Herbst, E., Leung, C.M.: 1989, *Astrophys. J. Suppl.* **69**, 271.
Herbst, E.: 1995, *Ann. Rev. Phys. Chem.* **46**, 27.
Herbst, E.: 2000, in Astrochemistry: From Molecular Clouds to Planetary Systems, IAU Symp. 197, eds. Minh Y.C., van Dishoeck E.F., ASP Publ.
Herbst, E., Terzieva, R., Talbi, D.: 2000a, *Mon. Not. Roy. Astron. Soc.* **311**, 869.
Hildebrand, R.H.: 1983, *Q. J. R. Astron. Soc.* **24**, 267.
Hildebrand, R.H.: 1988, *Q. J. R. Astron. Soc.* **29**, 327.
Hirota, T., Yamamoto, S., Mikami, H., Ohisi, M.: 1998, *Astrophys. J.* **503**, 717.
Ho, P.T.P., Townes, C.H.: 1983, *Ann. Rev. Astron. Astrophys.* **21**, 239.
Hodapp, K.–W.: 1994, *Astrophys. J. Suppl.* **94**, 615.
Hodapp, K–W., Ladd, E.F.: 1995, *Astrophys. J.* **453**, 715.
Hogerheijde, M.R., van Dishoeck, E.F., Blake, G.A., van Lagevelde, H.J.: 1997, *Astrophys. J.* **489**, 293.
Hogerheijde, M.R., van Dishoeck, E.F., Blake, G.A., van Lagevelde, H.J.: 1998, *Astrophys. J.* **502**, 315.
Hogerheijde, M.R., van Dishoeck, E.F., Salberda, J.M., Blake, G.A.: 1999, *Astrophys. J.* **513**, 350.
Hollenbach, D.J., Tielens, A.G.G.M.: 1997, *Ann. Rev. Astron. Astrophys.* **35**, 179.
Houlahan, P., Scalo, J.: 1992, *Astrophys. J.* **393**, 172.
Hu, E.M.: 1981, *Astrophys. J.* **248**, 119.
Hunter, J.H.Jr., Whitaker, R.W., Lovelace, R.V.E.: 1997, *Astrophys. J.* **482**, 852.
Hunter, J.H.Jr., Whitaker, R.W.: 1989, *Astrophys. J. Suppl.* **71**, 777.
Hurt, R.L., Barsony, M.: 1996, *Astrophys. J.* **460**, L45.

Irvine, W.M., Schloerb, F.P.: 1984, *Astrophys. J.* **282**, 516.
Jansen, D.J.: 1995, PhD thesis, University of Leiden, Leiden.
Jansen, D.J., van Dishoeck, E.F., Black, J.H.: 1994, *Astron. Astrophys.* **282**, 605.
Jeans, J.H.: 1928, Astronomy and Cosmogony, p.340, Cambridge UK: Cambridge Univ. Press.
Johansson, L.E.B., Greve, A., Booth, R.S. et al.: 1998, *Astron. Astrophys.* **331**, 857.
Johns–Krull, C.M., Valenti, J.A., Hatzes, A.P., Kanaan, A.: 1999, *Astrophys. J.* **510**, L41.
Joy, A.H.: 1942, *Publ. Astron. Soc. Pacific*, **54**, 15.
Jones, A.P., Tielens, A.G.G.M., Hollenbach, D.J.: 1996, *Astrophys. J.* **469**, 740.
Juvela, M.: 1997, *Astron. Astrophys.* **322**, 943.
Juvela, M.: 1998, *Astron. Astrophys.* **329**, 659.
Kantharia, N.G., Anantharamaiah, K.R., Payne, H.E.: 1998a, *Astrophys. J.* **506**, 758.
Kantharia, N.G., Anantharamaiah, K.R., Goss, W.M.: 1998b, *Astrophys. J.* **504**, 375.
Kazes, I., Walmsley, C. M., Churchwell, E.: 1977, *Astron. Astrophys.* **60**, 293.
Keenan, P.C.: 1942, *Astrophys. J.* **96**, 101.
Kemper, C., Spaans, M., Jansen, D.J., Hogerheijde, M.R., van Dishoeck, E.F., Tielens, A.G.G.M.: 1999, *Astrophys. J.* **515**, 649.
Kenyon, J.J., Hartman, L.: 1995, *Astrophys. J. Suppl.* **101**, 117.
Kerr, F.J., Hindman, J.V., Gum, C.S.: 1959, *Aust. J. Phys.* **12**, 270.
Khavtassi, J.Sh.: 1955, *Bull. of Abastumani Astrophysical Observatory*, **18**, 29.
Khavtassi, J.Sh.: 1960, Atlas of Galactic Dark clouds, Tbilisi.
Kingdon, J.B., Ferland, G.J.: 1997, *Astrophys. J.* **477**, 732.
Kiss, Cs., Moór, A., Nikolić, S., Tóth, L.V.: 1997, in the Proc. of the XXX YERAC, *Acta Cosmologica*, Universitas Iagellonica, XXIII-2, pg. 95.
Kiss, Cs., Tóth, L.V., Moór, A., Sato, F., Nikolić, S., Wouterloot, J.G.A.: 2000, *Astron. Astrophys.* **363**, 755.
Kitamura, Y., Kawabe, R., Yamashita, T., Hayashi, M.: 1990, *Astrophys. J.* **363**, 180.
Kitamura, Y., Kawabe, R., Ishiguro, M.: 1992, *Publ. Astron. Soc. Jpn.* **44**, 407.
Knapp, G.R., Morris, M.: 1985, *Astrophys. J.* **292**, 640.
Kontinen, S., Harju, J., Heikkilä, A., Haikala, L.K.: 2000, *Astron. Astrophys.* **361**, 704.
Koyama, H., Inutsuka, S.-I.: 2000, *Astrophys. J.* **532**, 980.
Kramer, C., Degiacomi, C.G., Graf, U.U. et al.: 1998, Proc. SPIE 3357, 711. Advanced Technology MMW, Radio and Terahertz Telescopes. Phillips T.G. ed.
Kramer, C., Alves, J., Lada, C.J. et al.: 1999, *Astron. Astrophys.* **342**, 257.
Kuiper, T.B.H., Langer, W.D., Velusamy, T.: 1996, *Astrophys. J.* **468**, 761.
Kuiper, T.B.H., Kuiper, E.N.R., Dickinson, D.F., Turner, B.E., Zuckerman, B.: 1984, *Astrophys. J.* **276**, 211.
Kun, M.: 1982, *Afz*, **18**, 63.
Kun, M.: 1998, *Astrophys. J. Suppl.* **115**, 59.
Kun, M., Balázs, L.G., Tóth, I.: 1987, *Astrophys. & Sp. Sci* **134**, 211
Kun, M., Prusti, T.: 1993, *Astron. Astrophys.* **272**, 235.
Kun, M., Vinkó, J., Szabados, L.: 2000a, *Mon. Not. Roy. Astron. Soc.* **319**, 777.
Kun, M., Nikolić, S., Ábrahám, P.: 2000b, in the Proc. 33rd ESLAB Symp. *"Star formation from the small to the large scale"* ESA SP-445, eds. F. Favata, A. A. Kaas & A. Wilson, pg. 441.
Kutner, M.L., Ulich, B.L.: 1981, *Astrophys. J.* **291**, 188.
Lacy, J.H., Knacke, R., Geballe, T.R., Tokunaga, A.T.: 1994, *Astrophys. J.* **428**, L69.
Lada, C.J.: 1987, p.93 in Formation and Evolution of Low Mass Stars, eds. A.K. Dupree & M.T.V.T. Lago, Kluwer.
Lada, C.J.: 1999, in The Origin of Stars and Planetary Systems eds. Lada C.J., Kylafis N.D., Kluwer Academic Publishers.
Lada, C.J., Margulis, M., Dearborn, D.: 1984, *Astrophys. J.* **285**, 141.
Lada, C.J., Wilking, B.A.: 1984, *Astrophys. J.* **287**, 610.
Lada, C.J., Lada, E.A., Clemens, D.P., Bally, J.: 1994, *Astrophys. J.* **429**, 694.

Lahuis, F., van Dishoeck, E.F.: 2000, *Astron. Astrophys.* **355**, 699.
Lang, K.R.: 1992, *Astrophysical Data: Planets and Stars*, Springer-Verlag New York, Inc. pg. 144.
Langer, W.D.: 1978, *Astrophys. J.* **225**, 95L.
Langer, W.D., Wilson, R.W., Goldsmith, P.F., Beichman, C.A.: 1989, *Astrophys. J.* **337**, 355.
Langer, W.D., van Dishoeck, E.F., Bergin, E.A., Blake, G.A., Tielens, A.G.G.M., Velusamy, T., Whittet, D.C.B.: 2000, in Protostars and Planets IV, eds. Mennings V., Boss A.A., Russel S.S., Tucson: University of Arizona Press.
Lapinov, A.: 1989, *Sov. Astron.* **33**, 132.
Larson, R.B.: 1969, *Mon. Not. Roy. Astron. Soc.* **145**, 271.
Larson, R.B.: 1981, *Mon. Not. Roy. Astron. Soc.* **194**, 809.
Laureijs, R.J., Clark, F.O., Prusti, T.: 1991, *Astrophys. J.* **372**, 185.
Le Bourlot, J., Pineau des Forets, G., Roueff, E.: 1993, *Astrophys. J.* **416**, L87.
Le Bourlot, J., Pineau des Forets, G., Roueff, E.: 1995a, *Astron. Astrophys.* **297**, 251.
Le Bourlot, J., Pineau des Forets, G., Roueff, E.: 1995b, *Astron. Astrophys.* **302**, 870.
Lebrun, F.: 1986, *Astrophys. J.* **306**, L16.
Lee, Y.: 1994, *JKAS*, **27**, 159.
Lee, H.–H., Battens, R.P.A., Herbst, E.: 1996, *Astron. Astrophys. Suppl.* **119**, 111.
Leisawitz, D., Bash, F.N., Thaddeus, P.: 1989, *Astrophys. J. Suppl.* **70**, 737.
Lepp, S., McCray, R.: 1983, *Astrophys. J.* **269**, 560.
Leung, C.M., Liszt, H.S.: 1976, *Astrophys. J.* **208**, 732.
Leung, C.M., Brown, R.L.: 1977, *Astrophys. J.* **214**, 73L.
Li, Z.Y., Shu, F.H.: 1996, *Astrophys. J.* **472**, 211.
Liszt, H.S., Leung, C.M.: 1977, *Astrophys. J.* **218**, 396.
Lizano, S.: 1989, *RMxAA*, **18**, 11.
Loren, R.B., Mundy, L.G.: 1984, *Astrophys. J.* **286**, 232.
Lovas, F.J.: 1992, *J. Phys. Chem. Ref. Data*, **21**, 181-272.
Lucas, R.: 1974, *Astron. Astrophys.* **36**, 465.
Lucas, R.: 1976, *Astron. Astrophys.* **46**, 473.
Lynds, B.T.: 1962, *Astrophys. J. Suppl.* **7**, 1.
Magnum, J.G., Wootten, A.: 1993, *Astrophys. J. Suppl.* **89**, 123.
Mardones, D., Myers, P.C., Tafalla, M. et al.: 1997, *Astrophys. J.* **489**, 719.
Masson, C.R., Chernin, L.M.: 1993, *Astrophys. J.* **414**, 230.
Mather, J.C., Cheng, E.S., Cottingham, D.A. et al.: 1994, *Astrophys. J.* **420**, 439.
Mathis, J.S.: 1996, *Astrophys. J.* **472**, 643.
Matthews, B.C., Wilson, C.D.: 2000, *Astrophys. J.* **531**, 868.
McCall, B.J., Geballe, T.R., Hinkle, K.H., Oka, T.: 1999, *Astrophys. J.* **522**, 338.
Mendoza, E.E.: 1966, *Astrophys. J.* **143**, 1010.
Menten, K.M.: 1997, in Molecules in Astrophysics: Probes and Processes, IAU Symp. 178, ed. van Dishoeck E.F., Kluwer: Dordrecht.
Mestel, L.: 1985, in Protostars and Planets II, eds. Black D.C., Matthews M.S., Tucson: Univ.Arizona Press.
Mestel, L.: 1965, *Q. J. R. Astron. Soc.* **6**, 161.
Mestel, L., Spitzer, L.: 1956, *Mon. Not. Roy. Astron. Soc.* **116**, 503.
Meyers, K.A., Snow, T.P., Federman, S.R., Breger, M.: 1983, *Astrophys. J.* **288**, 148.
Mezger, P.G., Smith, L.F.: 1977, in Star Formation, IAU Symp. 75, eds. de Jong T., Maeder A., Dordrecht: Reidel.
Millar, T.J., Farquhar, P.R.A., Willacy, K.: 1997, *Astron. Astrophys. Suppl.* **121**, 139.
McCall, B.J., Geballe, T.R., Hinkle, K.H., Oka, T.: 1999, *Astrophys. J.* **522**, 338.
McKee, C.F.: 1990, in The Evolution of the Interstellar Medium, ed. Blitz L., ASP Conf.Series Vol. 12.
McKee, C.F.: 1995, in The Physics of the Interstellar and Intergalactic Medium, eds. Ferrara A., McKee C.F., Heiles C., Shapiro P.R., ASP Conf. Series Vol. 80.

Mollaaghababa, R., Gottlieb, C.A., Vrtilek, J.M., Thaddeus, P.: 1991 *Astrophys. J.* **368**, L19.
Montmerle, T., Koch–Miramond, L., Falgarone, E., Grindlay, J.E.: 1983, *Astrophys. J.* **269**, 182.
Morata, O., Estalella, R., López, R., Planesas, P.: 1997, *Mon. Not. Roy. Astron. Soc.* **292**, 120.
Moreira, M.C., Yun, J.L., Vásquez, R., Torelles, J.M.: 1997, *Astron. J.* **113**, 1371.
Moriarty–Schieven, G.H., Snell, R.L.: 1988, *Astrophys. J.* **332**, 364.
Motte, F., André, P.: 2001, *Astron. Astrophys.* **365**, 440.
Motte, F., André, P., Neri, R.: 1998, *Astron. Astrophys.* **336**, 150.
Mouschovias, T.Ch.: 1976, *Astrophys. J.* **207**, 141.
Mouschovias, T.Ch., Spitzer, L.: 1976, *Astrophys. J.* **210**, 326.
Mouschovias, T.Ch., Paleologou, E.V.: 1980, *Astrophys. J.* **237**, 877.
Muller, C.A., Westerhout, G.: 1957, *Bull. Astron. Inst. Neth.* **13**, 151.
Myers, P.C.: 1995, in Molecular Clouds and Star Formation, Proc. of the 7th Guo–Shoujing Summer School in AStrphysics, Wuxi, china, ed. Yuan C., Singapore: World Press.
Myers, P.C., Benson, P.J.: 1983, *Astrophys. J.* **266**, 309.
Myers, P.C., Fuller, G.A., Goodman, A.A., Benson, P.J.: 1991, *Astrophys. J.* **376**, 561.
Myers, P.C., Ladd, E.F.: 1993, *Astrophys. J.* **413**, L47.
Myers, P.C., Dame, T.M., Thaddeus, P. et al.: 1986, *Astrophys. J.* **301**, 398.
Nakano, T.: 1979, *Publ. Astron. Soc. Jpn.* **31**, 697.
Nejad, L.A.M., Williams, D.A., Charnley, S.B.: 1990, *Mon. Not. Roy. Astron. Soc.* **246**, 183.
Nejad, L.A.M., Wagenblast, R.: 1999, *Astron. Astrophys.* **350**, 204.
Nikolić, S.: 1998, in the Proc. of the XII Nacional Conference of Yugoslav Astronomers, *Publ. Astron. Obs. Belgrade* **65**, 93.
Nikolić, S., Kiss, Cs., Johansson, L.E.B., Wouterloot, J.G.A., Tóth, L.V.: 2001, *Astron. Astrophys.* **367**, 694.
Nikolić, S., Johansson, L.E.B., Harju, J.: 2002, *Astron. Astrophys.* submitted December.
Nikolić, S., Kun, M.: 2003, *Astron. Astrophys.* submitted January.
Nilsson, A., Bergman, P., Hjalmarson, Å.: 2000, *Astron. Astrophys. Suppl.* **144**, 441.
Nummelin, A., Bergman, P., Hjalmarson, Å. et al.: 1998, *Astrophys. J. Suppl.* **117**, 427.
Nummelin, A., Bergman, P.: 1999, *Astron. Astrophys.* **341**, L59.
Obayashi, A., Fukui, Y., Kun, M., Sato, F., Yonekura, Y.: 1998, *Astron. J.* **115**, 247.
Ogawa, H.S., McMullin, D., Judge, D.L., Canfield, L.R.: 1990, *Journal of Geophysical Research*, **95**, 4291.
Olmi, L., Cesaroni, R., Neri, R., Walmsley, C.M.: 1996 *Astron. Astrophys.* **315**, 565.
O'Linger, J., Wolf–Chase, G.A., Barsony, M., Ward–Thompson, D.: 1999, *Astrophys. J.* **515**, 696.
Osterbrock, D.E.: 1989, Astrophysics of Gaseous Nebuale and Active Galactic Nuclei, University Science, California.
Padoan, P., Juvela, M., Bally, J., Nordlund, Å.: 1998, *Astrophys. J.* **504**, 300.
Padoan, P., Juvela, M., Bally, J., Nordlund, Å.: 2000, *Astrophys. J.* **529**, 259.
Park, Y.-S., Kim, J., Minh, Y.C.: 1999, *Astrophys. J.* **520**, 223.
Parker, E.N.: 1979, Cosmical Magnetic Fields, Oxford Univ. Press.
Patel, N.A., Goldsmith, P.F., Heyer, M.H., Snell, R.L., Pratap, P.: 1998, *Astrophys. J.* **507**, 241.
Pineau des Forêts, G., Roueff, E., Flower, D.R.: 1992, *Mon. Not. Roy. Astron. Soc.* **258**, 45.
Pirogov, L., Zinchenko, I., Lapinov, A., Myshenko, V., Shul'Ga, V.: 1995, *Astron. Astrophys. Suppl.* **109**, 333.
Plambeck, R.L., Snell, R.L.: 1995, *Astrophys. J.* **446**, 234.
Plambeck, R.L., Snell, R.L., Loren, R.B.: 1983, *Astrophys. J.* **266**, 321.
Polk, K.S., Knapp, G.R., Stark, A.A., Wilson, R.W.: 1988, *Astrophys. J.* **332**, 432.

Preibisch, T.: 1997, *Astron. Astrophys.* **320**, 525.
Raga, A.C., Cabrit, S.: 1993, *Astron. Astrophys.* **278**, 267.
Rawlings, J.M.C., Hartquist, T.W., Menten, K.M., Williams, D.A.: 1992, *Mon. Not. Roy. Astron. Soc.* **255**, 471.
Rawlings, J.M.C., Hartquist, T.W., Williams, D.A., Falle, A.E.G.: 2002, *Astron. Astrophys.* **391**, 681.
Richer, J., Shepherd, D., Cabrit, S., Bachiller, R., Churchwell, E.: 2000, in Protostars and Planets IV, eds. Mannings V., Boss A., Russell S., Tucson: Univ. Arizona Press.
Rohlfs, K., Wilson, T.L.: 1996, Tools of Radio Astronomy, Springer-Verlag Berlin Heidelberg New York.
Roshi, D.A., Anantharamaiah, K.R.: 2000, *Astrophys. J.* **535**, 231.
Rosvick, J.M., Davidge, T.J.: 1995, *Publ. Astron. Soc. Pacific*, **107**, 49.
Sancisi, R.: 1974, in IAU Symposium 60, Galatic Radio Astronomy, eds. Kerr F.J., Simonson S.C., Dordrecht: Reidel.
Sandell, G., Höglund, B., Kislyakov, A.G.: 1983, *Astron. Astrophys.* **118**, 306.
Sandford, S.A., Allamandola, L.J.: 1990, *Astrophys. J.* **355**, 357.
Sato, F., Fukui, Y.: 1989, *Astrophys. J.* **343**, 773.
Sato, F., Mizuno, A., Nagahama, T. et al.: 1994, *Astrophys. J.* **435**, 279.
Schlegel, D.J., Finkbenier, D.P., Davis, M.: 1998, *Astrophys. J.* **500**, 525.
Schleuning, D.A., Vaillancourt, J.E., Hildebrand, R.H. et al.: 2000, *Astrophys. J.* **535**, 913.
Scalo, J.: 1986, *Fund. Cosm. Phys.* **11**, 1.
Schwartz, P.R., Gee, G., Huang, Y.-L.: 1988, *Astrophys. J.* **327**, 350.
Schwartz, R.D.: 1975, *Astrophys. J.* **195**, 631.
Scott, G.B.I., Freeman, C.G., McEwan, M.J.: 1997, *Mon. Not. Roy. Astron. Soc.* **290**, 636.
Scoville, N.Z.: 1985, in Protostars and Planets II, eds. Black D.C., Matthews M.S., Tucson: Univ.Arizona Press.
Scoville, N.Z., Solomon, P.M.: 1974, *Astrophys. J.* **187**, L67.
Scoville, N.Z., Irvine, W.M., Wannier, P.G., Predmore, C.R.: 1977, *Astrophys. J.* **216**, 320.
Seitter, W.C.: 1975, Bonner Spectral Atlas II., Ferdinand Dümmler Verlag.
Shalabiea, O., Greenberg, J.M.: 1994, *Astron. Astrophys.* **290**, 266.
Shalabiea, O., Greenberg, J.M.: 1995, *Astron. Astrophys.* **296**, 779.
Shu, F.H.: 1977, *Astrophys. J.* **214**, 488.
Shu, F.H.: 1991, in The Physics of Star Formation and Early Stellar Evolution, eds. Lada C.J., Kylafis N.D., Kluwer Academic Publishers.
Shu, F.H., Adams, F.C., Lizano, S.: 1987, *Ann. Rev. Astron. Astrophys.* **25**, 23.
Shu, F.H., Lizano, S., Ruden, S.P., Najita, J.: 1988, *Astrophys. J.* **328**, L19.
Shu, F.H., Ruden, S.P., Lada, C.J., Lizano, S.: 1991a, *Astrophys. J.* **370**, L31.
Snyder, L.E., Hollis, J.M., Buhl, D.: 1977, *Astrophys. J.* **215**, L87.
Sobolev, V.V.: 1960, Moving Envelopes of Stars, Cambridge: Harvard University Press.
Solomon, P.M., Klemperer, W.: 1972, *Astrophys. J.* **178**, 389.
Solomon, P.M., Sanders, D.B.: 1985, in Protostars and Planets II, eds. Black D.C., Matthews M.S., Tuscon: Univ.Arizona Press.
Solomon, P.M., Rivolo, A.R., Barrett, J.W., Yahil, A.: 1987, *Astrophys. J.* **319**, 730.
Snell, R.L., Scoville, N.Z., Sanders, D.B., Erickson, N.R.: 1984, *Astrophys. J.* **284**, 176.
Spaans, M., van Langevelde, H.J.: 1992, *Mon. Not. Roy. Astron. Soc.* **258**, 159.
Spitzer, L.: 1978, Physical Processes in the Interstellar Medium, New York: Wiley.
Spitzer, L.: 1968, in Nebulae and Interstellar Matter, Stars and Stellar Systems, eds. Middlehurst S.B., Aller L.H., Chicago: Univ.Chicago Press.
Stahler, S.W., Walter, F.M.: 1993, in Protostars and Planets III.
Stahler, S.W., Shu, F.H., Taam, R.E.: 1980, *Astrophys. J.* **242**, 226.
Stark, A.A., Gammie, C.F., Wilson, R.W. et al.: 1992, *Astrophys. J. Suppl.* **79**, 77.
Strong, A.W., Mattox, J.R.: 1996, *Astron. Astrophys.* **308**, L21.
Strong, A.W., Bennett, K., Bloemen, H. et al.: 1994, *Astron. Astrophys.* **292**, 82.

Stutzki, J., Bensch, F., Heithausen, A., Ossenkopf, V., Zielinsky, M.: 1998, *Astron. Astrophys.* **336**, 697.
Suzuki, H.Y., Ohishi, M., Kaifu, N., Ishikawa, S. et al.: 1992, *Astrophys. J.* **392**, 551.
Swings, P., Rosenfeld, L.: 1937, *Astrophys. J.* **86**, 483.
Tafalla, M., Bachiller, R., Wright, M.C.H.: 1994, *Astrophys. J.* **432**, L127.
Tafalla, M., Mardones, D., Myers, P.C. et al.: 1998, *Astrophys. J.* **504**, 900.
Talbi, D., Ellinger, Y., Herbst, E.: 1996, *Astron. Astrophys.* **314**, 688.
Talbi, D., Herbst, E.: 1998, *Astron. Astrophys.* **333**, 1007.
Taylor, D.K., Dickman, R.L., Scoville, N.Z.: 1987, *Astrophys. J.* **315**, 104.
Taylor, S.D., Morata, O., Williams, D.A.: 1996, *Astron. Astrophys.* **313**, 269.
Taylor, S.D., Morata, O., Williams, D.A.: 1998, *Astron. Astrophys.* **336**, 309.
Terzieva, R., Herbst, E.: 2000, *Mon. Not. Roy. Astron. Soc.* **317**, 563.
Tielens, A.G.G.M., Hagen, W.: 1982, *Astron. Astrophys.* **114**, 245.
Tielens, A.G.G.M., Hollenbach, D.: 1985, *Astrophys. J.* **291**, 772.
Tielens, A.G.G.M., Whittet, D.C.B.: 1997, in Molecules in Astrophysics: Probes and Processes, IAU Symp. 178, ed. van Dishoeck E.F., Kluwer, Dordrecht, 45.
Torrelles, J.M., Rodríguez, L.F., Cantó, J., Carral, P., Marcaide, J. et al.: 1983, *Astrophys. J.* **274**, 214.
Tóth, L.V., Walmsley, C.M.: 1994, *IBVS*, 4107.
Tóth, L.V., Walmsley, C.M.: 1996, *Astron. Astrophys.* **311**, 981.
Tóth, L.V., Kun, M.: 1997, *IBVS*, 4492.
Tóth, L.V., Haikala, L.K., Liljeström, T., Mattila, K.: 1995, *Astron. Astrophys.* **295**, 755.
Tóth, L.V., Kiss, Cs., Moór, A.: 1996, in The Role of Dust in the Formations of Stars, ESO workshop, ed. Käufl, H.U., Springer.
Townes C.H., Schawlow A.L.: 1975, *Microwave Spectroscopy*, Dover Publications Inc., New York
Turner, B.E., Pirogov, L., Minh, Y.C.: 1997, *Astrophys. J.* **483**, 325.
Ulich, B.L., Haas, R.W.: 1976, *Astrophys. J. Suppl.* **30**, 247.
Van Dishoeck, E.F.: 1998, in The Molecular Astrophysics of Stars and Galaxies, eds. Hartquist T.W. and Williams D.A., Oxford University Press.
Van Dishoeck, E.F., Black, J.H.: 1986, *Astrophys. J. Suppl.* **66**, 109.
Van Dishoeck, E.F., Black, J.H.: 1988, *Astrophys. J.* **334**, 771.
Van Dishoeck, E.F., Blake, G.A.: 1998, *Ann. Rev. Astron. Astrophys.* **36**, 317.
Van Dishoeck, E.F., Hogerheijde, M.R.: 1999, The Physics of Star Formation and Early Stellar Evolution II eds. C.J. Lada and D.Kylafis, Dordrecht: Kluwer.
Van Dishoeck, E.F., Black, J.H., Phillips, T.G., Gredel, R.: 1991, *Astrophys. J.* **366**, 141.
Van de Hulst, H.C.: 1945, *Ned. Tijdschr. Natuurk.* **11**, 201.
Van den Bergh, S., Tammann, G.A.: 1991, *Ann. Rev. Astron. Astrophys.* **29**, 363.
Van der Tak Floris, F.S., van Dishoeck, E.F., Evans, N.J.II, Bakker, E.J., Blake, G.A.: 1999, *Astrophys. J.* **522**, 991.
Van der Veen, W.E.C.J., Huggins, P.J., Matthews, H.E.: 1998, *Astrophys. J.* **505**, 749.
Van der Werf, P.P., Goss, W.M., Van den Bout, P.A.: 1988, *Astron. Astrophys.* **201**, 311.
Vrba, F.J., Strom, K.M., Strom, S.E.: 1976, *Astron. J.* **81**, 958.
Wadiak, E.J., Wilson, T.L., Rood, R.T., Johnston, K.L.: 1985, *Astrophys. J.* **295**, L43.
Walmsley, C.M., Churchwell, E., Nash, A., Fitzpatrick, E.: 1982, *Astrophys. J.* **258**, L75.
Wannier, P.G., Lichten, S.M., Morris, M.: 1983, *Astrophys. J.* **268**, 727.
Ward–Thompson, D., Scott, P.F., Hills, R.E., André, P.: 1994, *Mon. Not. Roy. Astron. Soc.* **268**, 276.
Ward–Thompson, D., Chini, R., Krugel, E., André, P., Bontemps, S.: 1995, *Mon. Not. Roy. Astron. Soc.* **274**, 121.
Wardle, M.: 1998, *Mon. Not. Roy. Astron. Soc.* **298**, 507.
Weinreb, S., Barrett, A.H., Meeks, M.L., Henry, J.C.: 1963, *Nature*, **200**, 829.
Wheelock, S.L. et al.: 1994, IRAS Sky survey Atlas Explanatory Supplement, JPL Publication 94-11, Pasadena: JPL.

Whittet, D.C.B., Gerakines, P.A., Tielens, A.G.G.M., Adamson, A.J., Boogert, A.C.A. et al.: 1998, *Astrophys. J.* **488**, L159.
Williams, D.A.: 1993, in Dust and Chemistry in Astronomy, eds. Millar T.J., Williams D.A., IOP Publishing, Bristol pg. 143.
Williams, J.P., Bergin, E.A., Caselli, P., Myers, P.C., Plume, R.: 1998, *Astrophys. J.* **503**, 689.
Wilking, B.A., Schwartz, R.D., Fanetti, T.M., Friel, E.D.: 1997, *Publ. Astron. Soc. Pacific*, **109**, 569.
Wilking, B.A., Claussen, M.J., Benson, P.J. et al.: 1994, *Astrophys. J.* **431**, L119.
Wilson, T.L., Rood, R.: 1994, *Ann. Rev. Astron. Astrophys.* **32**, 191.
Wilson, T.L., Henkel, C., Hüttemeister, S., Dahmen, G., Linhart, A., Lemme, C., Schmid-Burgk, J.: 1993, *Astron. Astrophys.* **276**, L29.
Wilson, R.W., Jefferts, K.B., Penzias, A.A.: 1970, *Astrophys. J.* **161**, L43.
Wolf, M.: 1923, *AN*, **219**, 109.
Wolf–Chase, G.A., Barsony, M., O'Linger, J.: 2000, *Astron. J.* **120**, 1467.
Wolf–Chase, G.A., Barsony, M., Wootten, A.H. et al.: 1998, *Astrophys. J.* **501**, L193.
Wolk, S.J., Walter, F.M.: 1996, *Astron. J.* **111**, 2066.
Wolkovitch, D., Langer, W.D., Goldsmith, P.F., Heyer, M.: 1997, *Astrophys. J.* **477**, 241.
Wu, Y., Huang, M., He, J.: 1996, *A&ASS*, **115**, 283.
Wyrowski, F., Schilke, P., Walmsley, C.M.: 1999, *Astron. Astrophys.* **341**, 882.
Xiang, D., Turner, B.T.: 1995, *Astrophys. J. Suppl.* **99**, 121.
Yonekura, Y., Dobashi, K., Mizuno, A. et al.: 1997, *Astrophys. J. Suppl.* **110**, 21.
Yorke, H.W., Bodenheimer, P., Laughlin, G.: 1993, *Astrophys. J.* **411**, 274.
Yorke, H.W., Bodenheimer, P., Laughlin, G.: 1995, *Astrophys. J.* **443**, 199.
Yun, J.L., Moreira, M.C., Afonso, J.M., Clemens, D.P.: 1999, *Astron. J.* **118**, 990.
Yun, J.L., Moreira, M.C., Torrelles, J.M., Alfonso, J.M., Santos, N.C.: 1996, *Astron. J.* **111**, 841.
Zhou, S., Wu, Y., Evans, N.J. II, Fuller, G.A., Myers, P.C.: 1989, *Astrophys. J.* **346**, 168.
Zhou, S.D., Evans, H.J., Kompe, C., Walmsley, C.M.: 1993, *Astrophys. J.* **404**, 232.
Zinchenko, I., Forsstroem, V., Lapinov, A., Mattila, K.: 1994, *Astron. Astrophys.* **288**, 601.
Zuckerman, B., Evans, N.J.II.: 1974, *Astrophys. J.* **192**, L149.
Zuckerman, B., Palmer, P.: 1974, *Ann. Rev. Astron. Astrophys.* **12**, 279.
Zweibel, E.G.: 1998, *Astrophys. J.* **499**, 746.
Zweibel, E.G., Josafatsson, K.: 1983, *Astrophys. J.* **270**, 511.